



저작자표시-비영리-변경금지 2.0 대한민국

이용자는 아래의 조건을 따르는 경우에 한하여 자유롭게

- 이 저작물을 복제, 배포, 전송, 전시, 공연 및 방송할 수 있습니다.

다음과 같은 조건을 따라야 합니다:



저작자표시. 귀하는 원저작자를 표시하여야 합니다.



비영리. 귀하는 이 저작물을 영리 목적으로 이용할 수 없습니다.



변경금지. 귀하는 이 저작물을 개작, 변형 또는 가공할 수 없습니다.

- 귀하는, 이 저작물의 재이용이나 배포의 경우, 이 저작물에 적용된 이용허락조건을 명확하게 나타내어야 합니다.
- 저작권자로부터 별도의 허가를 받으면 이러한 조건들은 적용되지 않습니다.

저작권법에 따른 이용자의 권리는 위의 내용에 의하여 영향을 받지 않습니다.

이것은 [이용허락규약\(Legal Code\)](#)을 이해하기 쉽게 요약한 것입니다.

[Disclaimer](#)

Doctoral Thesis

EFFECT OF STRONG ACIDS ON
HYDROLYSIS OF POLYAMIDE
MEMBRANES AND ITS APPLICATION

Byung-Moon Jun

Department of Urban and Environmental Engineering
(Environmental Science and Engineering)

Graduate School of UNIST

2018

**EFFECT OF STRONG ACIDS ON
HYDROLYSIS OF POLYAMIDE
MEMBRANES AND ITS APPLICATION**

Byung-Moon Jun

Department of Urban and Environmental Engineering
(Environmental Science and Engineering)

Graduate School of UNIST

Effect of strong acids on hydrolysis of polyamide membranes and its application

A thesis/dissertation
submitted to the Graduate School of UNIST
in partial fulfillment of the
requirements for the degree of
Doctor of Philosophy of Science

Byung-Moon Jun

12. 19. 2018 of submission

Approved by



Advisor

Young-Nam Kwon

Effect of strong acids on hydrolysis of polyamide membranes and its application

Byung-Moon Jun

This certifies that the thesis/dissertation of Byung-Moon Jun is
approved.

12. 19. 2018 of submission

signature



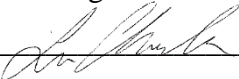
Advisor: Young-Nam Kwon

signature



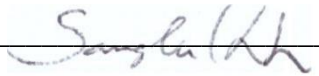
Jaeweon Cho: Thesis Committee Member #1

signature



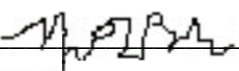
Changha Lee: Thesis Committee Member #2

signature



Sang Kyu Kwak: Thesis Committee Member #3

signature



In-Chul Kim: Thesis Committee Member #4;

ABSTRACT

Water resource is essential for humans and many places on the earth, and there needs to solve freshwater shortage caused by water pollution by industrial and farming activities. Nanofiltration (NF) technique has been attracted a lot during past decades, because of its unique characteristics which are utilizing separation mechanisms of both solution diffusion (as in reverse osmosis) and sieving (as in ultrafiltration), resulting to obtain high rejection of divalent salts and organic molecules with low molecular weight (M_w from 200 to 1000) at low operating pressure. Currently, commercial NF polyamide (PA) thin-film composite (TFC) membranes have been generally produced by interfacial polymerization method using piperazine (aliphatic amine monomer) or *m*-phenylenediamine (MPD, aromatic amine monomer) reacting with trimesoyl chloride (TMC, acyl chloride monomer). The interfacial polymerization methods using piperazine/MPD and TMC are one of the most effective methods to fabricate TFC NF membranes, because the thin/dense polyamide selective layer can make high water flux at low driving-pressure, and the permeable properties can be optimized by several fabrication factors (*e.g.*, monomer concentrations, effective additives, reaction times, and curing time/temperature for post-treatment).

The NF technique has been broadly applied to treatment/recycle of the target compounds in acidic conditions: (I) exclusion of heavy metals and sulfate ions in the mining and metal industry, (II) recycling of phosphorus in sewage sludge, (III) treatment of nitric acids in the picture tube production, (IV) regeneration of acidic effluents in dairy cleaning-in-place processes, (V) purification of acidic effluents in the pulp and paper industry, and (VI) separation of plentiful acids such as HBF_4 , HCl , HNO_3 , H_2SO_4 , H_3BO_3 in effluents from rinsing, fermentation, and extraction processes. Additionally, NF technique can be applied to wastewater containing HCl , HBr and HI from semiconductor's etching process. Acid-stable NF membranes are needed to apply above processes which operate with acidic condition. However, high performance commercial NF semi/full-aromatic PA membranes, which are fabricated by piperazine/MPD with TMC, are limited in the range of pH 2 to 11 in accordance with suppliers.

The previous studies were mainly investigated to effect of acidic conditions on PA membranes in the view of permeability. However, both changes of physical and chemical properties by degradation mechanism have not been systematically discussed for semi/full-aromatic membranes after exposure to various acidic conditions up to now. Therefore, a detailed research needs to elucidate effect of acidic degradation on physical and chemical properties of PA membranes using various analytical tools and computational calculation methods.

The overall objectives of this work is to systematically examine the effect of the acidic conditions on semi/full-aromatic PA membranes in terms of changes of physical/chemical properties, and to suggest mechanism to explain changed the properties as well as applications for practical fields via various analytical tools: Scanning Electron Microscopy (SEM), Attenuated Total Reflectance-Fourier Transform Infrared spectroscopy (ATR-FTIR), X-ray photoelectron spectroscopy (XPS), Time-of-Flight Secondary Ion Mass Spectrometry (ToF-SIMS), contact angle analyzer, electrophoretic light scattering spectrophotometer, filtration tests, and density functional theory (DFT) computational calculations.

Experimental results from degradation by acid showed different tendency between semi and full-aromatic PA membrane using acidic aqueous solution (15wt% sulfuric acid). According to analyses of the membrane's physical and chemical properties (*e.g.*, SEM, ATR-FTIR, XPS, and filtration tests), full-aromatic PA membrane had relatively higher acid-stability than semi-aromatic PA membrane. These degradations by acid cause conversion of an amide group to carboxyl and amine groups measured by ToF-SIMS results. Furthermore, these converted carboxyl and amine groups decreased the contact angle and increased the absolute value of the zeta potential semi-aromatic PA membranes. These difference of acid-stability between semi and full-aromatic PA membrane is resulted from relatively lower energy barrier of semi-aromatic PA membrane in the RDS step. These energy barrier results in the RDS had a close relationship with protonated amides' twist angle (τ_D), which shows representative and quantitative value for resonance of amide group. However, full-aromatic PA membrane with relatively higher acid-stability were also severely degraded when it exposed to pH 0 acidic solution containing hydrogen halides. For example, in ATR-FTIR results, amide II band (N-H) in 1541 cm^{-1} and amide I band (C=O) in 1663 cm^{-1} after degradation by hydrogen halides tended to decrease due to halogenation reacted with halogens generated by oxidation of hydrogen halides. In addition, water flux after exposure to hydrogen halides tended to severely decrease with increasing exposure time, resulted from broken hydrogen bonding due to halogenation.

Meanwhile, acid-catalyzed hydrolysis, which causes conversion amide group into amine and carboxyl group, were applied to post-treatment of semi-aromatic PA membrane in terms of practical applications (*e.g.*, water softening and enrichment of antibiotics). Post-treatment by sulfuric acid in the range of pH 0 to 2 increased membrane's hydrophilicity, pore size, and absolute value of surface charge. In accordance with change of surface characteristics, mixture selectivity ($\text{Na}^+/\text{Mg}^{2+}$) for water softening was improved about 2.6 times in acidic conditions. Optimized post-treatment membranes were applied to the enrichment of antibiotics as well, and the membrane had higher water flux and competitive antibiotics rejection compared to other commercial or fabricated membranes. That is, operation time of optimized membrane was improved about 2 to 3 times than virgin semi-aromatic membrane.

Contents

Abstract	I
Contents	IV
List of figures	VII
List of tables	XII
Appendix A. Nomenclature and abbreviation.....	XIV
I. Chapter 1. Introduction	1
1.1 Problem statement and significance	2
1.2 Objectives of this work.....	4
1.3 Scope of this work.....	4
1.4 Outline of this work.....	6
II. Chapter 2. Background and literature review	7
2.1 Classification of membrane	8
2.2 Pressure-driven process	9
2.3 Polyamide (PA) membrane.....	11
2.3.1 Cross-sectional structures of TFC PA membrane	13
2.3.2 Interfacial polymerization.....	14
2.3.3 Characterizations of polyamide membrane.....	17
2.3.3.1 Scanning electron microscopy (SEM)	18
2.3.3.2 Attenuated total reflectance-Fourier transform infrared spectroscopy (ATR-FTIR)	20
2.3.3.3 X-ray photoelectron spectroscopy (XPS)	22
2.3.3.4 Contact angle.....	25
2.3.3.5 Zeta potential (ζ)	27
2.3.3.6 Time-of-flight secondary ion mass spectrometry (ToF-SIMS)	30
2.4 Acid-catalyzed hydrolysis of amide group	33
2.5 Acidic degradation of PA membranes.....	35
III. Chapter 3. Study on acid-catalyzed hydrolysis of polyamide NF membranes in terms of surface characterization and DFT calculation.....	38
3.1 Introduction.....	40
3.2 Materials and methods.....	43
3.2.1 Chemicals and materials.....	43
3.2.2 Characterization of membranes	43
3.2.2.1 Scanning electron microscopy (SEM)	43

3.2.2.2 Attenuated total reflectance-Fourier transform infrared spectroscopy (ATR-FTIR)	44
3.2.2.3 X-ray photoelectron spectroscopy (XPS)	44
3.2.2.4 Contact angle	44
3.2.2.5 Zeta potential	45
3.2.2.6 Time-of-flight secondary ion mass spectrometry (ToF-SIMS)	45
3.2.3 Permeation experiments of membrane soaked in acid	45
3.2.4 Computational calculation methods	46
3.2.4.1 Calculation details	46
3.2.4.2 Model systems	47
3.2.4.3 Out-of-plane deformation and energy calculations	47
3.3 Results and discussion	49
3.3.1 Characterization of membrane soaked in acid	49
3.3.1.1 Effect of sulfuric acid on morphology (SEM)	49
3.3.1.2 Chemical surface property change of polyamide NF membrane by sulfuric acid	50
3.3.1.3 Effect of sulfuric acid on hydrophilicity and surface charge of polyamide NF membranes	57
3.3.2 Permeation of the virgin and hydrolyzed membranes	60
3.3.3 Computational analysis to interpret degradation of NE70 and NE90	62
3.4 Conclusions	66
IV. Chapter 4. Investigation of degradation by sulfuric acid and hydrogen halides on full-aromatic polyamide NF membrane in terms of surface/permeability properties	67
4.1 Introduction	69
4.2 Materials and methods	74
4.2.1 Chemicals and materials	74
4.2.2 Membrane degradation protocol	74
4.2.3 Characterization of membranes	75
4.2.3.1 Scanning electron microscopy (SEM)	75
4.2.3.2 Attenuated total reflectance-Fourier transform infrared spectroscopy (ATR-FTIR)	75
4.2.3.3 X-ray photoelectron spectroscopy (XPS)	75
4.2.3.4 Contact angle	76
4.2.3.5 Zeta potential	76
4.2.4 Filtration tests	76

4.3 Results and discussion-----	78
4.3.1 Characterizations of degraded membranes -----	78
4.3.1.1 Effect of degradation by acid on surface morphology (SEM)-----	78
4.3.1.2 Effect of degradation by acid on change of membrane surface's chemical bond and atomic percentages (ATR-FTIR and XPS)-----	79
4.3.1.3 Effect of degradation by acid on change of membrane surface's hydrophilicity and surface charge (contact angle and zeta potential)-----	81
4.3.2 Effect of degradation by sulfuric acid (pH 0 to 2) on permeability properties	83
4.3.3 Effect of degradation by hydrogen halides (pH 0) on permeability properties	87
4.4 Conclusions-----	90
V. Chapter 5. Acid-catalyzed hydrolysis of semi-aromatic polyamide NF membrane and its application to water softening and antibiotics enrichment-----	91
5.1 Introduction-----	93
5.2 Materials and methods-----	96
5.2.1 Chemicals and materials-----	96
5.2.2 Characterization of membranes -----	97
5.2.2.1 ATR-FTIR and SEM -----	97
5.2.2.2 Contact angle and zeta potential-----	97
5.2.2.3 Molecular weight cut off (MWCO) and pore size of membranes -----	98
5.2.3 Filtration tests -----	98
5.2.4 Ideal selectivity and mixture selectivity-----	99
5.2.5 Antibiotics separation and enrichment -----	100
5.3 Results and discussion-----	101
5.3.1 Characterization of virgin and post-treated membrane-----	101
5.3.1.1. Effect of post-treatment on chemical structure of membrane and surface morphology-----	101
5.3.1.2 Effect of post-treatment on permeability and salt rejection-----	103
5.3.1.3 Effect of post-treatment on hydrophilicity and surface charge (Contact angle and zeta potential)-----	105
5.3.2 Application of post-treated membrane to water softening-----	107
5.3.3 Application of post-treated membrane in enrichment of antibiotics-----	113
5.4 Conclusions-----	121
VI. Chapter 6. Summary and conclusions -----	122
References -----	125

LIST OF FIGURES

Figure 1.1	The reaction scheme and procedure most commonly used for TFC NF membranes -	2
Figure 1.2	Schematic diagram of research scope -----	5
Figure 2.1	Schematic diagram of (a) cross flow filtration and (b) dead-end filtration -----	11
Figure 2.2	The three main Lewis structure of amide group using resonance model -----	12
Figure 2.3	Schematization for twist angle (τ) -----	12
Figure 2.4	Schematic illustration of a TFC membrane. A crosslinked PA selective (active) layer is supported on a porous PSf membrane cast on a polyester fabric-----	13
Figure 2.5	Chemical structure of polysulfone -----	13
Figure 2.6	(A) Schematic description of the process during interfacial polymerization. Reactant A (initially dissolved in the aqueous phase, piperazine or MPD in this case) and reactant B (dissolved in the organic phase, TMC in this case) diffuses toward each other and reacts to form polymer film C (PA in this case). (B) The TEM image shows the structure of ridge and valley by a PA layer. The boundary between the dark parts (right of the micrograph) and bright parts (left of the micrograph) of the film represents the densely cross-linked active layer. The black spot at the bottom of the micrograph shows part of the film-supporting structure-----	14
Figure 2.7	AFM images of different commercial PA membranes' active layers. (a) LE, (b) SW30HR, (c) HL, (d) NTR729HF, (e) DK and (f) SG. (a) and (b) were made from MPD and TMC. Others were fabricated using piperazine and TMC-----	16
Figure 2.8	SEM surface (a) and cross-sectional (b-d) images of polymerizable bi-continuous microemulsion membrane with magnification from 10k to 40k -----	19
Figure 2.9	Working principle of the SEM using schematic illustration -----	19
Figure 2.10	Schematic illustration related the horizontal ATR accessory and formula to calculate penetration depth -----	21
Figure 2.11	Schematic illustration for the XPS process, which shows photoionization of an atom from a 1s electron -----	22
Figure 2.12	Example of XPS survey spectrum from tin (Sn), which shows multiplet splitting peaks in p and d orbitals -----	23
Figure 2.13	Schematic diagram of the XPS instrumentation-----	24
Figure 2.14	The method related measurement of contact angle (a) sessile drop method, (b) captive bubble method, respectively-----	26

Figure 2.15 Schematic illustration for charge spreading of the ionic species which near to the membrane surface (the electrical double layer) and the resultant zeta potential with increasing distance from the membrane surface----- 28

Figure 2.16 Schematic representation of a collision event that can lead to the formation of liberated SI capable of being captured in a detector. Primary ion (red) impacts upon sample surface (grey), thereby transferring energy to the sample, which is then distributed through different atoms (grey lines). This process can lead to the ejection of SI from close to the surface (green), which is then possible to observe with an analyzer ---- 30

Figure 2.17 Total processes to analyze mass spectra of sample surface. (a) primary ion beam collimates on sample surface and occurs SIs, (b) extraction of secondary ions, (c) repeated process for specified area, and (d) produced mass spectra using detection of ejected SIs----- 31

Figure 2.18 Schematic illustration of ToF analysis ----- 32

Figure 2.19 Schematic diagram of dual beam ToF-SIMS equipment. And, the SIs are ejected from surface of sample by a primary ion gun. Ejected SIs are collected by the flight tube, and subsequently detected at a microchannel plate. Mass spectra to analyze chemical information on the surface of sample can be measured by depending on instrumental operation mode----- 32

Figure 2.20 Reaction pathways of the piperazine-amide hydrolysis reaction under acidic conditions initiated from (a) O-protonation and (b) N-protonation ----- 33

Figure 2.21 Reaction pathways of polyacrylamide polymer under acid-catalyzed hydrolysis initiated (a) O-protonation and (b) N-protonation with combining second and third parts as explained in Fig. 2.20 ----- 34

Figure 2.22 Salt rejection of the full-aromatic virgin (■) and modified (coated) (▲) membranes with increasing filtration times until 2 months with aqueous acidic solution containing 0.5 M HCl and 2,000 ppm NaCl. The operating condition is 1.5 MPa pressure and room temperature ----- 35

Figure 2.23 Copper rejections of NF membranes (BPT-NF-2, BPT-NF-1, and Desal KH as acid-resistant NF membranes with Desal-5 DK and NF 270 as semi-aromatic PA membranes) during 2 months' filtration times. Feed solution contains 8 wt% H₂SO₄ and 25g/L CuSO₄. Operating pressure and temperature are 30 bar and 40°C, respectively----- 36

Figure 3.1 Surface morphology observed by SEM for NF membranes versus exposed time in aqueous acid solution----- 49

Figure 3.2 ATR-FTIR spectra of virgin and acid hydrolyzed membranes: (a) NE40, (b) NE70, and (c) NE90 NF polyamide membrane from 1000 cm⁻¹ to 4000 cm⁻¹. Absorbance was

normalized to compare intensity for investigation of effect of acid solution on NF membranes-----	51
Figure 3.3 XPS spectra of (a) NE40, (b) NE70, and (c) NE90 NF polyamide membrane with increasing acid-soaking time-----	52
Figure 3.4 The ToF-SIMS spectra of virgin NE70 and NE90 membranes, hydrolyzed NE70 for 7 Days and hydrolyzed NE90 for 63 Days-----	56
Figure 3.5 Comparison of measured surface contact angles of NF membranes along with increasing acid-soaking time-----	58
Figure 3.6 Zeta potential of the (a) NE70 virgin and NE70 7 Days, and (b) NE90 virgin and NE90 63 Days-----	59
Figure 3.7 Permeation properties (water flux and rejection) of NF membranes with increasing acid-soaking time (tested at 75 psi, using 2,000 ppm NaCl or MgSO ₄ single solution)- -----	60
Figure 3.8 (a) Change of Gibbs free energy (ΔG at T = 25 °C) diagram of the degradation reactions of NE70 and NE90. The colored values at transition states (TS 1 and TS 2) in the graph indicate the energy barrier for the reaction, and the colored values at Step 3 and Step 4 indicate the relative Gibbs free energy of the product to the reactant. O and N in parentheses indicate the protonated sites. (b) Schematic reaction mechanism. Red-dotted circles indicate the protonated sites-----	63
Figure 3.9 From top to bottom, monomer, dimer and trimer of NE70 and NE90 are presented, respectively. Blue dashed line indicates intermolecular hydrogen bonding (HB). Carbon, hydrogen, oxygen and nitrogen atoms are colored gray, white, red, and blue, respectively-----	64
Figure 3.10 The monomer structures of NE70 (a) and NE90 (b). Out-of-plane deformations (τ_D) values are calculated from the sets of atoms as follows; For NE70, τ_D : C1-N-C3-O, C2-N-C3-C4 and for NE90, τ_D : C1-N-C3-O, H-N-C3-C4-----	65
Figure 3.11 Out-of-plane deformations (τ_D) profiles of NE70 (a) and those of NE90 (b). O and N indicate the N protonated and O protonated structures of NE70 and NE90, respectively. Note that τ_D 's of dimer and trimer were calculated by averaging the values of each protonated site. (c) The correlation between activation energy at the rate determining step (<i>i.e.</i> , Step 2 to Step 3 in Fig. 3.8 (a)) and τ_D at Step 2 (Fig. 3.8 (a)). The dotted line indicates a linear trend line. O and N in parenthesis indicate the protonated sites --	65
Figure 4.1 Schematic description of possible pathway of halogenated polyamide due to halogenation generated by hydrogen halides and oxygen-----	73

Figure 4.2	SEM images of the surface of the active layer of the NE90 virgin (a) and degraded membranes soaked in pH 0 (b) H ₂ SO ₄ (c) HCl, (d) HBr, and (e) HI until 63 Days for exposure times -----	78
Figure 4.3	ATR-FTIR spectra of the NE90 virgin and degraded membranes soaked in pH 0 (a) H ₂ SO ₄ (b) HCl, (c) HBr, and (d) HI until 63 Days for exposure times -----	80
Figure 4.4	Atomic percent of halogen in the degraded membranes after exposure to pH 0 HCl, HBr, and HI until 63 Days-----	80
Figure 4.5	Zeta potential of the NE90 virgin and degraded membranes soaked in pH 0 H ₂ SO ₄ , HCl, HBr, and HI until 63 Days for exposure times -----	82
Figure 4.6	The effect of compaction on membrane flux and salt rejection of the NE90 virgin membrane kept in Milli-Q water (tested at 75 psi, using Milli-Q, 2,000 ppm NaCl and MgSO ₄ single electrolyte solution) -----	83
Figure 4.7	The effect of sulfuric acid's pH (pH 0-2) and exposure time on membrane flux and salt rejection of the NE90 membrane (tested at 75 psi, using Milli-Q, 2,000 ppm NaCl and MgSO ₄ single electrolyte solution) -----	85
Figure 4.8	Schematic diagram of possible mechanisms to change membrane performance due to different pH condition of sulfuric acid -----	86
Figure 4.9	The effect of halogen halide (pH 0) and exposure time on membrane flux and salt rejection of the NE90 membrane (tested at 75 psi, using Milli-Q, 2,000 ppm NaCl and MgSO ₄ single electrolyte solution) -----	88
Figure 4.10	Schematic diagram of possible mechanisms to change membrane performance due to different acidic condition -----	89
Figure 5.1	Schematic diagram of (a) piperazine-amide chemical structure and (b) acid-catalyzed hydrolysis reaction of the amide group -----	95
Figure 5.2	ATR-FTIR spectra of semi-aromatic NE70 virgin and post-treated polyamide membranes under (a) pH 0, (b) pH 0.25, (c) pH 0.5, (d) pH 0.75, (e) pH 1, and (f) pH 2 conditions with characteristic bands from 1000 cm ⁻¹ to 4000 cm ⁻¹ related to the membrane polyamide active layer and polysulfone support layer. Absorbance peaks at wavenumbers 1634 and 1587/1488 cm ⁻¹ are attributed to the amide (I) band of semi-aromatic polyamide and polysulfone layer, respectively -----	102
Figure 5.3	Surface morphology of virgin NE70 (a) and post-treated membranes from (b) to (k) measured by SEM in terms of strength of acid and post-treatment time -----	103
Figure 5.4	Permeation properties (water flux and rejection) of virgin and post-treated membranes with increasing strength of acid and post-treatment time (tested at 75 psi, using 2,000 ppm NaCl or MgSO ₄ single solution) -----	104

Figure 5.5 Zeta potential of the NE70 virgin and post-treated membrane by pH 0.25 acidic solution for 7, 14, and 28 days----- 106

Figure 5.6 Ideal selectivity of NE70 virgin and post-treated membranes under acidic solution ranging from pH 0 to 2 with increasing post-treatment time ----- 108

Figure 5.7 ATR-FTIR's peak intensity ratio of representative polysulfone support layer (1587 cm^{-1}) to polyamide layer (1634 cm^{-1}) for comparison of degrees of ideal selectivity with increasing acid concentration or exposure time to acidic solution----- 109

Figure 5.8 (a) PEGs and (b) Sugars rejection curves of NE70 virgin and post-treated membranes in pH 0.25 acidic solution for 7, 14, and 28 days for MWCO measurement (tested with 1000 ppm PEG aqueous solution and 200 ppm sugars aqueous solution under 10 bar)-
----- 113

Figure 5.9 Schematic illustration of PEG and sugar's rejection in (a) larger and (b) smaller pore case----- 115

Figure 5.10 Comparison of NE70 virgin and post-treated membranes in pH 0.25 acidic solution for 7 and 14 days in terms of erythromycin (ERY) enrichment during the feed solution permeated from 4L to 1L (a) water flux, (b) ERY/NaCl rejection, (c) concentration of NaCl in feed, and (d) concentration of ERY in feed (tested at 150 psi, using mixture of 100 ppm ERY/ 10 g L^{-1} NaCl at pH 8.8 because chemicals were used without further purification)----- 118

Figure 5.11 Comparison of NE70 virgin and post-treated membrane by pH 0.25 acidic solution for 7 and 14 days in terms of vancomycin (Van) enrichment during the feed solution permeated from 4L to 1L (a) water flux, (b) Van/NaCl rejection, (c) concentration of NaCl in feed, and (d) concentration of Van in feed. (tested at 150 psi, using mixture of 100 ppm Van/ 10 g L^{-1} NaCl at pH 4.7 because chemicals were used without further purification)----- 119

LIST OF TABLES

Table 2.1	Categorization of membranes (bold type will be mainly discussed in this work) -----	8
Table 2.2	Physical/chemical characterization of membranes using various analytical tools (bold type will be mainly discussed in this work)-----	17
Table 2.3	Example of the common ATR crystals and their properties -----	21
Table 2.4	Permeability after exposure to various acidic conditions during 0 to 4 months for NF-45 membranes-----	37
Table 3.1	Relative atomic concentrations (C, N, O, and S) and composition ratios of polyamide NF membranes (virgin versus 63 Days soaking in acid) -----	53
Table 3.2	List of fragments which were detected by ToF-SIMS from the outermost surface of virgin and hydrolyzed membranes of NE70 and NE90 in negative (I) and positive mode (II and III)-----	54
Table 3.3	Permeation properties (water flux and rejection) of polysulfone support layer UF membranes with increasing acid-soaking time (tested at 75 psi, using 2,000 ppm NaCl or MgSO ₄ single solution)-----	61
Table 4.1	Chemical reaction for generating halogen gases by oxidation of hydrogen halides and gibbs energy in standard state (for one mole at 298K and 1 bar) -----	72
Table 4.2	Example of calculation to calculate normalized flux ² -----	77
Table 4.3	Contact angle of the NE90 polyamide membranes soaked in pH 0 H ₂ SO ₄ , HCl, HBr, and HI until 63 Days for exposure times -----	82
Table 5.1	Specifications of NE 40 and 70 membranes from supplier -----	96
Table 5.2	Contact angles of NE70 virgin and post-treated membranes by pH 0.25 acidic solution for 7, 14, and 28 days using Milli-Q water-----	105
Table 5.3	Permeation properties (water flux, rejection, and ideal selectivity) of NE40 virgin and post-treated membranes with increasing post-treatment time using 15 wt% sulfuric acid (tested at 75 psi, using 2,000 ppm NaCl or MgSO ₄ single solution) - -----	108
Table 5.4	Water flux, salt rejection, and ideal selectivity of NE70 virgin and optimized post-treatment membranes using single feed solution-----	111
Table 5.5	Water flux, salt rejection, and mixture selectivity of NE70 virgin and post-treated membranes using a NaCl/MgSO ₄ mixture solution in neutral and acidic conditions ---- -----	112
Table 5.6	Pore radius of NE70 virgin and post-treated membranes by pH 0.25 acidic solution for 7, 14, and 28 days estimated from neutral organic compound's rejection -----	114

Table 5.7	Relative enrichment ratio of salt to antibiotic ($\Delta C_{antibiotic}^{salt}$) and flux reduction ratio using NE70 virgin and post-treated membranes-----	116
Table 5.8	Comparison of the performance of NE70 control and optimized membranes in the separation of antibiotics with other published papers -----	120

Appendix A. Nomenclature and abbreviation

α_B^A	Membrane selectivity between A and B (-)
γ_{as}	Free energies between air and solid (N/m)
γ_{aw}	Free energies between air and water (N/m)
γ_{sw}	Free energies between solid and water (N/m)
$\Delta C_{antibiotic}^{salt}$	The amount of salt enrichment when unit amount of antibiotics is recovered (-)
ΔG	Changes of Gibbs free energy (Kcal/mol)
ϵ_0	Permittivity of the and vacuum (C/V/m)
ϵ_r	Permittivity of the liquid medium (C/V/m)
ζ	Zeta potential measured by electrophoresis method (mV)
η	Viscosity of liquid medium (psi·hr),
θ	The incidence angle (°)
θ_c	Contact angle (°)
τ_D	Twist angle (°)
J_w	Permeate water flux (L/m ² /hr)
L	The flight tube's length (m)
$\log P$	Partition coefficient (-)
M	Molarity (mol/L)
n_1	Refractive index of ATR crystal (-)
n_2	Refractive index of sample (-)

n_{21}	The ratio of n_2 to n_1 (-)
R	Salt rejection (%)
r_p	The radius of membrane pore (m)
r_s	The radius of solute (m)
t	Time-of-flight of the secondary ions (hr)
U	The monitoring particle's electrophoretic mobility ($m^2/V/hr$),
v	The accelerating potential (V)
W	The wavenumber (1/m)
AEPPS	N-AminoEthylPiperazine Propane Sulfonate
ATR-FTIR	Attenuated Total Reflectance-Fourier Transform InfraRed spectroscopy
CSA	CamphorSulfonic Acid
CTAB	CetylTrimethyl Ammonium Bromide
DFT	Density Functional Theory
ERY	ERYthromycin
FE-SEM	Field Emission-Scanning Electron Microscopy
HB	Hydrogen Bonding
IC	Ion Chromatography
ICP-MS	Inductively Coupled Plasma-Mass Spectrometry
IEP	IsoElectric Point
IP	Interfacial Polymerization
MF	MicroFiltration
MPD	M-PhenyleneDiamine

MWCO	Molecular Weight Cut Off
NF	NanoFiltration
PIP	PIPazine
PA	PolyAmide
PSf	PolySulfone
PTFE	PolyTetraFluoroEthylene
RDS	Rate Determining Step
RO	Reverse Osmosis
SEM	Scanning Electron Microscopy
SIs	Secondary Ions
TEA	TrimEthylAmine
TEM	Transmittance Electron Microscopy
TFC	Thin Film Composite
TMC	TriMesoyl Chloride
ToF-SIMS	Time of Flight-Secondary Ion Mass Spectrometry
TS	Transition States
UF	UltraFiltration
Van	Vancomycin
XPS	X-ray Photoelectron Spectroscopy

Introduction

1.1 Problem statement and significance

Water is important resource for humans and many places on the earth, and it is needed to solve fresh water shortage due to water pollution by industrial and farming activities. There are various methods that have been researched and applied to treat water such as chemical process using OH radical oxidation [1], biological process by aeration [2], and physical process through membrane technology. Above all, membrane technology is one of the promising methods to obtain drinking water by desalination/treatment of sea/brackish/waste water [3] due to lower operation and maintenance cost as well as less land space requirement, resulting from improvements of the membrane technology [4]. Membrane processes can be categorized by the pore size. Nanofiltration (NF) membrane, which has 0.5 to 2.0 nm of pore diameters, has been rapidly attracted during last decades because of its high rejection for divalent salts or organic molecules ($M_w \sim 200$ to 1000 g mol^{-1}) under low operating pressure [5]. These high rejection can be explained by both solution diffusion mechanism and steric/electrostatic sieving mechanism [6]. Currently, commercial NF polyamide (PA) thin-film composite (TFC) membranes have been widely fabricated by interfacial polymerization method using piperazine (aliphatic amine monomer) or m-phenylenediamine (MPD, aromatic amine monomer) reacting with trimesoyl chloride (TMC, acyl chloride monomer) [7, 8] as shown in Fig. 1.1. These IP technique is a good method to obtain TFC NF membranes, because the thin/dense PA active layer makes high water flux and salt rejection under low operating pressure, and the membrane performance can be optimized by numerous fabrication factors such as monomer/additives concentrations, reaction times, and post-treatment time/temperature (*e.g.*, curing process) [9].

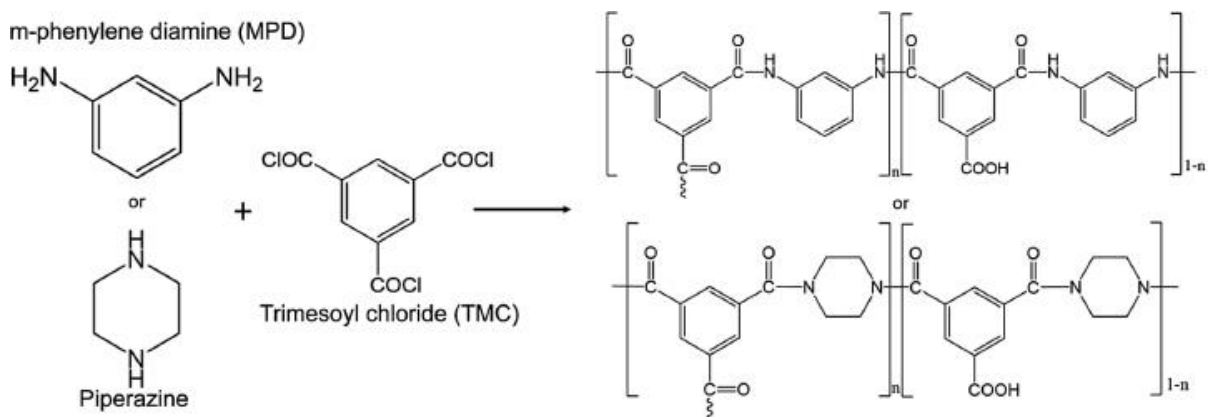


Figure 1.1 The reaction scheme and procedure most commonly used for TFC NF membranes [10].

Several application using NF membrane in terms of industrial effluent has been studied for removing or recycling of abundant acids like hydrochloric acid, sulfuric acid, fluoroboric acid, nitric acid, boric acid, and other valuable metals [11]. Potentially applicable examples are summarized as follows: purification of phosphoric and nitric acids [12, 13], purification of diluted acidic streams in dairy cleaning-in-place processes (CIP) [14], treatment of effluents in the pulp and paper industry [15], recovery of phosphorus from sewage sludge [16, 17], the removal of metals (*e.g.*, copper or gold) with a high sulfuric acid concentration [18], removal of sulfate ions from industrial effluents in the mining and metal industry [19], and the treatment of wastewater containing HCl, HBr and HI from etching process for semiconductors [20-22]. These acidic industrial effluents which contains low pH condition can be potentially removed and recycled through NF process [23], therefore, there needs NF membranes to tolerate low pH condition during the application. However, high performance commercial NF PA TFC membranes fabricated by piperazine/MPD and TMC limits to use application in industrial effluent, because NF membrane manufacturers limits to pH in the range of 2 - 11 by relatively low chemical stability [24]. Therefore, consideration for degradation of semi and full-aromatic PA membranes by acid is needed to apply above processes which have less than pH 2 acidic condition.

Recently, several studies have been conducted to investigate the change of PA membranes' permeability properties due to degradation by acidic conditions. Liu et al. [25] studied effect of 0.5 M HCl on lab-made full-aromatic PA membrane, and it was hydrolyzed after 30 Days filtration, resulting to increase permeations of water and salt. Tanninen et al. [26] performed acid-stability of semi-aromatic PA membranes (The Desal-5 DK and the NF 270 membrane) by filtration test using 8 wt% H₂SO₄ at 40°C for 2 months, and salt rejection was not maintained due to their insufficient acid-resistance during operation. These semi-aromatic PA membranes were also analyzed in the range of pH 1 to 13 by adjusting HCl and NaOH, and the results were that effect of membrane permeability at acidic condition (pH 1) was relatively lower than alkaline condition (pH 13) [27]. Another semi-aromatic PA membrane (the NF-45 membrane) showed acid-catalyzed hydrolysis, resulting from severely decreased sucrose retention when the membrane exposed to 20 wt% H₂SO₄ at 80°C for only 1 month [18]. Evidence for degradation of PA membranes by acid has been suggested by severely increased water flux and decreased salt/target rejection.

The previous studies were mainly investigated to effect of acid on PA membranes in terms of permeability, however, both changes of physico-chemical properties and degradation mechanism of semi/full-aromatic membranes after exposure to acidic conditions have not been systematically discussed to date. Therefore, an in-depth research needs to explain effect of acidic conditions on physical and chemical properties of PA membranes using various analytical tools and computational calculation methods.

1.2 Objectives of this work

The overall objectives of this work is to systematically investigate the effect of the acidic conditions on semi/full-aromatic PA membranes in terms of changes of physico-chemical properties, and to suggest mechanism to explain changed the properties using various analytical tools and computational calculation methods. The more specific objective is as follows:

1. To systematically assess changes of physico-chemical properties of semi/full-aromatic PA membranes after exposure to various solution pH and acids.
2. To identify and suggest the mechanism of changed surface characterization and permeability of semi/full-aromatic PA membranes due to acidic degradation.
3. To utilize degradation phenomenon on semi-aromatic PA membranes in the view of practical applications.

1.3 Scope of this work

This study consists of (1) characterization of semi/full-aromatic PA membranes, (2) acidic degradation experiments, (3) investigation of acidic degradation on semi/full-aromatic PA membranes in terms of physico-chemical properties, (4) explanation of the acidic degradation mechanism, and (5) utilization of acidic degradation on semi-aromatic PA membranes in the view of practical applications.

The scope of this work is described in Fig 1.2. Commercially available NF PA membranes, *Toray Chemical Korea*© piperazine (PIP)-based NE40/70 membranes and m-phenylene diamine (MPD)-based NE90 membrane, were systematically investigated to explain effect of acidic degradation on physico-chemical properties of PA membranes. A series of acidic degradation experiments were performed under 2 different conditions which are in the range of H₂SO₄ pH 0 to 2, and various acids containing H₂SO₄ and hydrogen halides (HCl, HBr, and HI). Physico-chemical properties of the membranes were studied before and after exposure to acidic conditions using various analytical tools: Scanning Electron Microscopy (SEM), Attenuated Total Reflectance-Fourier Transform Infrared spectroscopy (ATR-FTIR), X-ray photoelectron spectroscopy (XPS), Time-of-Flight Secondary Ion Mass Spectrometry (ToF-SIMS), contact angle analyzer, electrophoretic light scattering spectrophotometer, and filtration tests. Density functional theory (DFT) calculation was also conducted

to reveal the different acid-resistance between the piperazine-based and MPD-based polyamide membranes in terms of reaction energies and twist angles. Acidic degradation mechanism on PA membranes were investigated using the experimental/DFT calculation analyses, and comparison of the physico-chemical properties between virgin and degraded membranes.

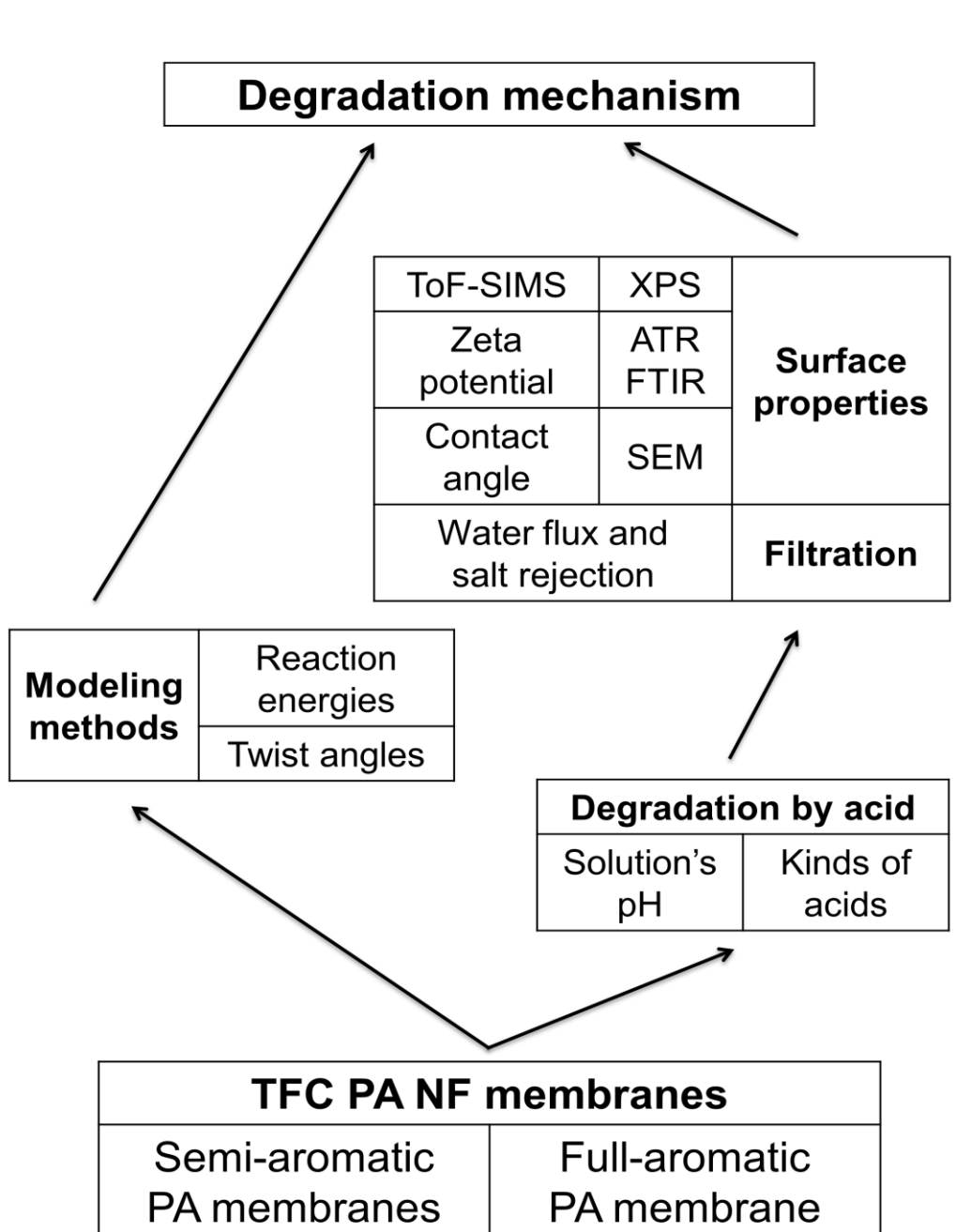


Figure 1.2 Schematic diagram of research scope.

1.4 Outline of this work

This thesis consists of six chapters. Chapter 1, 2 and 6 are the introduction, background and related research, and summary and conclusions, respectively. Research contents and explanation are presented in Chapter 3, 4, and 5. Chapter 5 was already published in Chemical Engineering Journal (Chemical Engineering Journal 332 (2018) 419–430).

Chapter 3 studied that two commercially available NF polyamide TFC membranes fabricated by two amine monomers (piperazine or MPD) with acyl chloride (TMC) as representative polyamide NF membranes. The effect of acidic aqueous solution (15wt% sulfuric acid) on the membrane's physico-chemical properties were systemically investigated.

Chapter 4 conducted that systematical physical and chemical characterization to explain the effect of degradation by sulfuric acid in the range of pH 0 to 2 as well as hydrogen halides at pH 0 on MPD-based full-aromatic membrane. The importance of halogenation caused by oxidation of hydrogen halides on full-aromatic membrane was discussed in detail.

Chapter 5 investigated surface characterization and permeability of a commercial NF semi-aromatic polyamide TFC membrane during the post-treatment of the membrane via acid-catalyzed hydrolysis under various acidic conditions. The hydrolysis condition was optimized based on the characterization study, and the membrane was modified for use in water softening and antibiotics enrichment processes.

Last part is the appendix which gives list of abbreviations and symbols used in this thesis, then references subsequently followed.

Background and literature review

Chapter 2

This chapter introduces background and related research on classification of membrane, pressure-driven process, chemical properties of amide bond, basic principles of analytical tools, acidic degradation of amide group and PA membranes.

2.1 Classification of membrane

The important factor of membrane process depends on membrane. Membrane exists naturally (biological membrane) or made by synthesis using chemical compounds (synthetic membrane). These membranes play the role as a barrier between two phases. Synthetic membrane can be divided by pore size, structure, and materials. A brief summary of each membrane is as follows [28, 29] (Table 2.1).

Table 2.1 Categorization of membranes (bold type will be mainly discussed in this work).

Biological membrane	Living membrane (ex. Living cell membranes where the energy is provided by ATP)			
	Non-living membrane (ex. Liposomes and vesicles from phospholipids)			
Synthetic membrane	Pore size	Microfiltration: 0.05 – 5 μm		Separation principle: size exclusion
		Ultrafiltration: 1 – 100 nm		
		Nanofiltration: ~ 1 – 10 nm		Separation principle: solution-diffusion
		Reverse osmosis: < 2 nm		
	Structure	Symmetric membrane		(Cylindrical) porous membrane
				Nonporous (homogeneous) membrane
		Asymmetric membrane:		(Integrally) asymmetric membranes
				Thin film composite membranes
	Material	Organic	Liquid membrane (ex. Carrier-mediated transport)	
			Synthetic polymeric membrane	Relatively Hydrophilic Cellulose esters Polycarbonate (PC)

			Polysulfone/poly(ether sulfone) (PSf/PES) Polyimide/poly(ether imide) (PI/PEI) Polyamide (PA) Polyetheretherketone (PEEK)
			Relatively Hydrophobic Polytetrafluoroethylene (PTFE, Teflon) Poly(vinylidene fluoride) (PVDF) Polypropylene (PP) Polyethylene (PE) Polysulfone (PSf)
		Inorganic	Ceramic membrane: alumina (Al ₂ O ₃), zirconia (ZrO ₂), titania (TiO ₂) silicium carbide (SiC)
			Metal membrane: stainless steel, palladium, tungsten, silver

2.2 Pressure-driven process

The principle of membrane process is allowing pure water to transport through the membrane but exclude most of the solutes or macromolecules in the solution. Pressure-driven membranes can be categorized by their physical properties in water treatment processes, and they are consisted of microfiltration (MF), ultrafiltration (UF), nanofiltration (NF), reverse osmosis (RO) processes along the pore size and applied pressure. A detailed explanation of each process is as follows: [29]

- 1) **Microfiltration:** a pressure-driven process which operates at low applied pressure (0.1 – 2 bar) to filtrate large particles (with pore size from 50nm to 5 μm), proteins, and bacteria (size > 0.1 μm). Separation mechanism is size exclusion. MF is mostly applied in analytical applications, sterilization for food, pharmaceuticals, ultrapure water for semiconductors, clarification for beverages, cell harvesting membrane bioreactor, and water treatment.

- 2) **Ultrafiltration:** a pressure-driven process (1 – 10 bar) of which membrane pore size (1 – 100 nm) is between MF membrane and NF membrane to filtrate finer particles and molecules of molecular weight above about 10,000. Separation mechanism is also size exclusion. Main application of UF is separating macromolecules and colloids from a solution, such as dairy, food, metallurgy for oil-water emulsions and electropaint recovery, textile, pharmaceutical for enzymes, antibiotics and pyrogens, automotive for electropaint, and water treatment.
- 3) **Nanofiltration:** a pressure-driven process (10 – 25 bar) of which membrane pore size (1 – 10 nm) is between UF membrane and RO membrane to filtrate permeation of low molecular weight (200 - 20,000 daltons) substances. Separation principle of NF is solution-diffusion. NF is applied to separate desalination of brackish water, removal of micropollutants, water softening, waste water treatment, retention of dyes for textile industry.
- 4) **Reverse osmosis:** a pressure-driven process which operated at 15 – 25 bar for brackish water and 40 – 80 bar for seawater. RO membrane has less than 2 nm pore size. Separation principle of RO is similar with NF, which operates under solution-diffusion mechanism. RO is used to separate single charge ion like sodium, chloride ion in desalination process. Main applications of RO are desalination of brackish and seawater, production of ultrapure water in electronic industry, and concentration of food juice, sugars, and dairy industry.

Flow directions or filtration methods affect a high influence on separation performances during operation. Figure 2.1 shows two types of flow filtration which are (a) cross flow and (b) dead-end filtration. The feed stream is applied tangential direction to the membrane as shown in Fig. 2.1 (a), resulting to minimize membrane fouling and maintain a high water flux and recovery [30]. When the feed solution is applied perpendicular direction to the membrane, it enables rapid separation of target compounds as shown in Fig. 2.1 (b). However, dead-end filtration results in a easily build-up of fouling phenomenon on the membrane surface, resulting to severely decrease water flux [30]. Therefore, NF or RO processes which need high applied pressure are typically operated by cross flow filtration method.

In order to measure water flux (J_w) and salt rejection (R) of membranes, which are one of the main parameters to assess membrane performance, following equation (2.1 and 2.2) has been widely used [29].

$$J_w = \frac{\Delta \text{ weight}}{\Delta \text{ time} \times \text{effective membrane area} \times \text{water density}} \left(\frac{\text{L}}{\text{m}^2\text{h}} \text{ or LMH} \right) \quad (2.1)$$

$$R = \left(1 - \frac{[\text{Salt}]_{\text{permeate}}}{[\text{Salt}]_{\text{feed}}} \right) \times 100 (\%) \quad (2.2)$$

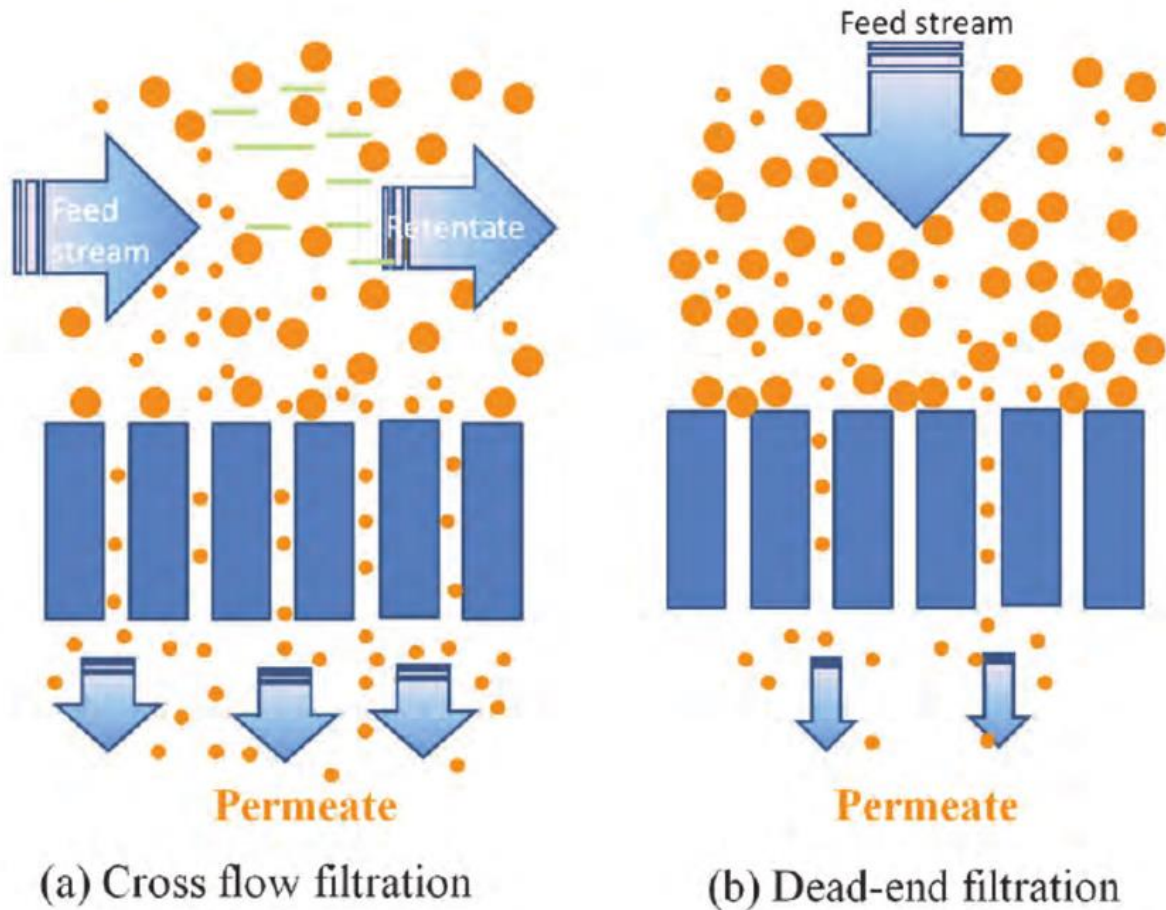


Figure 2.1 Schematic diagram of (a) cross flow filtration and (b) dead-end filtration [30]

2.3 Polyamide (PA) membrane

A supreme membrane condition to apply separation process is that the membrane has high chemical, thermal, and mechanical durability as well as low cost for fabrication. Polyamide structure has been widely used as commercial NF membranes due to its high permeability, selectivity and stability [31].

There has been much research on amide because proteins are consist of amide groups, and they play an important role in biological processes [32]. Amide group means the organic compound which contain -CONH- group. The chemical stability of amide bond comes from inherent three main Lewis resonance structure as described in Fig 2.2. In other words, left and right structure of Fig 2.2 shows sp^3 and sp^2 hybridization of the nitrogen, respectively, resulting to a partial double bond characteristic of the C-N bond. Therefore, these resonance structures explain amide's planarity and their natural stability.

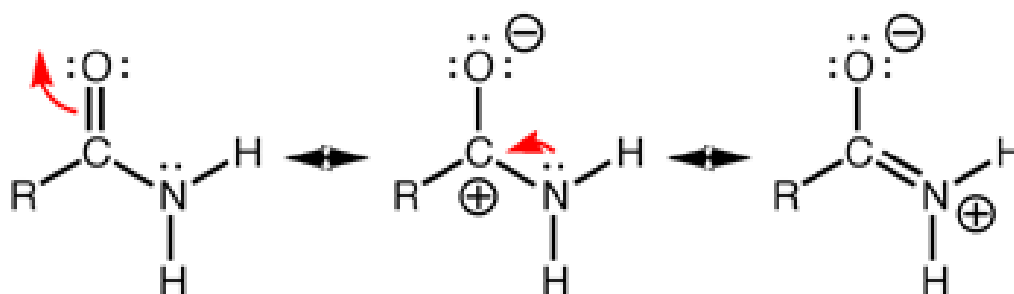


Figure 2.2 The three main Lewis structure of amide group using resonance model [33].

As described above paragraph, amide bond's stability is affected by its partial double bond delocalization between the nitrogen lone pair of amide and the carbonyl π_{CO} bond [34]. These amount of delocalization can be quantitatively calculated by twist angle (τ) as shown in Fig. 2.3, and the angle means between $\text{C}_1\text{-C}_2\text{-O}$ plane and lone pair of nitrogen atom. These twist angle, amount of distortion of C-N amide bond, have been calculated by computational modeling method [35-39]. That is, lower twist angle value is close to planar structure, resulting to increase chemical stability due to higher resonance structure. It is good agreement to previous studies which explain increasing hydrolytic rate of amide bond in acid and base with increasing distortion of C-N bond (twist angle) [34-36, 40].

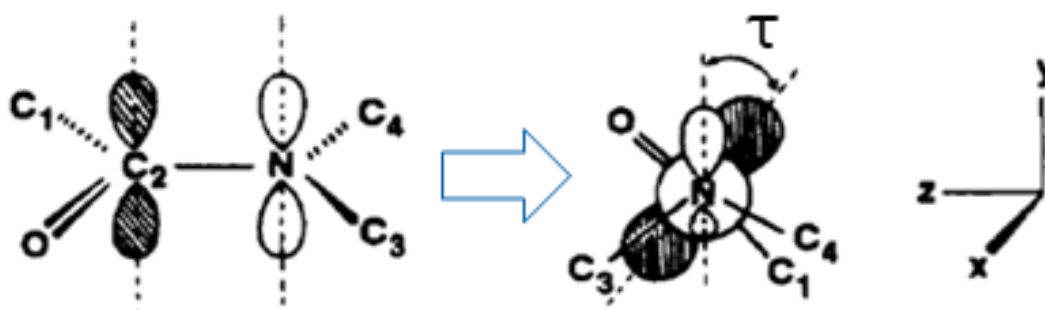


Figure 2.3 Schematization for twist angle (τ) [41].

As a result of its chemical properties of amide bond, PA structure has been broadly utilized in NF membranes. Detail explanation of the PA membrane such as cross-sectional structure, fabrication method, and characterization methods are summarized below section (2.3.1 to 2.3.3).

2.3.1 Cross-sectional structures of TFC PA membrane

An ideal conditions of membrane in the separation process are high water flux and salt rejection in terms of production cost. Therefore, asymmetric TFC membrane which consisted of ultra-thin selective layer and porous support layer have dominated in the NF/RO commercial membrane market from 1980's. General structure of TFC membrane is described in Fig. 2.4, and porous PSf support layer (Fig. 2.5), which has good thermal and chemical stability [42], is fabricated on reinforcing polyester fabric due to mechanical strength.

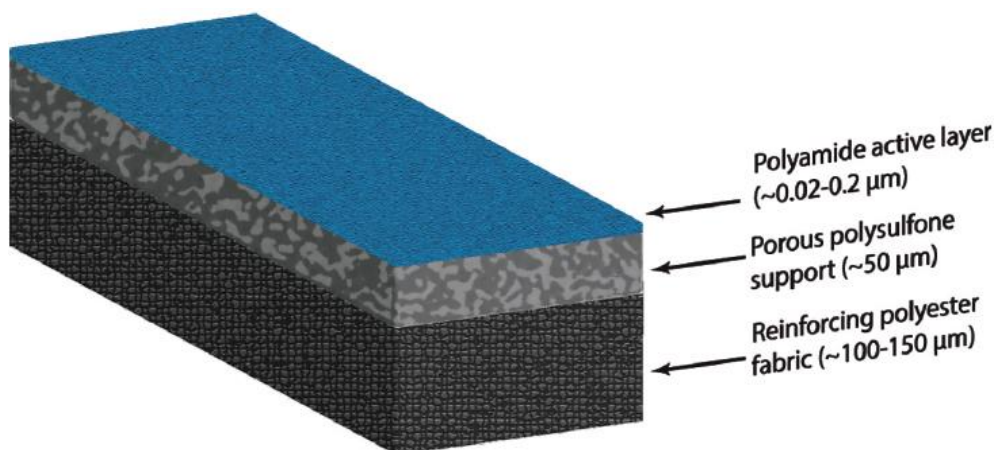


Figure 2.4 Schematic illustration of a TFC membrane. A crosslinked PA selective (active) layer is supported on a porous PSf membrane cast on a polyester fabric [10].

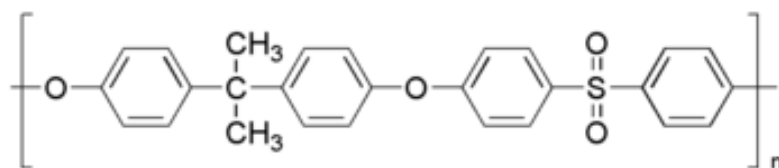


Figure 2.5 Chemical structure of polysulfone.

2.3.2 Interfacial polymerization

Interfacial polymerization (IP) is the most famous method for fabrication of commercial TFC PA membranes, and it has been tremendously developed after firstly suggested by Mogan in 1965 [43]. Interfacial polymerization technique in optimizing independently the properties of active layer and support layer, various kinds of TFC membranes have been widely and successfully developed [43]. The several factors such as solvent type, concentration of monomers, reaction time, and post-treatment conditions can affect the membrane performance by different structural morphology and composition of the selective layer [44]. Most of PA NF membranes have been produced by piperazine (aliphatic amine monomer) or m-phenylenediamine (MPD, aromatic amine monomer) reacting with trimesoyl chloride (TMC, acyl chloride monomer) [7, 8] as already explained in section 1.1, because both polymerization and cross-linking during IP are fast even though low concentration of acyl halide is used [45].

The process of IP is summarized as follows: (1) a porous support membrane is soaked in an aqueous solution which contains amine monomers to saturate porous support membrane before reaction with TMC. (2) excess amine aqueous solution on the surface of support membrane is removed by a rolling machine or air knife for reacting with TMC. (3) the amine saturated support membrane is soaked in a water-immiscible organic solvent solution which contains aromatic acyl halide. (4) when the amine-saturated support membrane is soaked in the aromatic acyl halide solution, a thin and densely cross-linked active layer is fabricated on the interfacial layer between organic phase and aqueous phase during IP. The process of above-mentioned interfacial polymerization is described in Fig 2.6.

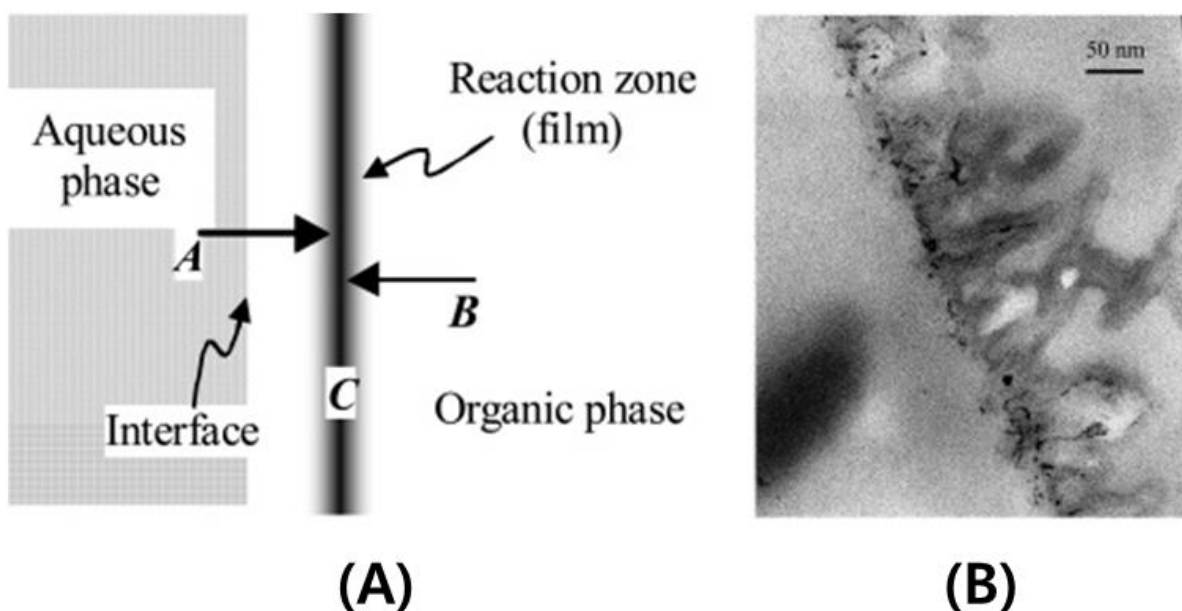


Figure 2.6 (A) Schematic description of the process during interfacial polymerization. Reactant A (initially dissolved in the aqueous phase, piperazine or MPD in this case) and reactant B (dissolved in the organic phase, TMC in this case) diffuses toward each other and reacts to form polymer film C (PA in this case). (B) The TEM image shows the structure of ridge and valley by a PA layer. The boundary between the dark parts (right of the micrograph) and bright parts (left of the micrograph) of the film represents the densely cross-linked active layer. The black spot at the bottom of the micrograph shows part of the film-supporting structure [46].

The chair structure of the piperazine amine molecule in its lowest energy state makes the thin active layer difficult to compact, providing a large free volume inside the active layer and high permeability of water molecules through the thin layer [47]. Meanwhile, the membrane fabricated by MPD and TMC has a very unique surface characteristic which has a ridge and valley structure rather than smooth surface by piperazine amine. Kwak et al. [48] proved that this rough ridge and valley structure increased effective surface area, resulting higher water transport and thus water flux. The reason why formation of ridge and valley structure will be explained followed paragraph based on IP process.

Polyamide film of formation on the support membrane surface is initiated by volcano-like reaction where the amine monomers erupt from surface pores of the support layer during the IP, because the amine monomer continuously can diffuse into organic solvent contrasting the acyl halide unable to diffuse into aqueous solution [49]. After eruption of the amine monomers, the amine monomers also can diffuse sideways continuously, resulting integral polyamide film is formed [49]. As a result, the initial polyamide tufts reaching earlier a high molecular weight than the laterally smooth base film develops into ridges, and the lateral film linking the initial tufts becomes valleys [49]. This ridge and valley structure of the surface appears in full-aromatic PA membrane prepared by MPD and TMC, on the other hand, other TFC membranes fabricated by aliphatic amines (*e.g.*, piperazine) have smoother surface due to relatively low solubility and diffusivity of amine monomer in organic solvent [49]. Figure 2.7 shows structural differences between active layers prepared by semi-aromatic poly(piperazinamide) membrane (Figure 2. 7 (c) to (f)) and MPD/TMC based fully aromatic membrane (Figure 2. 7 (a) and (b)) [50].

Further enhancement of membrane performance has been achieved by addition of effective additives. Amhed et al. [51] investigated the effect of trimethylamine (TEA) added as an acid acceptor during IP, and reported that the TEA can not only prevent protonation of amine monomer, but also keep reactivity of amine monomer, causing enhanced amount of cross-linking and a subsequent increase in salt rejection. The addition of TEA dosed with camphorsulfonic acid (CSA) was also reported to form thinner and smoother surfaces with 30% enhancement of water flux [9]. Mansourpanah et al. [52] studied the additive effect of cationic surfactant on membrane performance and showed that

cetyltrimethyl ammonium bromide (CTAB) increases water flux without loss of salt rejection because of the enlarged free-volume in the active layer.

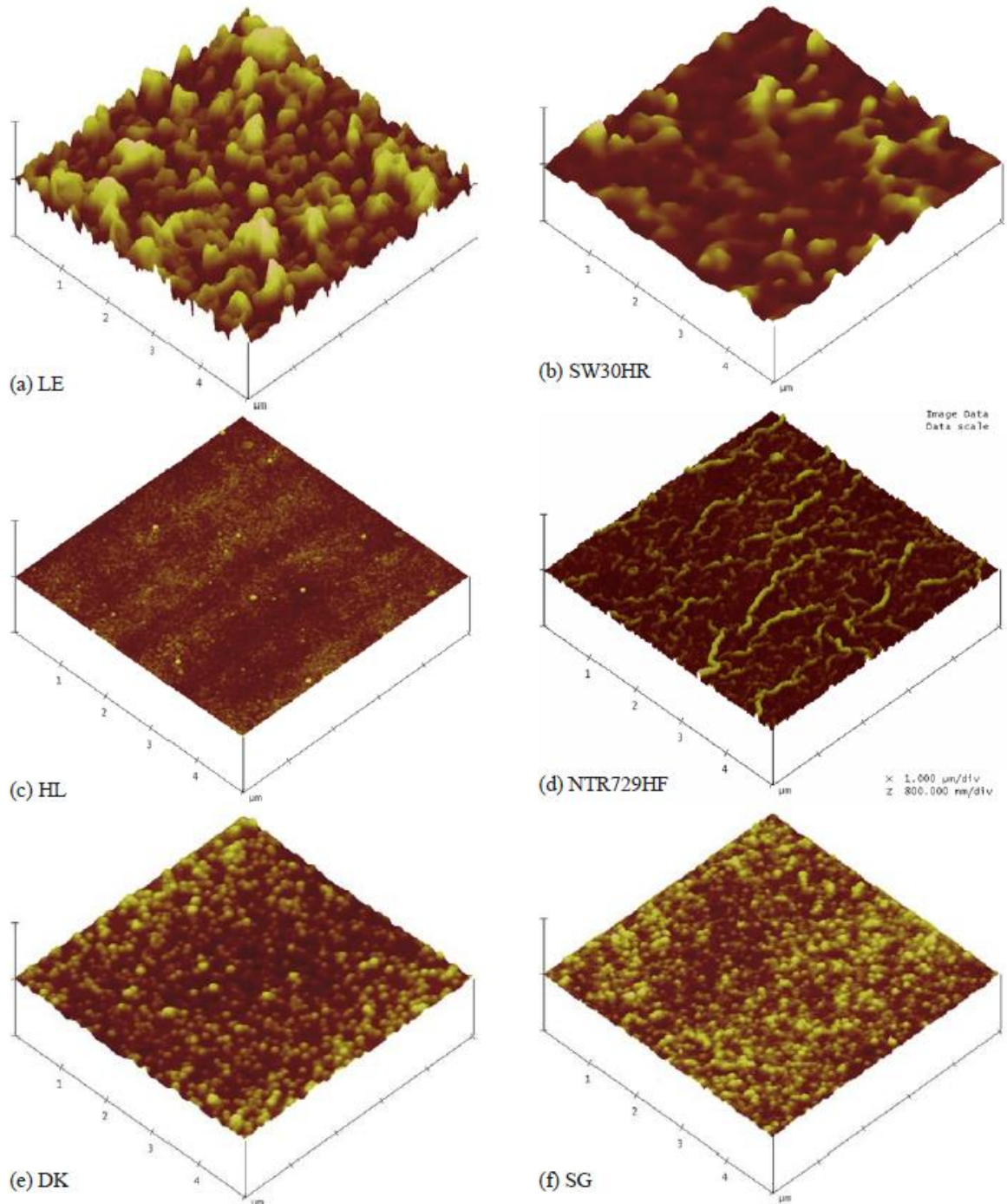


Figure 2.7 AFM images of different commercial PA membranes' active layers. (a) LE, (b) SW30HR, (c) HL, (d) NTR729HF, (e) DK and (f) SG. (a) and (b) were made from MPD and TMC. Others were fabricated using piprazine and TMC [50].

2.3.3 Characterizations of polyamide membrane

Membrane performance (water flux and salt rejection) is directly related with combination of pore size and distribution, thickness, and surface area/hydrophilicity/charge. Each physical/chemical characteristic of PA membrane can be characterized by numerous analytical tools. Table 2.2 summarizes membrane characteristics and several analytical equipment [53-55].

Table 2.2 Physical/chemical characterization of membranes using various analytical tools (bold type will be mainly discussed in this work).

Membrane characteristics	Analytical tools
Pore size and distribution	Thermoporometry, Permporometry, Mercury intrusion test
Mechanical properties	Universal Testing Machine (UTM)
Thickness	Scanning Electron Microscope (SEM) Time-of-Flight Secondary Ion Mass Spectrometry (TOF-SIMS)
Surface and cross section images	Scanning Electron Microscope (SEM) Transmittance Electron Microscopy (TEM)
Surface conductive and roughness (topography)	Atomic Force Microscope (AFM)
Membrane hydrophilicity	Contact angle instrument
Membrane zeta potential	Zeta potential analyzer
Elemental composition	X-ray photoelectron spectroscopy (XPS) Energy-dispersive X-ray spectroscopy (EDX) Time-of-Flight Secondary Ion Mass Spectrometry (TOF-SIMS)
Transmittance of functional groups	Fourier transform infrared spectroscopy (FTIR) Raman spectroscopy

The following section explains the basic principles and analytical methods of these equipment (bold type) to investigate physico-chemical characteristics of PA membranes. In addition, some of the previous studies are suggested to interpret specific phenomenon (*e.g.*, fouling) using their characteristics.

2.3.3.1 Scanning electron microscopy (SEM)

Scanning electron microscopy (SEM) has been widely applied to analyze membrane because of (1) the relatively high resolution surface as well as cross-sectional images, (2) fast measurement times rather than AFM, and (3) easy preparation of measuring sample compared to TEM [56].

There are many previous researches to utilize SEM equipment as measurement of polymer's surface and cross-sectional images. For instance, Galiano et al. [57] characterized the their developed membranes, and the membranes were fabricated by addition of a polymerizable bi-continuous microemulsion (PBM) layer on a scaffold PES UF membrane. These surface and cross-sectional images of developed membranes with homeomorphic structure are clearly measured by SEM as shown in Fig. 2.8. The PBM layer consists of randomly distributed water channels (dark space in Fig. 2.8) and polymer channels (white space in Fig. 2.8) on top-surface of the membrane, and the width of water channels are also clearly measured (about 30 to 50 nm). In addition, effect of PBM coating on thickness of the developed membrane was clearly investigated as described in Fig. 2.8 (about 1 μm thickness). Therefore, surface topography or cross-sectional images from measurement of SEM equipment are suitable to obtain effect of post-treatment or additional coating on morphology structure of the membrane.

The brief process of SEM measurement is scanning the surface of sample using a focused electrons beam. That is, ejected secondary electrons and backscattered electrons from the sample surface are collected by the specific detector, and subsequently produced sample's morphology using the SEM software [56]. Working principle of SEM equipment is summarized in following paragraph.

Figure 2.9 shows a schematic illustration of the main working principle for SEM equipment [58]. Firstly, an electron gun discharges the electrons. Secondly, the electrons penetrate the condenser/objective lens with acceleration voltage, resulting to produce the electrons from specimen (about nanoscale diameter). These phenomenon happens due to bombardments by interaction between the electron beam and surface of specimen. Thirdly, when the electron beam in a straight line scans over the surface of specimen, specific detector simultaneously measures the electron signals. Finally, the signals are altered to the brightness at corresponding spots in accordance with the amount of detected electrons, so the corresponding electron images can be obtained from a video screen as shown in Fig. 2.9. Through this principle of the SEM equipment, it is utilized to measure clear membrane surface as well as cross-sectional images.

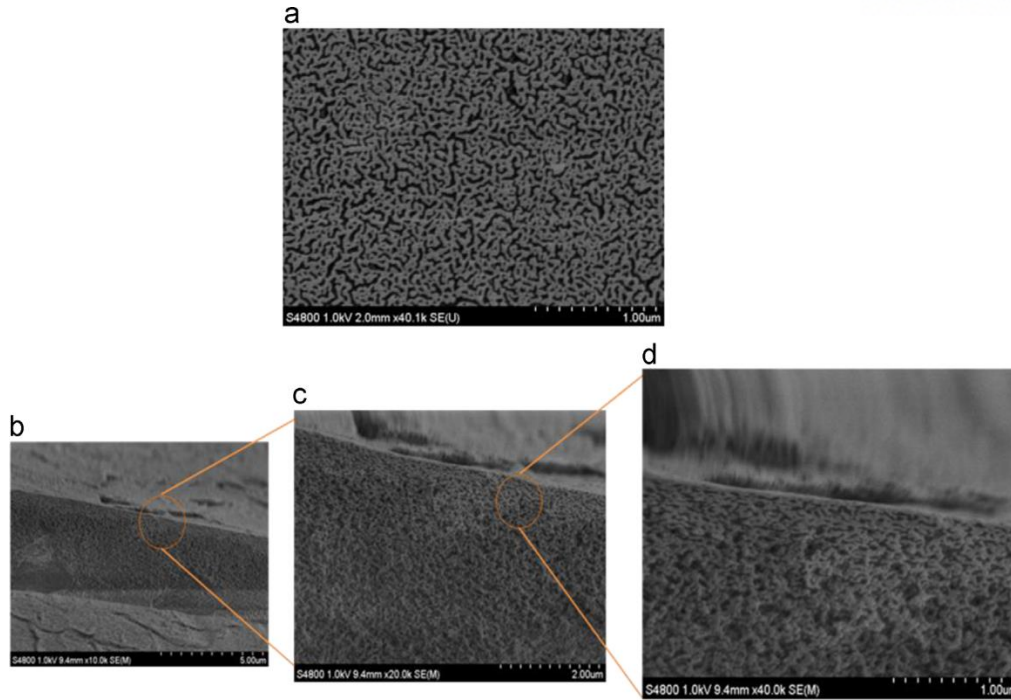


Figure. 2.8 SEM surface (a) and cross-sectional (b–d) images of polymerizable bi-continuous microemulsion membrane with magnification from 10k to 40k [57].

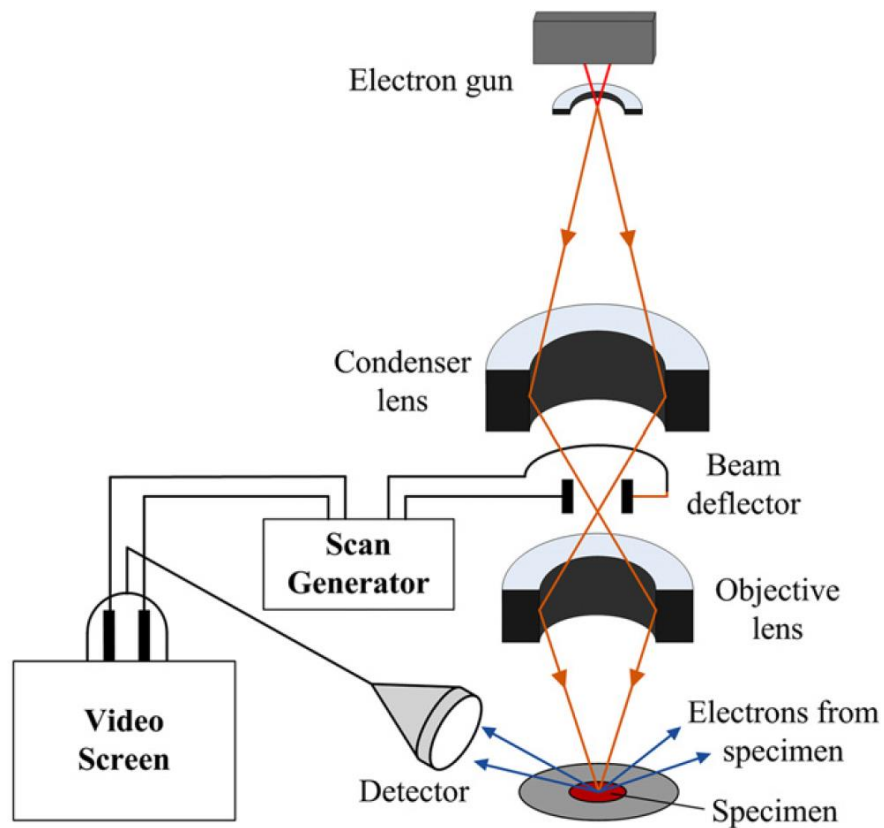


Figure. 2.9 Working principle of the SEM using schematic illustration [58].

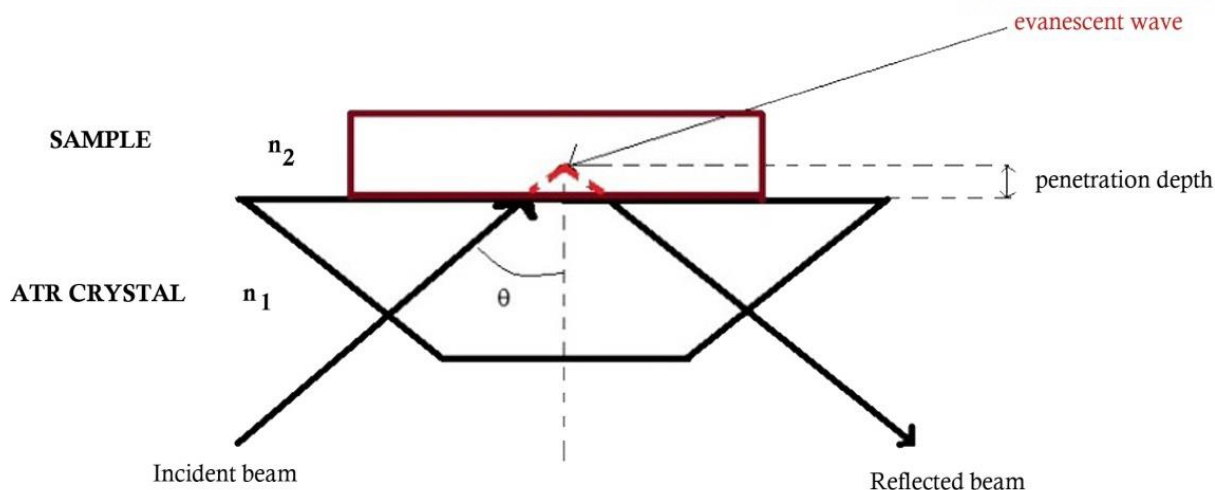
2.3.3.2 Attenuated total reflectance-Fourier transform infrared spectroscopy (ATR-FTIR)

An attenuated total reflectance-Fourier transform infrared spectroscopy (ATR-FTIR) has been applied to measure functional groups of membrane surface, and the FTIR based equipment is a great tool to perform functionality of the membrane surface such as polyamide membrane, modified membrane, and so on. That is, FTIR spectroscopic technique is the one of the most widely used measurement method to study chemical functional groups of membrane surface [56].

The main principle of FTIR technique is examination related to the molecular vibrations which overlap with frequencies of IR range from 10^{12} to 10^{14} Hz. A molecular vibration is the atoms' motion within a molecule when the whole molecule has constant rotational/translational motion. That is, normal modes of vibration are occurred when the IR frequency is equal to a specific molecular vibration, and the normal modes consists of symmetric/asymmetric stretching and in plane/out of plane bending [56].

The highlight to measure FTIR is interferogram, which utilizes different optical paths between splitted two beams from a single source. In other words, difference between the former and the latter beam is a signal produced by the difference of path length due to refractive index changes and irregularities of surface. These differences between two beams' distance and frequency can be converted into an actual spectrum using the mathematical Fourier transformation method [59].

Depends on specimen analyzing technique, there are popular FTIR instruments subdivided by transmission, diffuse reflectance spectroscopy (DRIFTS), ATR, and specular reflectance/reflection-absorption [56]. Above all, ATR is powerful tool to assess the surfaces of membrane compared to bulk chemical compounds, so it has been utilized to measure amount of chemical modification in contradistinction to virgin membrane surfaces. This tool usually connects to the FTIR instrument as an additional accessory. Figure 2.10 shows schematic illustration for the horizontal ATR accessory, and several crystal materials with a high refractive index can be used as an ATR accessory during ATR-FTIR operation. Penetration depth can be calculated using Eq. 2-5, and this value is affected by wavenumber, incident beam angle, and refractive index of used crystals [60]. The several crystal materials and their properties are summarized in Table 2.3. Numerous internal IR beam's reflections create an evanescent wave (in Fig. 2.10), and they interact with the surface of sample. That is, before the beam goes to the detector through the crystal, the evanescent wave is attenuated by the absorption of sample surface [56]. Lastly, the presence of particular absorption bands is used to match the corresponding functional groups of sample surface. These ATR-FTIR measurement can be conducted to measure functionality of membrane surface.



$$\text{Penetration depth } (d_p) = \frac{1}{2\pi W n_1 (\sin^2 \theta - n_{21}^2)^{\frac{1}{2}}} \quad (2-3)$$

where W is the wavenumber, n_1 is the ATR crystal's refractive index, θ is the incidence angle, n_2 is refractive index of sample, and n_{21} is the ratio of n_2 to n_1 (n_2/n_1).

Figure 2.10 Schematic illustration for the horizontal ATR accessory and formula to calculate penetration depth [59].

Table 2.3 Example of the common ATR crystals and their properties [59].

Material	Refractive index	Wavenumber range (cm ⁻¹)	d_p (μm)
Diamond	2.4	45000-2500	1.35-1.66
Germanium (Ge)	4	5500-870	0.65-0.73
Zinc Selenide (ZnSe)	2.41	20000-650	1.22-1.66
AMTIR (As/Ge/Se glass)	2.5	11000-750	1.46
Silicon (Si)	3.4	-	0.84-1.17
Thallium bromoiodide (KRS-5)	2.37	20000-250	1.22-1.73
Cd telluride (CdTe)	2.67	10000-450	-
Sapphire (Al ₂ O ₃)	1.74	25000-1800	-
Zinc Sulfide (ZnS)	2.2	17000-950	2.34
Cubic Zirconia (ZrO ₂)	2.15	25000-1800	-

2.3.3.3 X-ray photoelectron spectroscopy (XPS)

X-ray photon spectroscopy (XPS) is utilized to analyze quantitative elemental information on surface of sample. Principle of XPS is measurement of photo-emission phenomenon. When the atoms on sample surface obtain a sufficient electromagnetic energy by X-ray bombardment, the specific electrons can be ejected from the atoms [61]. That is, kinetic energy of the specific electrons is the same with the difference between the absorbed energy on photon and the binding energy of the specific electron at its orbital [56]. One of the example for photoionization of an atom which is ejected from 1s orbital electron is schematically described in Fig. 2.11 to explain the process of photo-emission [61].

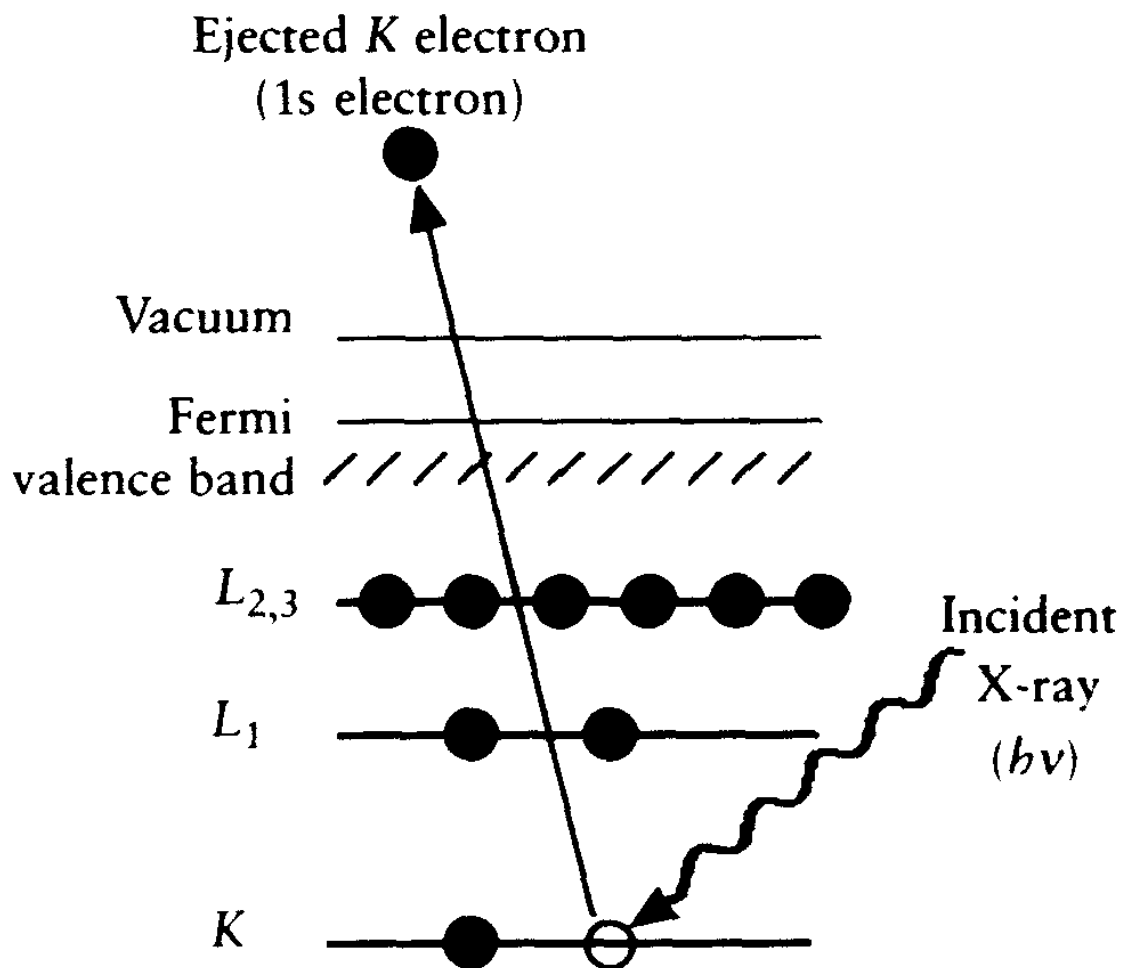


Figure 2.11 Schematic illustration for the XPS process, which shows photoionization of an atom from a 1s electron [61].

Detection of ejected electrons is XPS's main principle using the specific kinetic energy. XPS's data is usually plotted using the intensity on the y-axis versus binding energy, which is in the range of 1200 to 0 eV, on the x-axis as shown in Fig. 2.12. A particular element can be detected at the specific binding energy, however, overlap of peak shape can be also occurred when the analyses of sample surface containing mixture or complex materials. In some cases, the specific atoms within the bulk chemical compound are not able to detect due to attenuation by impacts of other atoms' emission at that spot. These disadvantages of XPS technique should be considered before measurement of the membrane sample which contains complex/bulk chemical compound.

Another characteristic of XPS measurement is occurrence of the multiplet peaks. Because s orbitals have only single peaks, the ejected electrons from s orbital are relatively easy to analyze. However, the ejected electrons from p, d and f orbitals can have multiplet peaks, and these multiplet peaks are able to be happened by coupling effect between the occupied outer shell's unpaired electron and unoccupied core orbital after photoionization. Figure 2.12 shows example of XPS survey spectrum from tin (Sn), which shows multiplet splitting peaks in p and d orbitals [61].

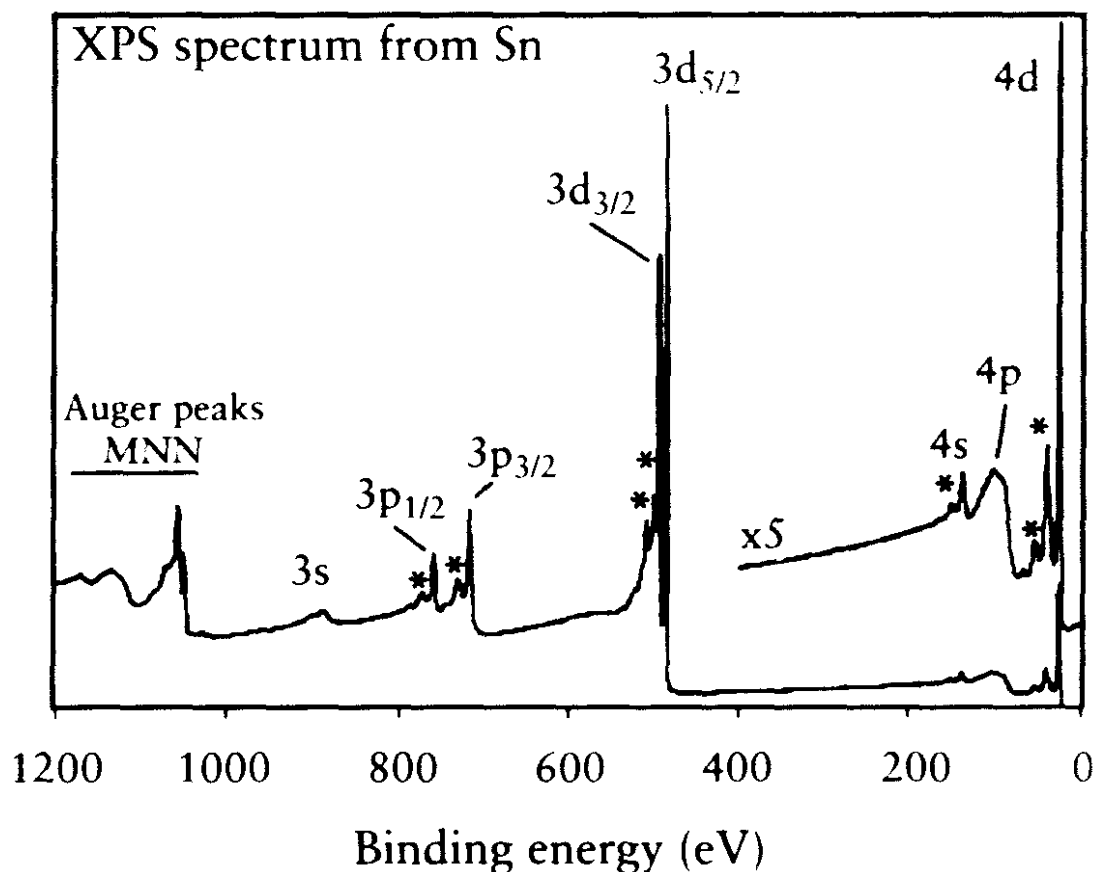


Figure 2.12 Example of XPS survey spectrum from tin (Sn), which shows multiplet splitting peaks in p and d orbitals [61].

The representative XPS instrumentation is made up an X-ray anode, an electron energy analyzer, an ultrahigh vacuum system, and data acquisition/analyses system as schematic described in Fig. 2.13. The measuring sample is mounted on sample stage in the preparation chamber with ultrahigh vacuum to irradiate by photons using X-ray. These X-rays are produced using impaction by electron gun onto an anode (*e.g.*, Al or Mg), and the anodes are chilled with water due to heat converted from electron energy during the XPS measurement. The X-rays generated by anode material are utilized to XPS technique, and the photon energy of Al or Mg is 1486.6 eV or 1253.6 eV, respectively. After bombardment of the X-rays on a sample surface, the photoelectrons emitted from the sample surface are separated into the vacuum chamber and then counted by the hemispherical energy analyzer. Finally, the counted data by energy analyzer are examined by the XPS software [62]. Therefore, these XPS measurement is applied to analyze atomic information on membrane surface.

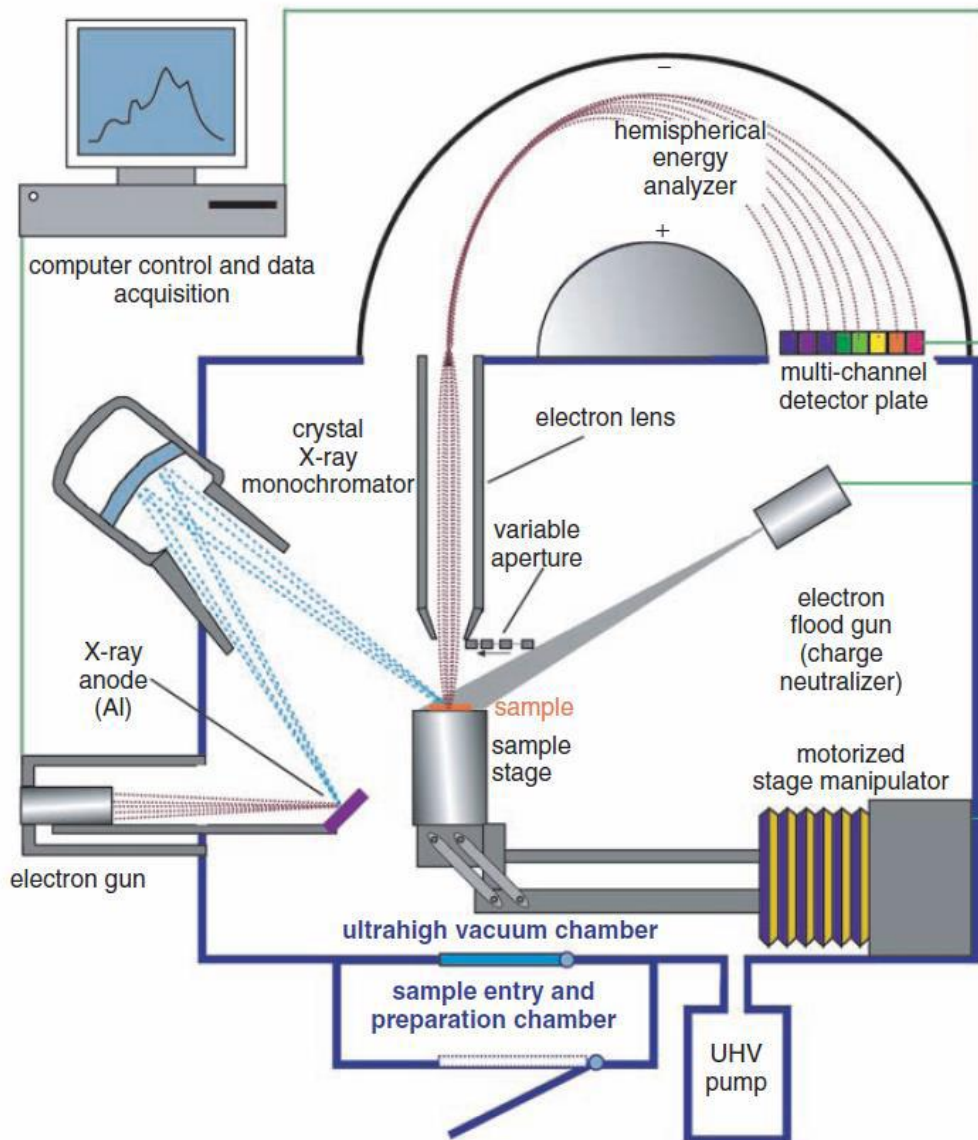


Figure 2.13 Schematic diagram of the XPS instrumentation [62].

2.3.3.4 Contact angle

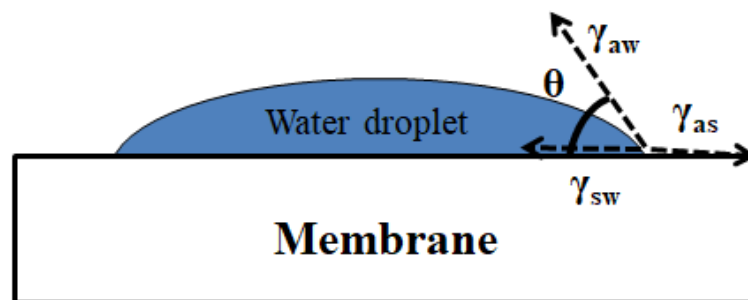
Surface properties such as hydrophilic or hydrophobic and surface charge can affect the membrane performance in the pressure-driven process. The common method to measure hydrophilicity of the membrane is based on measurement of a contact angle value by (1) captive bubble method which uses air bubble onto the immersed membrane, and (2) sessile drop method which measures deposition of a liquid droplet on the membrane surface [63]. Figure 2.14 represents schematic diagram for measurement of contact angle value. According to Young's Law, the air–water (γ_{aw}), air–solid (γ_{as}), and water–solid (γ_{sw}) free energies to the contact angle satisfy followed equation $\gamma_{as}-\gamma_{sw} = \gamma_{aw} \cos\theta_c$, and the law allows inferences about the relative hydrophilicity of different surface chemistries [64]. Thus, a hydrophobic surface (*e.g.*, $\theta_c > 90^\circ$) is less wettable as a result of the higher free energy of its water–solid interface ($\gamma_{as}-\gamma_{sw} < 0$) compared to a hydrophilic surface (*e.g.*, $\theta_c < 90^\circ$ and $\gamma_{as}-\gamma_{sw} > 0$) [64]. Values for contact angle of the membrane closely related with its surface features/functional group, for example, -OH, NH_2 group increases hydrophilicity of the membrane surface [44].

Hydrophilicity affects not only performance of the membrane but also less fouling in the pressure-driven process. The increase of hydrophilicity of the membrane surface can improve the permeate flux/rejection in pressure-driven process. Yu et al. [65] studied that interfacially synthesized thin film composite RO membrane was modified by poly(N-isopropylacrylamide-co-acrylamide). In this research, modified RO membrane showed that the membrane surface with high hydrophilicity enhanced about 20% of the water permeability without loss of rejection. The membrane surface of hydrophilic/hydrophobic is also an important factor in solute rejection during membrane applications. Kiso et al. [66] published that the rejection of hydrophobic molecules such as alkyl phthalates and mono-substituted benzenes by NF membranes has linear correlation between affinity of the solute and surface of the membrane expressed as the octanol/water partition coefficient ($\log P$). Therefore, hydrophobic interactions between the solute and surface of the membrane are the dominant mechanism for rejection of hydrophobic compounds.

Membrane surface property coated by hydrophilic polymer is a one of the method to improve hydrophilicity of the membrane surface as well as water flux/membrane fouling. Due et al. studied that a polyvinylidene fluoride (PVDF) membrane was modified by surface coating using a polyvinyl alcohol (PVA) aqueous solution followed by solid-vapor interfacial crosslinking to improve hydrophilicity [67]. The research was shown that the flux of the modified PVA/PVDF membrane was 14% higher than the unmodified PVDF membrane after 4 h filtration test and 95% higher after 18 h of filtration test when feed solution is surface water containing total organic carbon of 7 mg/l. Additionally, the hydrophilicity

of membrane surface by modified polysulfone [68] and thermo-responsive polymer [65] also improved fouling problem occurred by hydrophobic foulants such as organic pollutants and bovine serum albumin. The reason for improving fouling problem in the case of hydrophilic membrane is that hydrogen bonding interaction between membrane surface and water molecules makes thin water boundary which can prevent the approach of hydrophobic foulants on membrane surface [69]. However, in the case of hydrophobic membrane, the repulsion of water molecules from the hydrophobic membrane surface is a natural process due to increasing entropy and thus hydrophobic foulant molecules have an affinity to absorb onto membrane surface and dominate the boundary layer [44]. Therefore, improvement related to hydrophilicity of the membrane surface is important parameter to reducing membrane fouling with hydrophobic colloids and organic pollutants. Therefore, measurement of contact angle is important to investigate effect of hydrophilicity on membrane performance and fouling phenomenon.

(a) Sessile drop method



(b) Captive bubble method

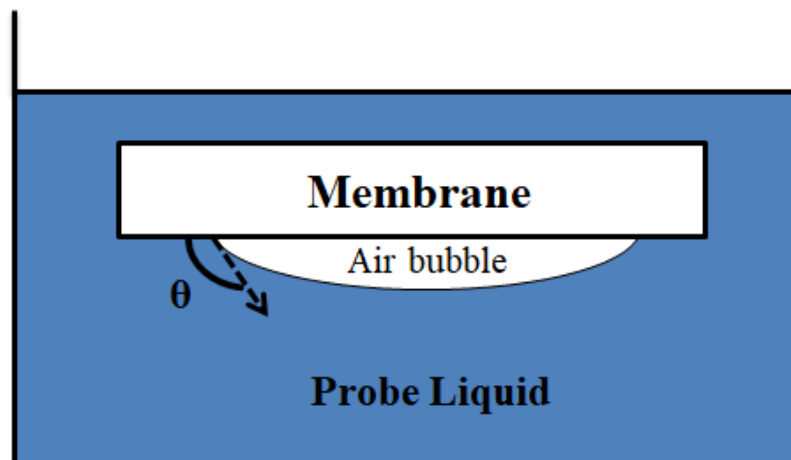


Figure 2.14 The method for measurement of contact angle (a) sessile drop method, (b) captive bubble method, respectively.

2.3.3.5 Zeta potential (ζ)

Polymeric filtration membranes (*e.g.*, polyamide membrane) or ion-exchange membranes naturally are ionizable characteristics at the membrane surface. Consequently, the sign (negative/positive) and amount of charge on membrane surface depends on condition of aqueous feed solutions such as ionic concentration and solution's pH. Feed solutions are normally complex mixtures which contains charge carrying substances such as surfactants, polyelectrolytes, ions, and macromolecules. The membrane's surface charge can be changed by complexation/interaction between charge carrying chemicals and the membrane surface. Because the complexation/interaction between membrane surfaces and these species in aqueous phase determines the membrane's surface charge, measurement of the zeta potential of the membrane is important parameter to explain membrane performances or fouling phenomenon.

The structure, charged species which near to the surface of membrane, is known as the electrical double layer (EDL) [56]. Charge spreading of the EDL is most concentrated at closest to the surface of membrane, and its potential decreases in accordance with increasing distance from the surface of membrane as shown in Fig. 2.15. Ions near to the surface of membrane are existed in the immobile Stern layer. This layer can be subdivided into the inner Helmholtz layer: (1) the layer containing partly dehydrated ions attached to the membrane surface electrostatically between the surface of membrane and the inner Helmholtz plane (IHP in Fig. 2.15), and (2) the outer Helmholtz layer containing fully hydrated ions which are counter-ions to the inner Helmholtz ions between the inner and outer Helmholtz planes (OHP in Fig. 2.15). In the immobile Stern layer, the charge spreading and electrical potential are measured by interactions between ions/dipoles and the surface of membrane. Ions can freely move by thermal driven motion where beyond the immobile Stern layer which is called by the diffuse Gouy-Chapman layer.

There are various methods to measure electrokinetic properties such as streaming potential, electro-osmosis, electrophoresis, and sedimentation potential. Because this work was conducted by electrophoresis method, only electrophoresis method is briefly summarized as follows: The ζ potential values of the membrane surface is measured by electrophoresis method using a quartz cell. When electric field exists in the electrophoresis chamber, an asymmetric electroosmotic flow happens through the membrane surface. Because of the amassment of the cations from the electrolyte solution, this electroosmotic flow allows to move the monitoring particles on the membrane surface. Then, the ζ potential values on the membrane surface can be calculated using the Smoluchowski equation (2-4) which uses electrophoretic mobility of the monitoring particles [70].

$$\zeta = \frac{4\pi\eta U}{\epsilon_r \epsilon_0} \quad (2-4)$$

where ζ is the ζ potential measured by electrophoresis method (mV), η is the viscosity of liquid medium (0.89×10^{-3} Pa s), U is the monitoring particle's electrophoretic mobility ($\text{cm}^2 \text{V}^{-1} \text{s}^{-1}$), ϵ_r and ϵ_0 are permittivity of the liquid medium (78.38) and vacuum ($8.854 \times 10^{-12} \text{ s m}^{-1}$), respectively.

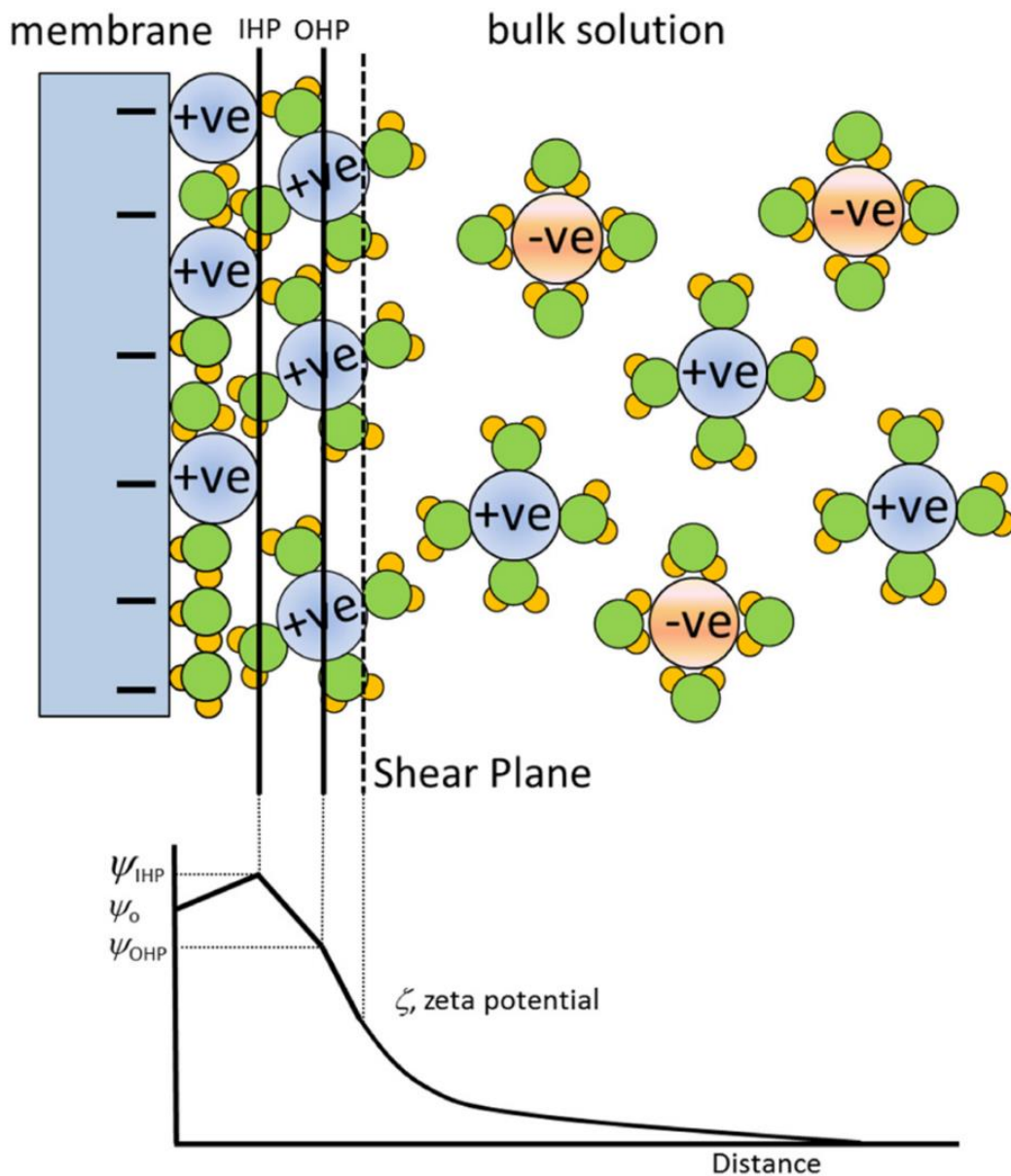


Figure. 2.15 Schematic illustration for charge spreading of the ionic species which near to the membrane surface (the electrical double layer) and the resultant zeta potential with increasing distance from the membrane surface [56].

Surface charge of membrane affects not only rejection of the charged organic/inorganic matters by the membrane but also different fouling tendency in the pressure-driven process.

Firstly, electrostatic interactions between charged organic solutes and a surface charge of membrane have often been published to be a rejection mechanism significantly [71]. Hu et al. studied that charged organics had higher rejections than neutral organics by negative charge of membrane surface because of electrostatic repulsion between charged of solute molecules and membrane surface [72]. The membrane surface of RO, NF and UF membranes frequently has a negative charge to increase the rejection of negatively charged natural organic matters by donnan exclusion effect [73]. Negative surface charge of the membranes are increased by increasing the pH of feed solutions due to a dissociation of carboxylic and sulfonic functional groups on membrane surface [44, 74], resulting increase rejection of negatively charged organic/inorganic matters.

Secondly, the electrostatic charge of membrane surface is a mainly important consideration for the decrease of membrane fouling when feed solution contains charged foulants. When surface of the membrane and the foulant have same charge, electrostatic repulsion forces between surface of the membrane and the foulants prevent the foulant deposition on the membrane surface thereby reducing the fouling [75]. For example, humic materials in aquatic environments are took into account to be the major element of natural organic matter (NOM), are refractory anionic macromolecules with low/moderate molecular weight [75]. Humic material contains both aromatic and aliphatic components with primarily carboxylic/phenolic functional groups [75]. Consequently, humic materials mostly are negatively charged in the pH range of natural waters [76]. Mika et al. showed that at pH 4–5 the membrane (NTR-7450 from Nitto Denko and Desal-5 from Osmonics/Desal company) has slightly negative charge and humic acid are almost uncharged thereby promoted fouling at pH 4-5 condition [77]. To solve this issue, polyvinyl alcohol (PVA) coated the membrane with highly negatively charged may show stable flux because of the strong electrostatic repulsion between membrane surface and negatively charged NOM [50]. Therefore, measurement of zeta potential is important to investigate effect of surface charge on membrane performance and fouling phenomenon.

2.3.3.6 Time-of-flight secondary ion mass spectrometry (ToF-SIMS)

TOF-SIMS is a kind of mass spectrometry technique to analyze chemical information such as elements and lower molecular weight compound using the detection of secondary ions (SIs). These SIs are generated from a target surface (*e.g.*, membrane surface) under vacuum state, and it is bombarded by a primary ion beam. To measure SIs for analyzing chemical information, the SIs, which generated from bombardment of primary ions on the sample's surface, are then extracted, and subsequently collected into a mass spectrometer.

Several processes are needed to measure SIMS. Firstly, the primary ion beam with high energy collimated on sample surface. Secondly, the primary ions with high energy collide with sample surface (described in grey circles in Fig. 2.16), and elastic/inelastic collisions transfers from partial primary ion's energy to the particles on sample surface. Thirdly, an atom/molecules, which received from partial primary energy during the ion bombardment, can be higher than the surface binding forces, then they are ejected from the sample surface (depicted in green circle in Fig. 2.16). Then, chemical information can be analyzed by these SIs. Total processes are well explained in Fig. 2.17 using schematic illustration.

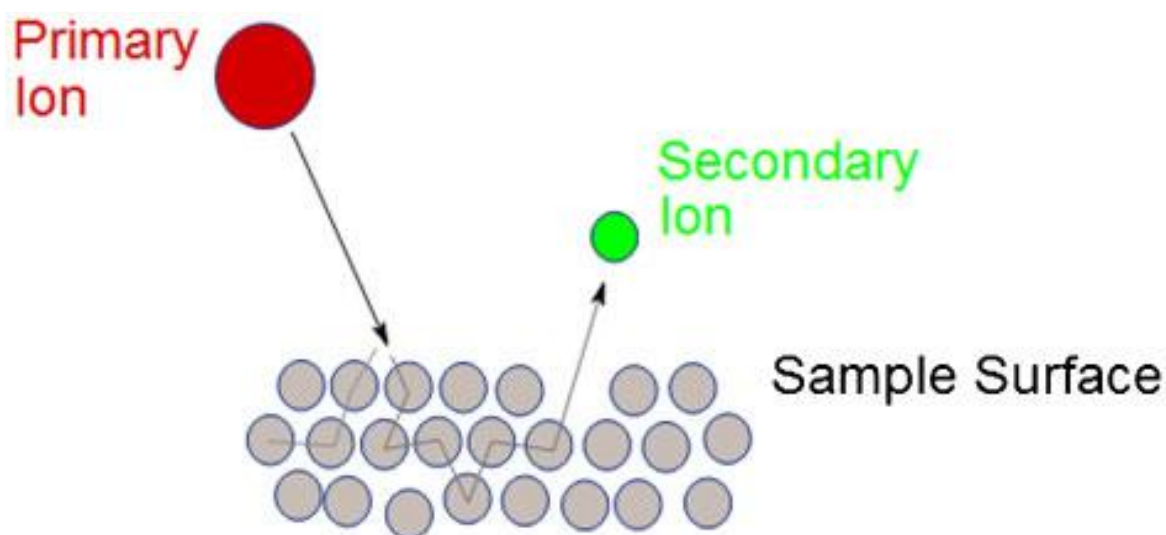


Figure. 2.16 Schematic representation of a collision event that can lead to the formation of liberated SI capable of being captured in a detector. Primary ion (red) impacts upon sample surface (grey), thereby transferring energy to the sample, which is then distributed through different atoms (grey lines). This process can lead to the ejection of SI from close to the surface (green), which is then possible to observe with an analyzer [78].

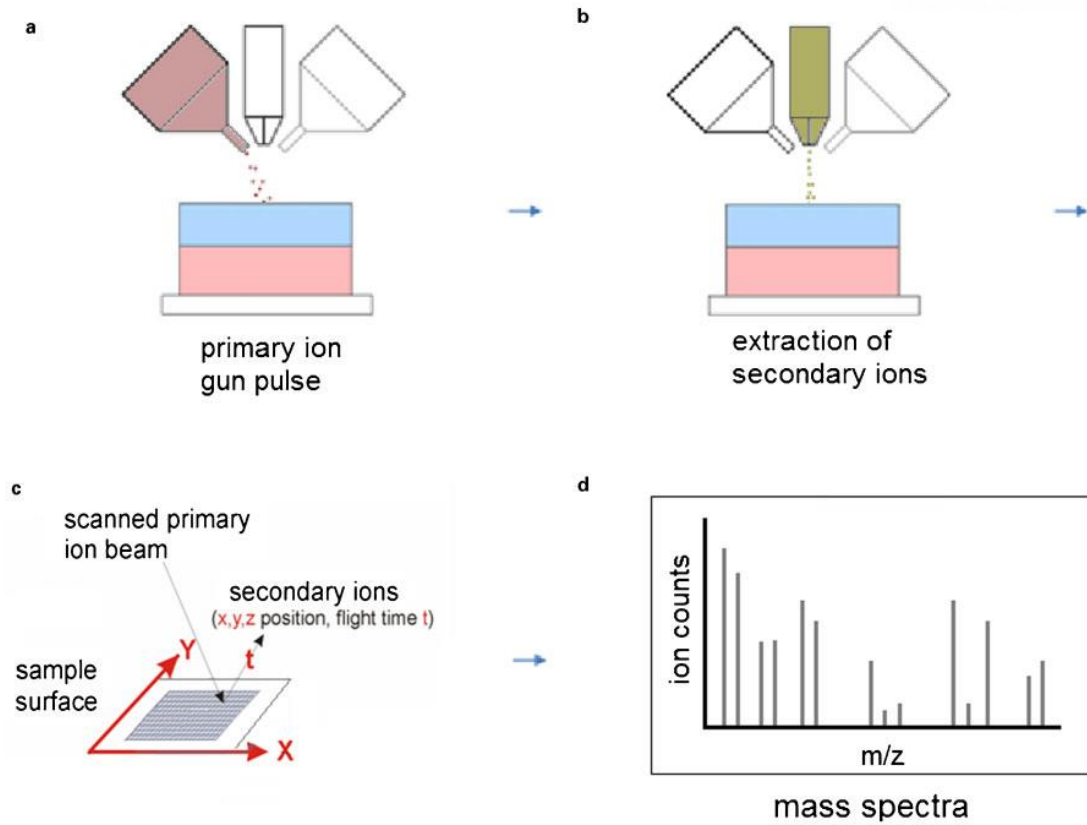


Figure. 2.17 Total processes to analyze mass spectra of sample surface. (a) primary ion beam collimates on sample surface and occurs SIs, (b) extraction of secondary ions, (c) repeated process for specified area, and (d) produced mass spectra using detection of ejected SIs [78].

When ejected SIs have the same kinetic energy and they are collected to a flight tube before entering a detector as shown in Fig. 2.18. These SIs' mass analysis is obtained by time-of-flight (ToF) method, and heavier masses needs more time to enter the detector compared to the lighter masses. The ratio of mass to charge (m/z) of the SIs is calculated by following the equation (2-5). Lastly, the SIs enter to detector which is a microchannel plate, giving the final signal output (Fig. 2.18).

$$\frac{m}{z} = \frac{2vt^2}{L^2} \quad (2-5)$$

where v is the accelerating potential, t is the ToF of the SIs, and L is the flight tube's length.

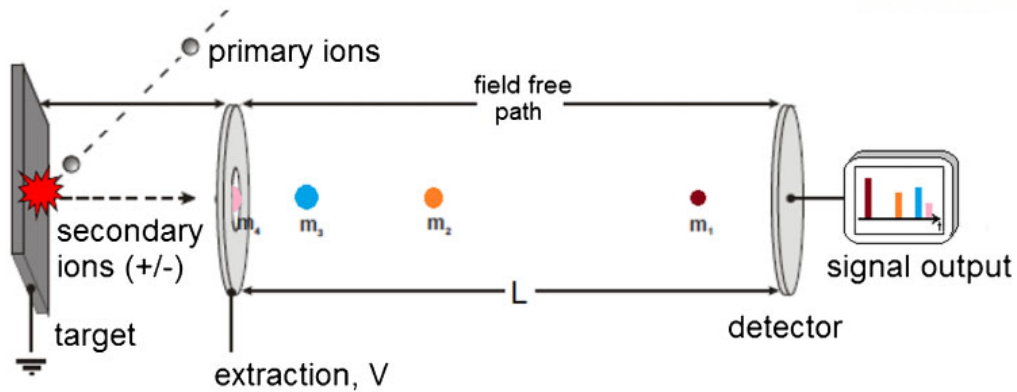


Figure. 2.18 Schematic illustration of ToF analysis [78].

Therefore, ToF-SIMS equipment has been utilized when biological or chemical samples are investigated to study detailed elemental and molecular information on the surface of samples. A schematic diagram of whole processes related to ToF-SIMS instrument are explained in Fig. 2.19.

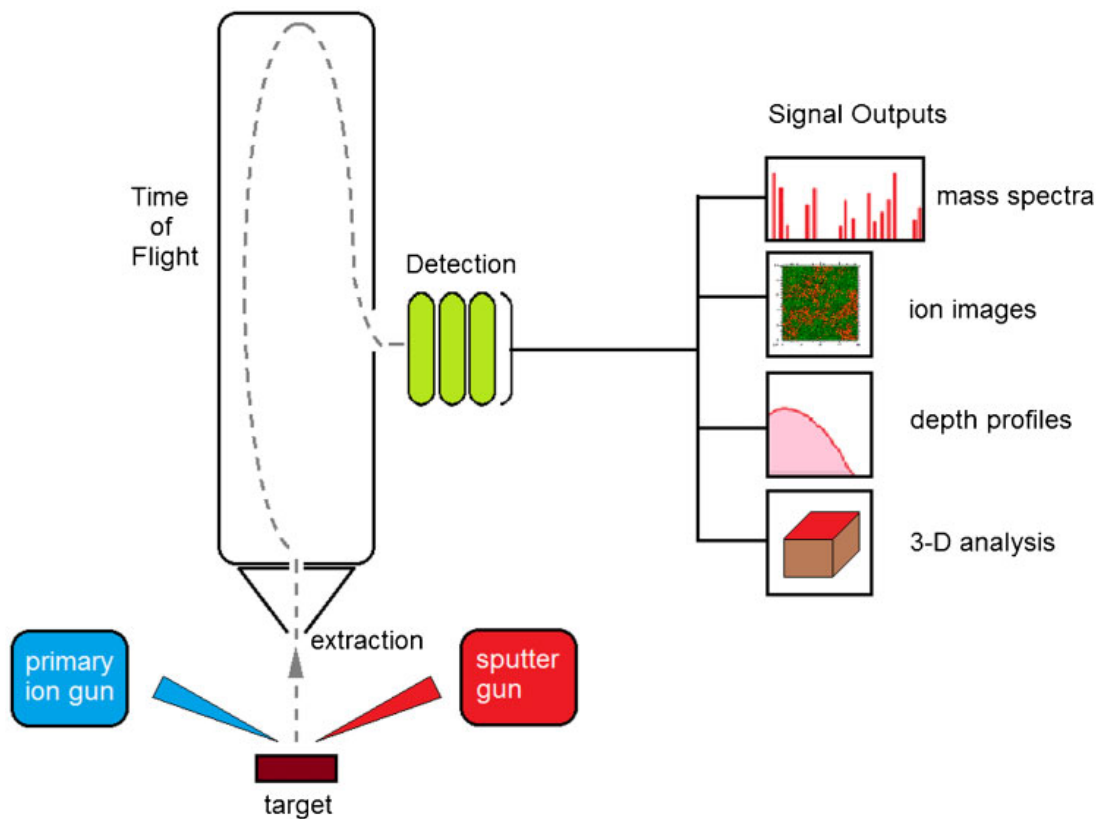


Figure. 2.19 Schematic diagram of dual beam ToF-SIMS equipment. The SIs are ejected from surface of sample by a primary ion gun. Ejected SIs are collected by the flight tube, and subsequently detected at a microchannel plate. Mass spectra to analyze chemical information on the surface of sample can be measured by depending on instrumental operation mode [78].

2.4 Acid-catalyzed hydrolysis of amide group

Amide hydrolysis has been studied significantly due to the biological importance of proteolytic reactions [32]. The amide hydrolysis reactions conducted under acidic conditions can be subdivided into four reaction steps [32, 79-81]. Figure 2.20 shows the scheme for reaction pathways of the acid-catalyzed hydrolysis reaction of piperazine-amide, which is one of the example for amide group. The piperazine-amide hydrolysis is initiated by either an O-protonated or N-protonated pathway under acidic conditions. In the first step, the two pathways are in competition and protonation of the oxygen or nitrogen in the amide group, and thus the dominant pathway for the subsequent reaction, is determined based on activation energy [81]. The second step of the piperazine-amide hydrolysis reaction occurs by nucleophilic attack of first water molecular to carbon at carbonyl bond of piperazine-amide group, followed by formation of a dihydroxy tetrahedral intermediate and removal of one proton at attached first water molecule by a second water molecule [79]. Thirdly, nitrogen for amide or oxygen of carbonyl group additionally reacts with a proton in the case of O- and N- protonation, respectively [80, 81]. At last, the C-N piperazine-amide bond breaks, causing depolymerization of the amide group into carboxyl and amine groups [32, 79-81].

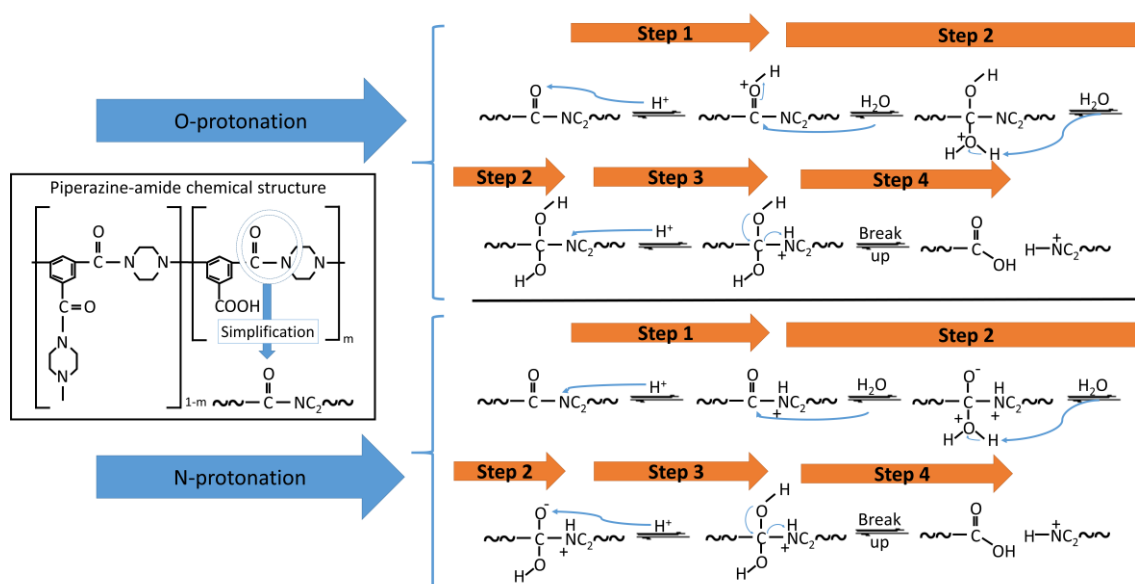


Figure. 2.20 Reaction pathways of the piperazine-amide hydrolysis reaction under acidic conditions initiated from (a) O-protonation and (b) N-protonation.

Meanwhile, according to Ma et al. [81], the second and third steps of the hydrolysis reaction were combined into the same transition state for calculating the polyacrylamide polymer using density functional theory (DFT) computational modeling method (Fig. 2.21).

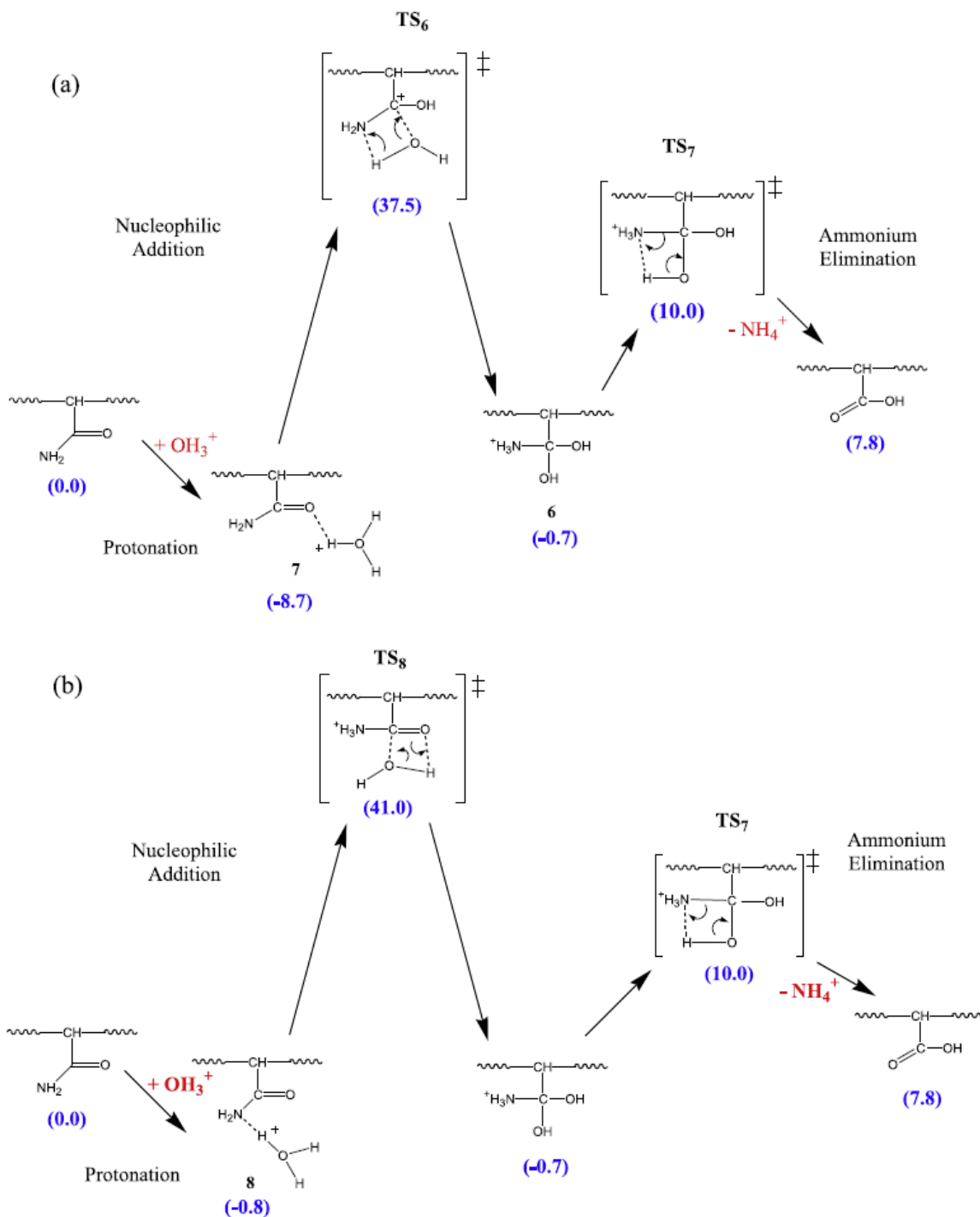


Figure. 2.21 Reaction pathways of polyacrylamide polymer under acid-catalyzed hydrolysis initiated (a) O-protonation and (b) N-protonation with combining second and third parts as explained in Fig. 2.20 [81].

2.5 Acidic degradation of PA membranes

Recently, numerous studies have been performed to investigate acidic degradation on PA membranes' physico-chemical properties. Liu et al. [25] investigated effect of coating by N-isopropylacrylamide-co-acrylamide copolymers on virgin full-aromatic PA membrane in terms of long-term acid stability using filtration of 0.5 M HCl. Figure 2.22 shows that 0.5 M HCl acidic condition affected hydrolysis of full-aromatic PA membrane after 30 Days filtration, resulting to decrease salt rejection. However, the author did not explain amide functionalities of degraded membrane (*e.g.*, amide I band in 1663 cm^{-1} (C=O stretching) or amide II band in 1541 cm^{-1} (N-H bending motion)) by ATR-FTIR technique. In summary, filtration property of full-aromatic PA membrane is deteriorated when the membrane is exposed to extreme acidic condition.

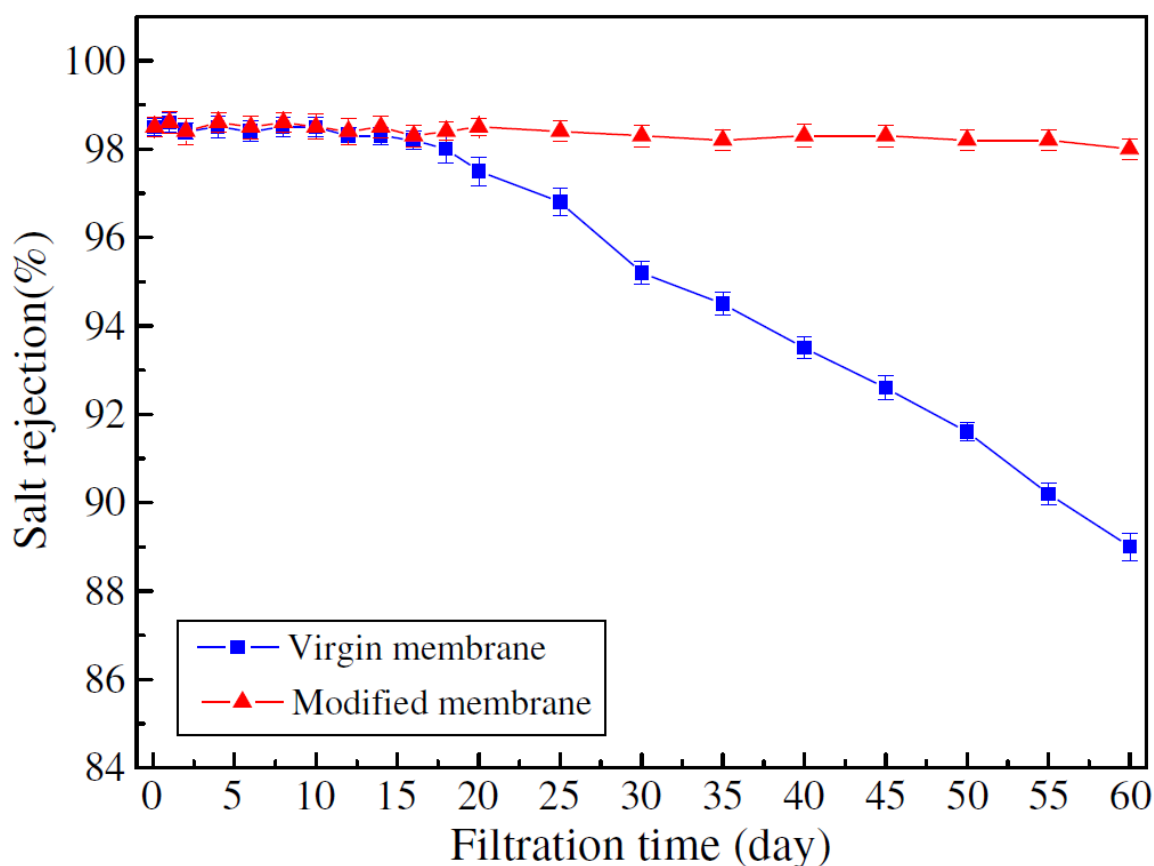


Figure. 2.22 Salt rejection of the full-aromatic virgin (■) and modified (coated) (▲) membranes with increasing filtration times until 2 months with aqueous acidic solution containing 0.5 M HCl and 2,000 ppm NaCl. The operating condition is 1.5 MPa pressure and room temperature [25].

In the case of semi-aromatic PA membrane, Tanninen et al. [26] studied acid-stability of semi-aromatic PA membranes (The Desal-5 DK and the NF 270 membrane) using filtration test containing 8 wt% H_2SO_4 and 25g/L $CuSO_4$ at 40°C during 2 months. Figure 2.23 explains 8 wt% H_2SO_4 acidic condition affected hydrolysis of semi-aromatic PA membranes after about 25 Days filtration, resulting to decrease copper rejection, on the other hand, acid-resistant NF membranes were almost maintained during operation. In this paper, the author did not also explain chemical analyses of amide group (*e.g.*, ATR-FTIR or XPS measurement).

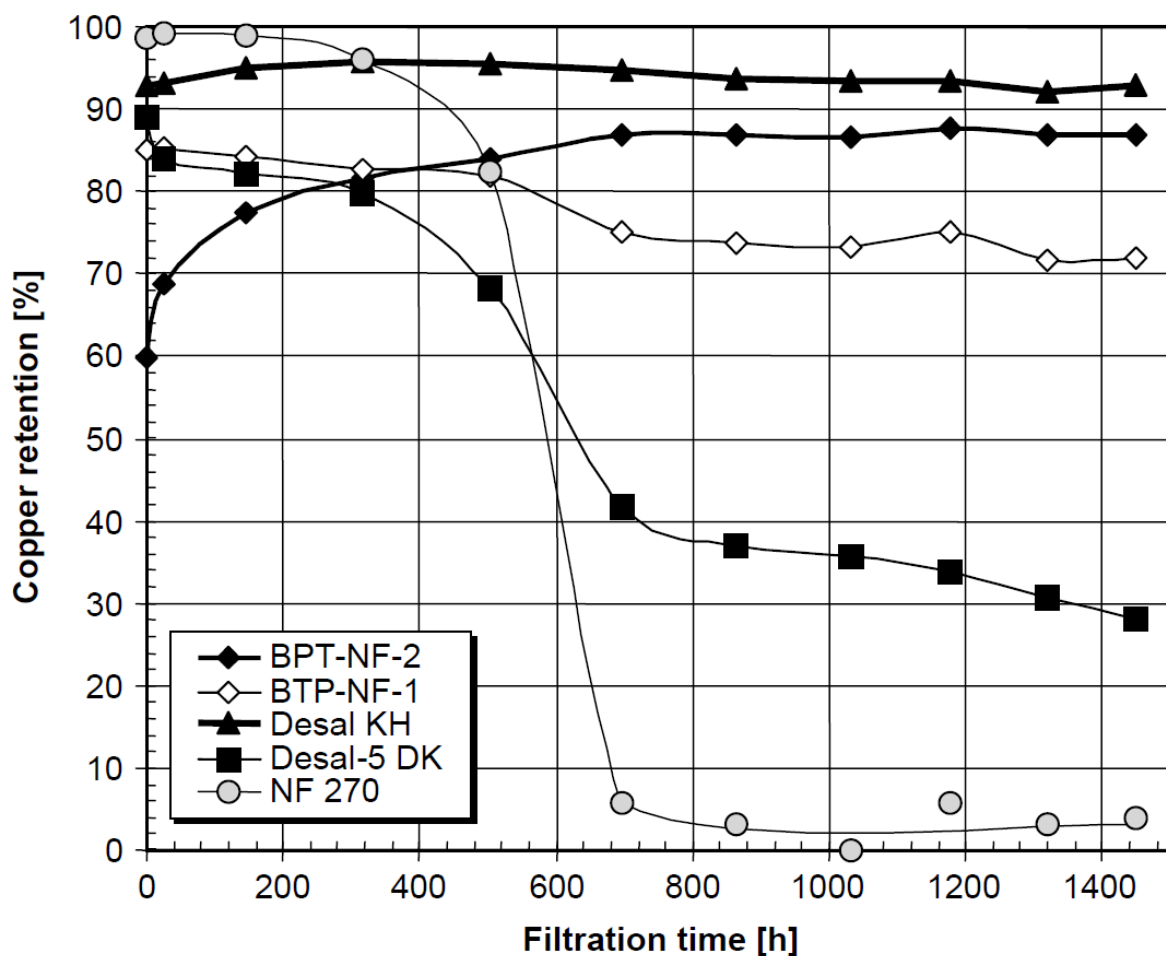


Figure. 2.23 Copper rejections of NF membranes (BPT-NF-2, BPT-NF-1, and Desal KH as acid-resistant NF membranes with Desal-5 DK and NF 270 as semi-aromatic PA membranes) during 2 months' filtration times. Feed solution contains 8 wt% H_2SO_4 and 25g/L $CuSO_4$. Operating pressure and temperature are 30 bar and 40°C, respectively. [26].

Moreover, another semi-aromatic PA membrane (the NF-45 membrane) showed similar results which are severely decreased sucrose/glucose retention due to acid-catalyzed hydrolysis when the membrane exposed to 5 wt% HNO₃ or 20 wt% H₂SO₄ at 80°C for only 1 month as shown in Table 2.4 [18]. Evidence for hydrolysis of PA membranes by acid was suggested by severely increased water flux and decreased sucrose and glucose rejection.

Table 2.4 Permeability after exposure to various acidic conditions during 0 to 4 months for NF-45 membranes [18].

Immersion solution	Temperature (°C)	Sucrose retention (%) after months				Glucose retention (%) after months				Permeability (l/h m ² bar) after months			
		0	1	2	4	0	1	2	4	0	1	2	4
5% HNO ₃	80	81	0			78	0			5.3	13		
	20	94	90	89	35	88	84	83	35	5.1	5.3	3.9	9.1
20% H ₂ SO ₄	80	83	0			79	0			5.8	26		
	20	80	72	49	2	77	68	45	2	6.9	7.2	8.2	19.2
12% H ₂ SO ₄	20	86	91	86		86	89	86		10	10.4	10.2	
H ₂ O	80	94	91	92	92	88	89	88	88	2.5	2.7	2.8	2.9
	20	79	76	82	78	76	71	73	75	8	8.1	8.4	8

To sum up, filtration property of semi/full-aromatic PA membranes are deteriorated when the membrane is exposed to extreme acidic condition. The previous studies were mainly investigated to effect of acid on PA membranes in the view of permeability, however, both changes of physico-chemical properties as well as degradation mechanism of semi/full-aromatic membranes after exposure to extreme acidic conditions have not been systematically discussed up to now. Hence, a detailed research needs to explain effect of severe acidic conditions on physical and chemical properties of PA membranes using various analytical tools (*e.g.*, ATR-FTIR, XPS, Zeta potential, and ToF-SIMS) and computational calculation methods.

***Study on Acid-catalyzed hydrolysis of
polyamide NF membranes
in terms of surface characterization and
DFT calculation***

Chapter 3

This chapter has been submitted:

Byung-Moon Jun, Su Hwan Kim, Sang Kyu Kwak, Young-Nam Kwon*,
'Study on Acid-catalyzed hydrolysis of polyamide NF membranes in terms
of surface characterization',
Water Research (WR-S-17-05712)

Abstract

We systematically investigated the effects of acidic aqueous solution (15wt% sulfuric acid) on the physical and chemical properties of commercially available nanofiltration (NF) polyamide membranes, using piperazine (PIP)-based NE40/70 membranes and m-phenylene diamine (MPD)-based NE90 membrane. Surface properties of the membranes were studied before and after exposure to strong acid using various analytical tools: Scanning Electron Microscopy (SEM), Attenuated Total Reflectance-Fourier Transform Infrared spectroscopy (ATR-FTIR), X-ray photoelectron spectroscopy (XPS), Time-of-Flight Secondary Ion Mass Spectrometry (ToF-SIMS), contact angle analyzer, and electrophoretic light scattering spectrophotometer. The characterization and permeation results showed piperazine-based NE40/70 membranes have relatively lower acid-resistance than MPD-based NE90 membrane. We also conducted density functional theory (DFT) calculation to reveal the different acid-tolerances between the piperazine-based and MPD-based polyamide membranes. The easiest protonation was found to be the protonation of oxygen in piperazine-based monomer, and the N-protonation of the monomer had the lowest energy barrier in the rate determining step (RDS). The calculations were well compatible with the surface characterization results. In addition, the energy barrier in RDS is highly correlated with the twist angle (τ_D), which determines the delocalization of electrons between the carbonyl π_{CO} bond and nitrogen lone pair, and the tendency of the twist angle was also maintained in longer molecules (dimer and trimer). This study clearly explained why the semi-aromatic membrane (NE40/70) is chemically less stable than the aromatic membrane (NE90) given the surface characterizations and DFT calculation results.

3.1 Introduction

Nanofiltration (NF) technology utilizing separation mechanisms of both solution diffusion (as in reverse osmosis) and sieving (as in ultrafiltration) has attracted lots of attention during past decades because of its high rejection of divalent salts and organic molecules with low molecular weight (200 – 1000 M_w) at low operating pressure [82, 83]. Currently, commercial NF polyamide thin-film composite (TFC) membranes have been widely fabricated by interfacial polymerization method using piperazine (aliphatic amine monomer) or m-phenylenediamine (MPD, aromatic amine monomer) reacting with trimesoyl chloride (TMC, acyl chloride monomer) [7, 8]. The interfacial polymerization using amine monomer (*e.g.*, piperazine or MPD) and acyl chloride monomer (*e.g.*, TMC) is one of the most effective methods to fabricate TFC NF membranes [84], since the thin/dense polyamide selective layer can make high water flux at low driving-pressure [85] and the selective performance can be optimized by several factors of fabrication such as monomer concentrations, effective additives, reaction times, and curing time/temperature for post-treatment [9].

The NF process has been applied to the purify phosphoric and nitric acids [12, 13], as well as diluted acidic streams in dairy cleaning-in-place processes (CIP) [14], to treat effluents in the pulp and paper industry [15], recover phosphorus from sewage sludge [16, 17], remove metals (*e.g.*, copper or gold) with a high sulfuric acid concentration [18], and sulfate ions from industrial effluents in the mining and metal industry [6, 19]. Furthermore, the application includes the removal or recycling of abundant acids like hydrochloric acid, sulfuric acid, fluoroboric acid, nitric acid, boric acid, and other valuable chemicals (copper or gold) [11, 23]. There has been a demand for acid-resistant NF membranes which have tolerate at low pH condition during the application. However, high performance commercial NF polyamide TFC membranes fabricated by piperazine or MPD with TMC are recommended for use only in the range of pH 2 to 11 [24].

There has been much research on hydrolysis of amide because of the great biological importance of proteolytic reactions [32]. An amide bond's stability is attributed to its partial double-bond character, which is affected by the delocalization of electrons between the carbonyl π_{CO} bond and the nitrogen lone pair of amide [34, 37, 39]. The amide bonds with rigid planar conformation have a short length of C-N bond [34], lowering the reactivity of nucleophilic attacks of water molecule toward the carbon of the carbonyl group and shifting the basicity of the amine's nitrogen. [86]. Acid-catalyzed hydrolysis reactions of amide may be subdivided into three or four reactions, depending on the combination of second and third reactions. For the hydrolysis reaction, protonation of oxygen (O) or nitrogen (N) occurs. The first reaction may involve N-protonation, which forms a tetrahedral

intermediate at the nitrogen in amide. The N-protonation in the amide group destabilizes the amide C-N bond by reducing delocalization of the lone-pair electrons of N or O of the carbonyl group, resulting in an increase in C-N bond length [38]. For example, in the twisted lactams case, N-protonation of the amide bond increases the distortion and length of the C-N bond [40], causing destabilization of the bond [34]. Another initial reaction of the amide hydrolysis reaction may involve O-protonation. The O- or N-protonation pathways were found to compete with each other [81]. That is, the amide hydrolysis reaction of the first step may proceed by either an O-protonated or N-protonated pathway, depending on the kinds of amide (undistorted amides are highly protonated at the oxygen) [38]. The protonation by acidic media twists the C-N bond to lose the resonance between nitrogen lone-pair electrons and carbonyl π bonds and consequently accelerates the rate of amide's hydrolysis [38, 39, 81]. In the second reaction of amide hydrolysis, nucleophilic attack by a water molecular on the carbon backbone is activated to form a dihydroxy tetrahedral intermediate, followed by the loss of a proton to a second water molecule [79]. This second step of the amide hydrolysis reaction is known as the rate determining step (RDS) for the acid-catalyzed hydrolysis [39]. Thus, solvent water plays an important role in acid-catalyzed hydrolysis reactions [79]. The third reaction is the protonation of basic intermediate (nitrogen of amide bond in O-protonation case or oxygen of carbonyl group in N-protonation) [80, 81]. According to Ma et al. [81], the second and third steps of the reaction were combined into the same transition state for calculating the polyacrylamide polymer. Finally, the last part is breaking of the C-N amide bond by transferring a proton from the hydroxyl group to the leaving nitrogen [32, 79-81, 87, 88].

As described above, the stability of the amide bond is influenced by the resonance between the nitrogen lone-pair electrons and carbonyl π_{CO} bond electrons [34]. That is, the distortion degree of the C-N amide bond is closely related to the rate of the amide's hydrolysis. The degree of the twist angle (τ) has been calculated by computational modeling method and reported by several researchers [35-39]. Wang et al. showed [35] that the most distorted C-N amide bond, among the several kinds of bicyclic anilides, underwent 11 orders of magnitude of the rate enhancement for acid-catalyzed hydrolysis due to high rate constant for H_2O attack on the protonated amide bond (RDS step) compared to relatively planar C-N amide bonds. That is, the most distorted bicyclic anilide was kinetically reactive in acid-catalyzed hydrolysis due to distortion of a C-N amide bond destabilized by loss of the resonance [35, 36]. Mujaka et al. [38] also reported that amides' hydrolysis rate was accelerated when the C-N bond is extremely twisted due to the orthogonality of the carbonyl π orbital and the lone pair of the nitrogen. Chemical stability in acid-catalyzed hydrolysis reaction can be relatively evaluated by calculation of the twist angle (shown destabilization by loss of the resonance) of protonated amide as the reactant in the RDS step [34-36, 40].

In this work, two commercially available NF polyamide TFC membranes fabricated by two amine monomers (piperazine or MPD) with acyl chloride (TMC) were chosen as representative polyamide NF membranes and the effect of acidic aqueous solution (15wt% sulfuric acid) on the membrane's physical and chemical properties were systemically investigated. Membrane acid-soaking tests were conducted by following the method reported by other researchers for membrane acid-stability characterization [11, 89], and the surface property changes were evaluated using SEM (scanning electron microscopy) as an observation of surface morphology, ATR-FTIR (attenuated total reflectance Fourier transform infrared spectroscopy) as a measurement of the chemical properties of the membrane surface, XPS (X-ray photoelectron spectroscopy) as a confirmation of atomic percentages' change, contact angle for surface's hydrophilicity, ToF-SIMS (Time-of-Flight Secondary Ion Mass Spectrometry) as a measurement of hydrolyzed functional group (carboxyl and amine group), and permeation experiments. To the best of our knowledge, this is the first study to use ToF-SIMS to evaluate changes in membrane properties after hydrolysis by acid. Furthermore, using density functional theory (DFT) calculation, we investigated the acid-catalyzed hydrolysis rate between piperazine-based polyamide membrane with MPD-based polyamide in terms of (1) calculation of reaction/transition-state energy during the acid-catalyzed hydrolysis, and (2) O/N- protonated twist angle (τ) of amide monomer, dimer, and trimer to study the effect of length of molecules on the twist angle.

3.2 Materials and methods

3.2.1 Chemicals and materials

Commercially available NE40, 70, and 90 thin-film composite (TFC) NF membranes were obtained from Toray Chemical Korea Inc (Korea) and used as a representative piperazine-based TFC NF polyamide membrane (NE40/70) and MPD-based TFC NF polyamide membrane (NE90). The base polysulfone (PSf) UF membrane used for comparison with the acid-hydrolyzed NF membrane was supplied by the Toray Chemical Korea Inc (Korea).

The following reagents were used without further purification: Sulfuric acid was purchased from DaeJung Chemicals (Korea) and the purity was 95%. Sodium chloride (NaCl) was obtained from Samchun Chemicals (Seoul, Korea), and magnesium sulfate ($\text{MgSO}_4 \cdot 7\text{H}_2\text{O}$) was purchased from Sigma-Aldrich for preparation of the permeation experiment. Milli-Q water (18 M Ω resistivity, Millipore®, Merck Millipore, Germany) was used as the solvent for soaking and rinsing the membrane samples as well as for preparing aqueous solutions.

3.2.2 Characterization of membranes

The membranes were exposed to the acid solution by to the methods reported by other researchers who conducted acid-resistance tests of membranes [11, 89]. The acid-soaking tests were conducted in Pyrex glass bottles with PTFE (polytetrafluoroethylene) cover. The TFC NF and UF membranes' coupons (10 × 15 cm²) were immersed in 1L of 15% (w/v) H₂SO₄ aqueous solution at 25 °C for 3, 7, 14, 28, and 63 Days. After that, the membrane samples were taken from the 15% sulfuric acid solution and rinsed thoroughly with de-ionized water, and then stored in Milli-Q water at room temperature until characterizations. Membrane samples for the analysis using SEM, ATR-FTIR, XPS, ToF-SIMS and goniometer were freeze-dried for at least 48 hrs in a vacuum freeze dryer (Biocryos, Korea); in contrast, wet membranes stored in Milli-Q water were used for measuring surface zeta potential and filtration performance.

3.2.2.1 Scanning electron microscopy (SEM)

Top surface images of the membranes were observed using Scanning Electron Microscopy (SEM) (Quanta 200, FEI, Hillsboro, OR, USA) to investigate the effect of acid- soaking on the surface

morphology of the membrane. The dried membrane was tightly mounted on a specimen by a carbon tape, then all samples were platinum coated at 20 mA and 2×10^{-3} mbar for 1 min in a Turbo Pumped High-Resolution Chromium Sputter Coater (K575X, EMITECH, Lohmar, Germany) to reduce image artifacts produced by electrostatic charge.

3.2.2.2 Attenuated total reflectance-Fourier transform infrared spectroscopy (ATR-FTIR)

Attenuated total reflectance-Fourier transform infrared spectroscopy (ATR-FTIR) was used to analyze the effect of acid-soaking on the chemical properties of the membrane surface using a Nicolet 6700 spectrometer (Thermo Scientific, Waltham, MA, USA) containing a flat plate germanium ATR crystal with an incident angle of 42° [90, 91]. OMNIC 8.1 software was used to apply the FTIR spectra, correct their baselines, and normalize the spectra. Dried membrane samples were scanned with nitrogen gas for purging continuously, and 64 scans of average spectra were calculated at wave numbers from 1000 to 4000 cm^{-1} with a resolution of 4 cm^{-1} for C=O stretching of both MPD-based amide and piperazine-based amide (1663 and 1634 cm^{-1} respectively).

3.2.2.3 X-ray photoelectron spectroscopy (XPS)

X-ray photoelectron Spectroscopy (XPS) (K Alpha, Thermo Scientific, USA) was applied to investigate the effect of acid-soaking on the change in the percentages of atoms in TFC NF membrane; these consisted of carbon (C), oxygen (O), nitrogen (N), and sulfur (S). Survey XPS spectra were measured by a sweeping range from 0 to 1000 eV of electron binding energy with a resolution of 1 eV. The X-ray beam penetrated about $5 \sim 10 \text{ nm}$ from the membrane surface for analysis of the elemental composition. In this work, the binding energy of C1s, O1s, N1s, S2s, and S2p was detected at 285, 531, 399, 231, and 167 eV, respectively [92].

3.2.2.4 Contact angle

Contact angle value of a membrane surface was confirmed to investigate effect of acid-soaking on surface's hydrophilicity by goniometer (Phoenix 300Plus, Surface & Electro Optics Co. Ltd., Korea). Contact angle of the membrane surface was measured by using sessile drops method. To obtain representative contact angles, 15 contact angle measurements were conducted on three separately prepared membranes coupons. All membrane samples were vacuum dried simultaneously during 48 hrs for same condition.

3.2.2.5 Zeta potential

Electrophoresis was performed to study the influence of acid-catalyzed hydrolysis on membrane surface charge according to the method published in our previous work [93]. Wet membrane samples kept in Milli-Q water over 1 Day were attached to a plate sample cell, then surface zeta potential of the membranes was measured using a 10mM NaCl electrolyte solution with polystyrene latex particles (diameter: 520 nm) (Otsuka Electronics, Osaka, Japan) from pH 3 to 9. The acidic or basic pH values were adjusted using 1N HCl or NaOH, respectively. The membranes' surface zeta potentials were measured three times by an electrophoretic light-scattering spectrophotometer (ELS-8000, Photal, Otsuka Electronics, Japan).

3.2.2.6 Time-of-flight secondary ion mass spectrometry (ToF-SIMS)

Fragments of the polymer before and after the acid-soaking test were detected by Time-of-Flight Secondary Ion Mass Spectrometry (ToF-SIMS) (TOF.SIM5, ION-TOF GmbH, Germany) in both positive-charge and negative-charge modes with a Bismuth gun (Bi^+). Analysis was performed under static conditions with a Bismuth (Bi^+) gun of 1 pA ion current and an energy of 25 keV. The ToF-SIMS spectra of the secondary ions were measured over mass ions (m/z) range from 0 to 100 or 120 in positive and negative mode, respectively. These lower masses range ions are much more matched exactly in ion abundance than higher masses [94]. The peak intensities of the secondary ions were normalized by total ion intensities detected in the spectrum to conduct qualitative comparison. Positive and negative mode was used to analyze the amine group and carboxyl group, respectively, because the amide group hydrolyzed to carboxyl and amine group through acid-catalyzed hydrolysis reaction as reported in already published research [79, 80, 87]. Table 3.2 shows the list of low-mass ions of elements and fragments, including carboxyl and amine groups that were detected by ToF-SIMS from the outermost surface of NE70/90 virgin and NE70 7 Days/NE90 63 Days membranes. Raw data for ToF-SIMS was sorted by Table 3.2 and reflected in Fig. 3.4 to compare the hydrolyzed amide groups in both NE70 and 90 membranes.

3.2.3 Permeation experiments of membrane soaked in acid

The TFC virgin NF membrane (NE40, 70, and 90) and acid-soaked membranes (3, 7, 14, 28, and 63 Days) were investigated to observe the effect of acid-soaking using a permeating test cells as described in another research [4]. Three membranes with 19.6 cm^2 effective area were tested at 1 L/min flow rates with 2,000 ppm concentration of NaCl or MgSO_4 as a feed single solution at room

temperature. The operating pressure for the permeation test was set to 150 psi for compaction during 1 hr, and then 75 psi for the performance test. The permeate water flux (J_w (L m⁻²h⁻¹ or LMH)) was measured after a 1 hr compaction step by mass change of the collected permeate sample in a Falcon tube at 25 °C per unit of effective membrane area and per unit time as shown in Eq. (3.1). The rejection, R (%), was calculated using single feed solution of 2,000 ppm NaCl or MgSO₄ (Eq. (3.2)). Rejection of ionic NaCl and MgSO₄ was determined based on the measurement of conductivity of the collected permeate and feed solution by a calibrated conductivity meter (Ultrameter IITM, Myron L Company, USA).

$$J_w = \frac{\Delta \text{ weight}}{\Delta \text{ time} \times \text{effective membrane area} \times \text{water density}} \left(\frac{\text{L}}{\text{m}^2\text{h}} \text{ or LMH} \right) \quad (3.1)$$

$$R = \left(1 - \frac{[\text{NaCl or MgSO}_4]_{\text{permeate}}}{[\text{NaCl or MgSO}_4]_{\text{feed}}} \right) \times 100 \text{ (\%)} \quad (3.2)$$

3.2.4 Computational calculation methods

3.2.4.1 Calculation details

The density functional theory (DFT) calculation was performed to elucidate the degradation mechanism of NE70 and NE90 polymer filters. All calculations were performed with the Dmol³ program, using the generalized gradient approximation (GGA) with the Perdew-Burke-Ernzerhof (PBE) functional to describe exchange-correlation energy [95-97]. All electron relativistic core treatment and 4.4 version of double numerical plus polarization (DNP) basis set were adopted to treat unreactive core-electron and atomic orbital basis sets, respectively. Spin polarized calculations were performed with the smearing value of 0.005 Ha. The convergence criteria for energy, force, and displacement were set to be 1.0×10⁻⁵ Ha, 0.002 Ha/Å, and 0.005 Å, respectively. The conductor-like screening model (COSMO) was implemented to every systems for the solution effect of water by applying the dielectric constant of 78.36 [98, 99].

Transition states (TS) of each reaction were found by complete single linear synchronous transit (LST) and quadratic synchronous transit (QST) methods [93, 100]. The LST method finds a transition state by linear interpolation of geometries between reactant and product to obtain an intermediate geometry having maximum energy. Subsequently, the energy minimization was followed in directions conjugate to the reaction pathway. The QST method, then, uses the intermediate geometry found by the LST method with three-point interpolation: an intermediate geometry, reactant, and product. These points were used for QST maximization, which was also followed by another energy minimization. This procedure continued until a stable point was located. In these calculations, the

threshold for the root mean square (RMS) forces on the atoms was set to be 0.01 Ha/Å. To confirm the transition state energy, TS optimization was repeated until only one imaginary vibrational mode was sought.

3.2.4.2 Model systems

The initial structures of monomers, dimers, and trimers of NE70 and NE90 were constructed by Conformers module in Materials Studio with the version of 2017R2 (Fig. 3.9) [101, 102]. COMPASS forcefield was adopted in this optimization, where the van der Waals and Coulomb interactions were treated using an atom-based cutoff distance of 12.5 Å [103, 104]. After initial molecular structures were constructed, the geometry optimization was performed by DFT calculations.

3.2.4.3 Out-of-plane deformation and energy calculations

To investigate the planarity of the amide bond, the degree of out-of-plane deformations (τ_D), where a smaller value represents a more stable resonance structure, was defined by following equation,

$$\tau_D = (Tor_{\cdot ABCD} + Tor_{\cdot A'BCD'}) / 2 \quad (3.3)$$

where $Tor_{\cdot ABCD}$ and $Tor_{\cdot A'BCD'}$ are the torsion angles of the set of atoms (*i.e.*, C1-N-C3-O and C2-N-C3-C4 for NE70, C1-N-C3-O and H-N-C3-C4 for NE90 in Fig. 3.10). Note that the term τ_D is often used to indicate the stability of molecules containing an amide bond [37, 38].

The degradation reactions of NE70 and NE90 were studied by calculating the changes of energy (ΔE) and Gibbs free energy (ΔG). ΔE represents the energy difference between the energy of the system at each step and that of Step 1 (Fig. 3.8 (a)), which we took as a reference value of the degradation mechanism, as shown below,

$$\Delta E = E - E_{\text{Step 1}} \quad (3.4)$$

ΔG of each system at $T = 25^\circ\text{C}$ was calculated as follows,

$$\Delta G^{25^\circ\text{C}} = \Delta H^{25^\circ\text{C}} - T\Delta S^{25^\circ\text{C}} \quad (3.5)$$

where $\Delta H^{25^\circ\text{C}}$ and $\Delta S^{25^\circ\text{C}}$ indicate the changes of enthalpy and entropy from Step 1, respectively. Thus, in an extended version, $\Delta G^{25^\circ\text{C}}$ can be expressed by

$$\begin{aligned}\Delta G^{25\text{ }^{\circ}\text{C}} &= H^{25\text{ }^{\circ}\text{C}} - H_{\text{Step 1}}^{25\text{ }^{\circ}\text{C}} - T(S^{25\text{ }^{\circ}\text{C}} - S_{\text{Step 1}}^{25\text{ }^{\circ}\text{C}}) \\ &= (U + PV)^{25\text{ }^{\circ}\text{C}} - (U + PV)_{\text{Step 1}}^{25\text{ }^{\circ}\text{C}} - T(S^{25\text{ }^{\circ}\text{C}} - S_{\text{Step 1}}^{25\text{ }^{\circ}\text{C}})\end{aligned}\quad (3.6)$$

where U is the molar internal energy, P is the pressure, V is the molar volume, and S is the molar entropy. By defining U' with motional degrees of freedom (*i.e.*, vibration (vib.), rotation (rot.), and translation (trans.)), the equation (3.6) can be rewritten as follows,

$$\Delta G^{25\text{ }^{\circ}\text{C}} = \Delta E + (U' + PV)^{25\text{ }^{\circ}\text{C}} - (U' + PV)_{\text{Step 1}}^{25\text{ }^{\circ}\text{C}} - T(S^{25\text{ }^{\circ}\text{C}} - S_{\text{Step 1}}^{25\text{ }^{\circ}\text{C}}) \quad (3.7)$$

where $U' = E_{\text{vib.}} + E_{\text{rot.}} + E_{\text{trans.}}$. Note that all terms are calculated once the system is optimized to the ground state.

3.3 Results and discussion

3.3.1 Characterization of membrane soaked in acid

3.3.1.1 Effect of sulfuric acid on morphology (SEM)

The surface morphological structures of NF membranes at various exposure time in aqueous acid were characterized by SEM images. Representative SEM images of the NF membranes are provided in Fig. 3.1, which shows that, the surface feature of the MPD-based NF virgin membrane appears to be the ridge-and-valley structure as general polyamide membrane [105]. Piperazine-based NE40/70 membranes were either smoother or grainier than the MPD-based NE90 membrane [105], because roughness has a strong correlation with amine monomer's solubility and slightly diffusivity [9], and the piperazine used in NF 40/70 has a low solubility/diffusivity in the organic solution (TMC). Compared to the MPD-based NE90 membrane, piperazine-based NE40/70 membranes' surface peeled off from the support layer after soaking in acid for 14 Days. These SEM images show that the MPD-based NE90 membrane has better acid-stability than the piperazine-based NE40/70 membranes.

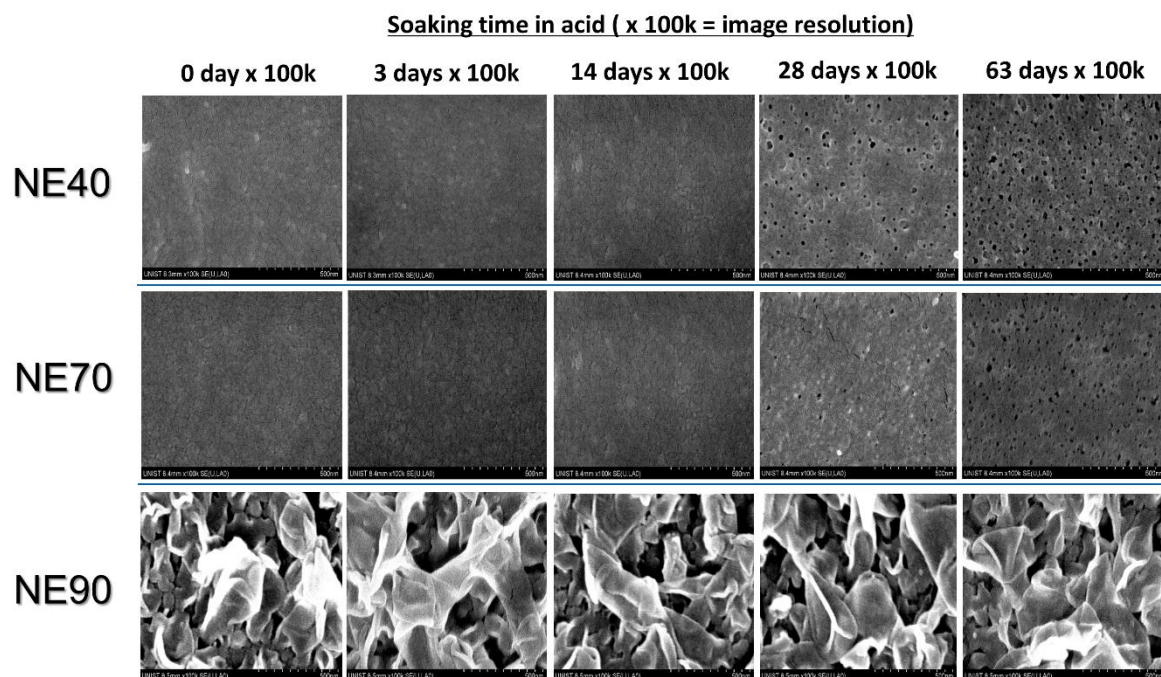


Figure 3.1 Surface morphology observed by SEM for NF membranes versus exposed time in aqueous acid solution.

3.3.1.2. Chemical surface property change of polyamide NF membrane by sulfuric acid

ATR-FTIR spectra were measured for investigation of the effect of acid solution on NF membranes. Figure 3.2 shows spectra of (a) NE40, (b) NE70, and (c) NE90 NF polyamide membrane from 1000 cm^{-1} to 4000 cm^{-1} , where related to the membrane polyamide active layer as well as the underlying PSf support layer as a result of the relatively large penetration depth of the IR [106]. Absorbance peaks at wavenumbers 1634 and 1663 cm^{-1} are attributed to the amide (I) band of poly(piperazineamide) and fully aromatic polyamide NF membrane, respectively [92]. PSf peaks at 1587 and 1488 cm^{-1} were measured in all NF virgin membrane [107], which clearly proved that PSf was used as a support layer for the NE40, 70, and 90 membranes. Furthermore, in the case of NE40/70 membranes, decreasing C=O stretching amide bond peak with increasing acid-soaking time supports that MPD-based NE90 membrane has better acid-stability than piperazine-based NE40/70 membrane as correlated results to surface morphology result in section 3.3.1.1.

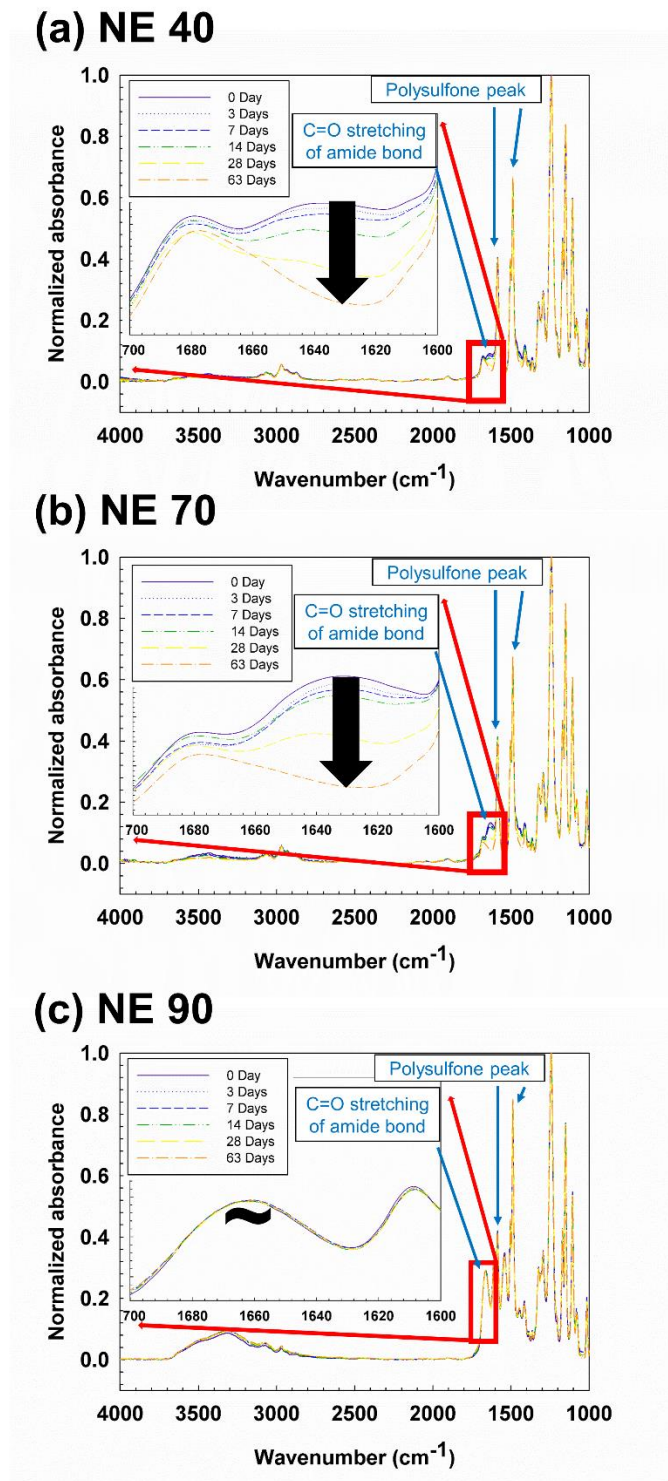


Figure 3.2 ATR-FTIR spectra of virgin and acid hydrolyzed membranes: (a) NE40, (b) NE70, and (c) NE90 NF polyamide membrane from 1000 cm^{-1} to 4000 cm^{-1} . Absorbance was normalized to compare intensity for investigation of effect of acid solution on NF membranes.

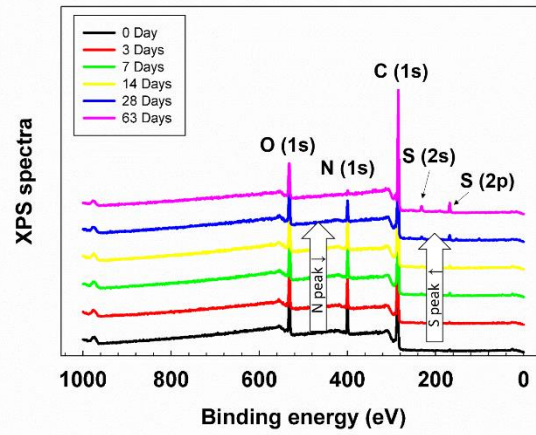
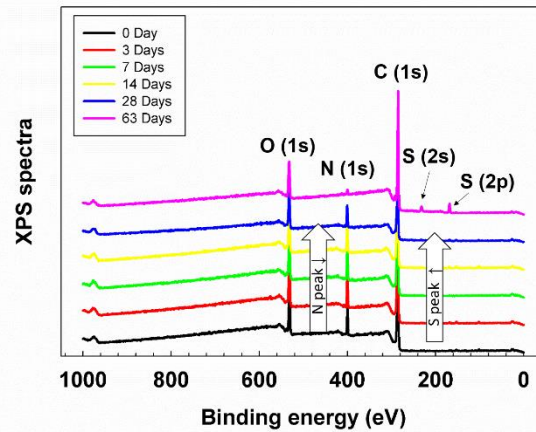
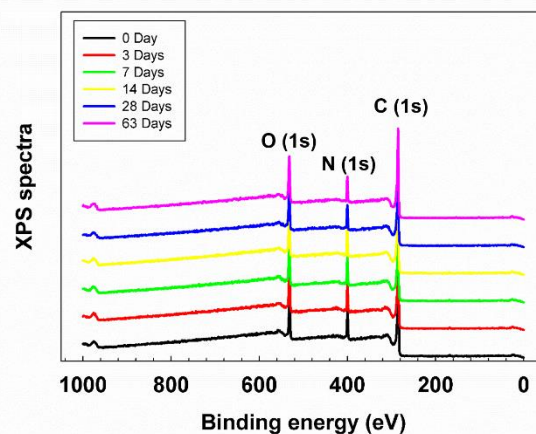
(a) NE40**(b) NE70****(c) NE90**

Figure 3.3: XPS spectra of (a) NE40, (b) NE70, and (c) NE90 NF polyamide membrane with increasing acid-soaking time.

XPS spectra were measured to investigate the percentages' change of atoms in TFC NF membranes (i.e., carbon (C), oxygen (O), nitrogen (N), and sulfur (S)) resulted from the exposure of the membranes to acid. Hydrogen (H) was not included in the XPS result, because XPS is not suitable for analyzing hydrogen atoms. Figure 3.3 contains XPS spectra versus binding energy of (a) NE40, (b) NE70, and (c) NE90 NF polyamide membranes in the range of 0 to 1,000 (eV) at various acid-soaking times. The binding energy of C1s, O1s, N1s, S2s, and S2p was detected at 285, 531, 399, 231, and 167 eV, respectively [92]. XPS peaks at binding energy 231 and 167 eV are attributed to the sulfur atoms, and these sulfur peaks were measured only in piperazine-based membranes (NE40/70) after soaking in acid for 28 Days. As ATR-FTIR results, these sulfur peaks were from the PSf support layer of the membrane, showing the peeling-off of the active layer on NF40/70 and proving better chemical stability in MPD-based polyamide membrane (NE90) than piperazine-based polyamide membranes. Table 3.1 summarizes quantitative values of the relative atomic concentrations (C, O, N, and S) as well as the composition ratios of polyamide NF membranes (virgin versus 63 Days soaking in acid). The molecular formulas of fully cross-linked or fully linear MPD-based polyamide are $C_{21}H_{16}O_3N_4$ and $C_{15}H_{10}O_4N_2$, respectively. Thus, theoretical C/O and N/O atomic ratios should exist in the range of 3.75~7 or 0.5~1.33 for C/O and N/O, respectively. For the piperazine-based fully aromatic polyamide, the molecular formula of fully cross-linked or fully linear polyamides are $C_{17}H_{19}O_3N_4$ and $C_{12}H_{12}O_4N_2$, respectively. Hence, theoretical C/O and N/O atomic ratios should exist in the range of 3~5.67 and 0.5~1.33 for C/O and N/O, respectively. As shown in Table 3.1, all virgin NF membranes exist between theoretical fully cross-linked and fully linear polyamides. However, NE40/70 63 Days sample of C/O atomic ratio is 6.6 and 6.5, respectively, and the range beyond the theoretical value resulted from PSf support layer. As explained in section 3.3.1.1 and the ATR-FTIR results, these C/O atomic ratios showed almost the same values as the PSf's monomer, which has a $C_{27}H_{20}O_4S$ formula with 6.75 C/O atomic ratio.

Table 3.1 Relative atomic concentrations (C, N, O, and S) and composition ratios of polyamide NF membranes (virgin versus 63 Days soaking in acid)

Membrane	Carbon (atomic %)	Oxygen (atomic %)	Nitrogen (atomic %)	Sulfur (atomic %)	C/O	N/O
NE40, virgin	73.0	15.3	11.7	~0	4.8	0.76
NE40, 63 Days	82.2	12.4	1.4	4.0	6.6	0.11
NE70, virgin	72.7	16.0	11.3	~0	4.5	0.71

NE70, 63 Days	82.2	12.6	1.8	3.4	6.5	0.14
NE90, virgin	74.7	14.4	10.9	~0	5.2	0.76
NE90, 63 Days	74.6	15.1	10.3	~0	4.9	0.68

Surface morphology (SEM images), ATR-FTIR, and XPS results supported that piperazine-based NE40/70 membrane has less chemical stability than MPD-based NE90 membrane. A ToF-SIMS experiment was, also, conducted to explain acid-catalyzed hydrolysis of the polyamide bond. An amide bond can be hydrolyzed to carboxyl and amine groups through acid-catalyzed hydrolysis reaction [79, 80, 87]. Table 3.2 shows a list of fragments which were detected by ToF-SIMS from the outermost surface of virgin and hydrolyzed NE70 and NE90 membranes in both negative ((I) for carboxyl group)) and positive ((II) and (III) for amine group) mode. The hydrolyzed NE70 membrane was exposed to the sulfuric acid for 7 Days, on the other hand, NE90 membrane was soaked in the acid solution for 63 Days.

Table 3.2 List of fragments which were detected by ToF-SIMS from the outermost surface of virgin and hydrolyzed membranes of NE70 and NE90 in negative (I) and positive mode (II and III).

(I) Carboxyl group-related fragments from virgin and hydrolyzed membranes of NE70/90 (NE70 and NE90 were exposed to acid for 7 Days and 63 Days, respectively)				
OH ⁻	CHO ⁻	CHO ₂ ⁻	C ₂ O ₂ ⁻	C ₂ HO ₂ ⁻
C ₃ O ₂ ⁻	C ₃ HO ₂ ⁻	C ₃ H ₂ O ₂ ⁻	C ₄ O ₂ ⁻	C ₄ HO ₂ ⁻
C ₄ H ₂ O ₂ ⁻	C ₄ H ₃ O ₂ ⁻	C ₅ O ₂ ⁻	C ₅ HO ₂ ⁻	C ₅ H ₂ O ₂ ⁻
C ₅ H ₃ O ₂ ⁻	C ₆ O ₂ ⁻	C ₆ HO ₂ ⁻	C ₆ H ₂ O ₂ ⁻	C ₆ H ₃ O ₂ ⁻
C ₇ O ₂ ⁻	C ₇ HO ₂ ⁻	C ₇ H ₂ O ₂ ⁻	C ₇ H ₃ O ₂ ⁻	C ₇ H ₄ O ₂ ⁻
(II) Amine group-related fragments from both virgin and hydrolyzed NE70 (NE70 was exposed to acid for 7 Days)				
NH ⁺	CN ⁺	CHN ⁺	CH ₂ N ⁺	CH ₃ N ⁺
C ₂ N ⁺	C ₂ HN ⁺	C ₂ H ₂ N ⁺	C ₂ H ₃ N ⁺	C ₂ H ₄ N ⁺

$C_2H_5N^+$	C_3N^+	C_3HN^+	$C_3H_2N^+$	$C_3H_3N^+$
$C_3H_4N^+$	$C_3H_5N^+$	$C_3H_6N^+$	$C_3H_7N^+$	C_4N^+
C_4HN^+	$C_4H_2N^+$	$C_4H_3N^+$	$C_4H_4N^+$	$C_4H_5N^+$
$C_4H_6N^+$	$C_4H_7N^+$	$C_4H_8N^+$	$C_4H_9N^+$	$C_4N_2^+$
$C_4HN_2^+$	$C_4H_2N_2^+$	$C_4H_3N_2^+$	$C_4H_4N_2^+$	$C_4H_5N_2^+$
$C_4H_6N_2^+$	$C_4H_7N_2^+$	$C_4H_8N_2^+$	$C_4H_9N_2^+$	
(III) Amine group-related fragments from both virgin and hydrolyzed NE90 (NE90 was exposed to acid for 63 Days)				
NH^+	NH_2^+	CN^+	CHN^+	CH_2N^+
C_2N^+	C_2HN^+	$C_2H_2N^+$	$C_2H_3N^+$	C_3N^+
C_3HN^+	$C_3H_2N^+$	$C_3H_3N^+$	$C_3H_4N^+$	C_4N^+
C_4HN^+	$C_4H_2N^+$	$C_4H_3N^+$	$C_4H_4N^+$	$C_4H_5N^+$
C_5N^+	$C_5H_1N^+$	$C_5H_2N^+$	$C_5H_3N^+$	$C_5H_4N^+$
$C_5H_5N^+$	C_6N^+	C_6HN^+	$C_6H_2N^+$	$C_6H_3N^+$
$C_6H_4N^+$	$C_6H_5N^+$	$C_6H_6N^+$		

Figure 3.4 summarizes the ToF-SIMS spectra of virgin and hydrolyzed NE70 and NE90 membranes in terms of mass to charge ratio (m/z) from 0 to 100 or 120 in positive and negative mode, respectively, because the lower masses range ions is well-matched in ion abundance than higher masses [94]. Figure 3.4 (a) and (c) shows the results in positive mode and Fig. 3.4 (b) and (d) in negative mode. More fragments could be detected if the polymer contains more of the specific molecule on the its outermost surface. Here, the NE70 membrane sample which was hydrolyzed by acid for 7 Days was investigated in ToF-Sims study as a representative hydrolyzed NE70 membrane, since further exposure for more than 7 Days makes the active skin polyamide layer of the NE70 peel off, as already observed by SEM, ATR-FTIR, and XPS study. When NE70 virgin membrane was compared with NE70 7 Days membrane in positive and negative mode (Fig. 3.4 (a) and (b)), the peak of 32 fragments out of a total of 39 fragments related to an amine group and 24 fragments out of a total of 25 fragments related to a carboxyl group increased. 56 fragments out of a total of 64 (about 88%) related to amine and carboxyl groups increased their intensities after exposure of the NE70 membrane to sulfuric acid for 7 Days. This

means that there is high possibility of increased number of amine and carboxyl groups by acid-catalyzed hydrolysis and the results are in good agreement with other researches [79, 80, 87]. However, when NE90 virgin membrane was compared with the membrane hydrolyzed for 63 Days in positive and negative mode (Fig. 3.4 (c) and (d)), the secondary ions' peak of 16 fragments out of 33 total fragments related to the amine group and 12 fragments out of 25 total fragments related to the carboxyl group increased. Hence, 28 fragments out of a total of 58 related to both amine/carboxyl group (about 48%) increased after soaking in acid for 63 Days. The NE90 membrane soaked for 63 Days in acid did not show the symptom of increased number of amine and carboxyl groups that resulted from acid-catalyzed hydrolysis. The NE90 membrane showed greater chemical stability than the NE70 membranes.

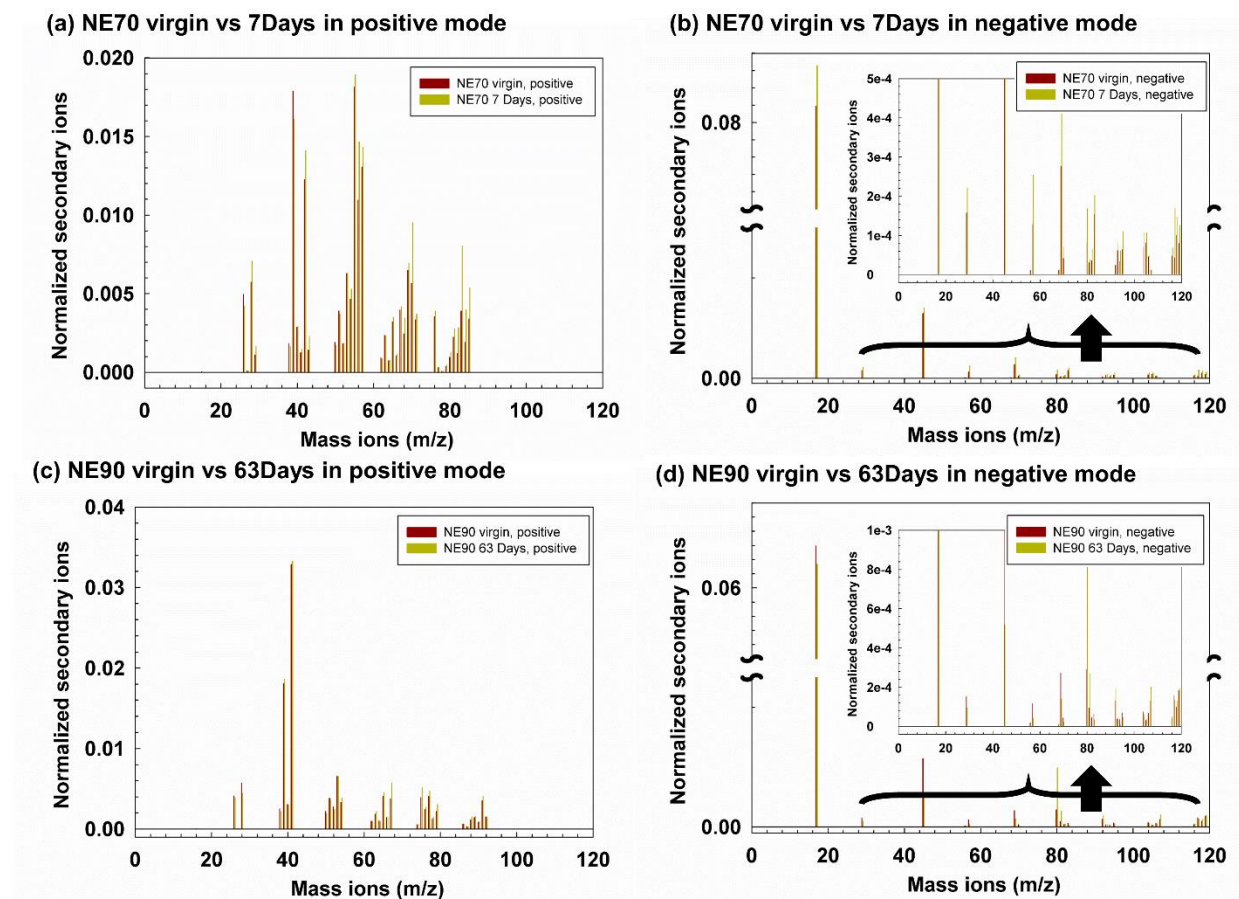


Figure 3.4 The ToF-SIMS spectra of virgin NE70 and NE90 membranes, hydrolyzed NE70 for 7 Days and hydrolyzed NE90 for 63 Days.

3.3.1.3 Effect of sulfuric acid on hydrophilicity and surface charge of polyamide NF membranes

The contact angle value of an NF membranes' surface was investigated to observe the effect of acid-soaking on the hydrophilicity of the membrane surface (Fig. 3.5). There was no observed influence of acid aqueous solution on the hydrophilicity of the MPD-based polyamide NE90 membrane, and this results are well compatible with the results showing high chemical stability of the membrane in sections 3.3.1.1 and 3.3.1.2. However, in the case of piperazine-based NE40 and NE70 membranes, the contact angle value slightly decreased until soaking time of 14 or 28 Days in acid and then increased until soaking time of 63 Days in acid. According to another research that reported the effect of charge on hydrophilicity [108], the hydrophilicity of the membranes increases (contact angle decreases) when the membranes are positively or negatively charged. The phenomenon, the more charged forms of the carboxylic acid or amine functional group is on the surface of the membrane the more hydrophilic the membrane become, the more hydrophilic than the neutral form, were also used to measure pK_a of membrane surface using contact angle titration [109]. Wamser, C.C. et. al [109] reported the pK_a value of surface carboxyl and amine functional groups was 6.8 and 9.3, respectively. Likewise, the contact angle value of NE40 and NE70 membrane sample monotonically decreased with soaking in acid until 14 or 28 Days, because the number of amine and carboxyl groups increased by acid-catalyzed hydrolysis of the amide bond, as shown in the ToF-SIMS result (Fig. 3.4). The contact angle value of the NE40/70 membranes continuously increased with increasing soaking time in acid from 14 or 28 Days to 63 Days due to hydrophobic PSf UF membrane ($\sim 68^\circ$) [110] as was already explained in the SEM, ATR-FTIR, and XPS results.

Electrophoresis zeta potential was measured to prove the change of membrane surface charge by acid-catalyzed hydrolysis. Figure 3.6 shows surface zeta potential of the (a) NE70 virgin and NE70 7 Days, and (b) NE90 virgin and NE90 63 Days. The surface of the NE70 PA membrane became more negative below the isoelectric point (IEP, \sim pH 4) and positive above IEP due to the protonation or deprotonation of the carboxyl group and amine group of piperazine, respectively [111]. The absolute value of the zeta potential increased after acid-catalyzed hydrolysis (with maintained IEP), because the acid-catalyzed hydrolysis of amides produced more positive charge of the amine groups and more negative charge of the carboxyl groups on the membrane surface. This result is in good agreement with the contact angle results (Fig. 3.5).

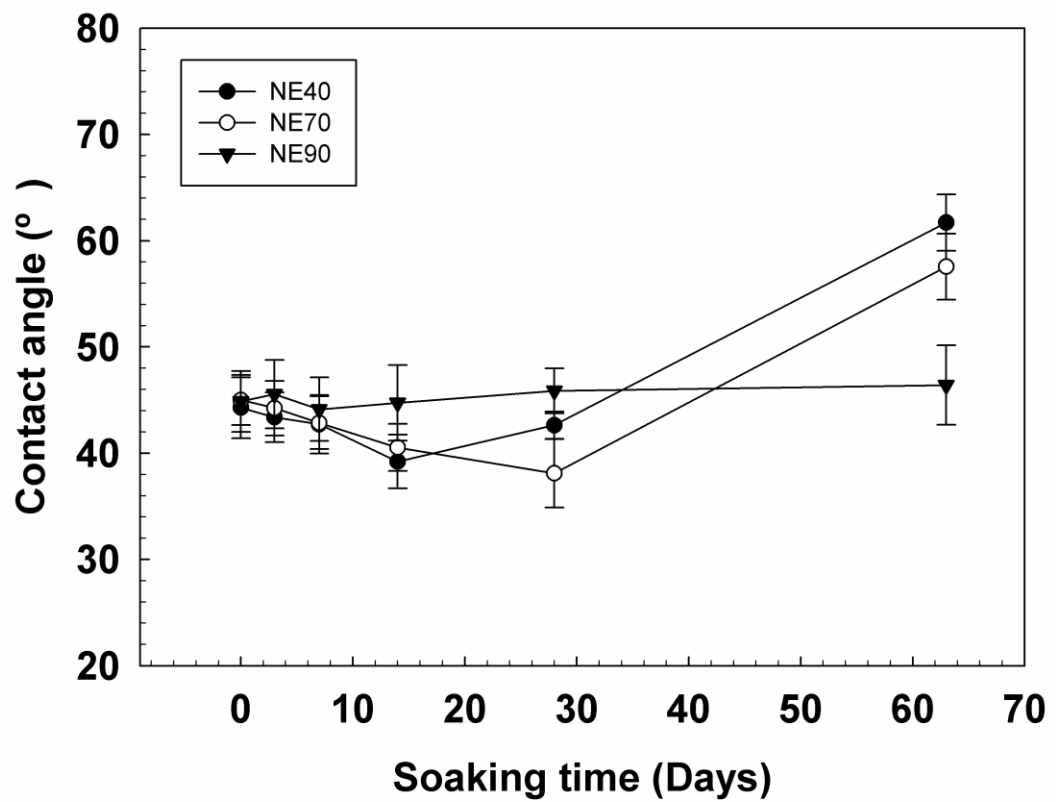
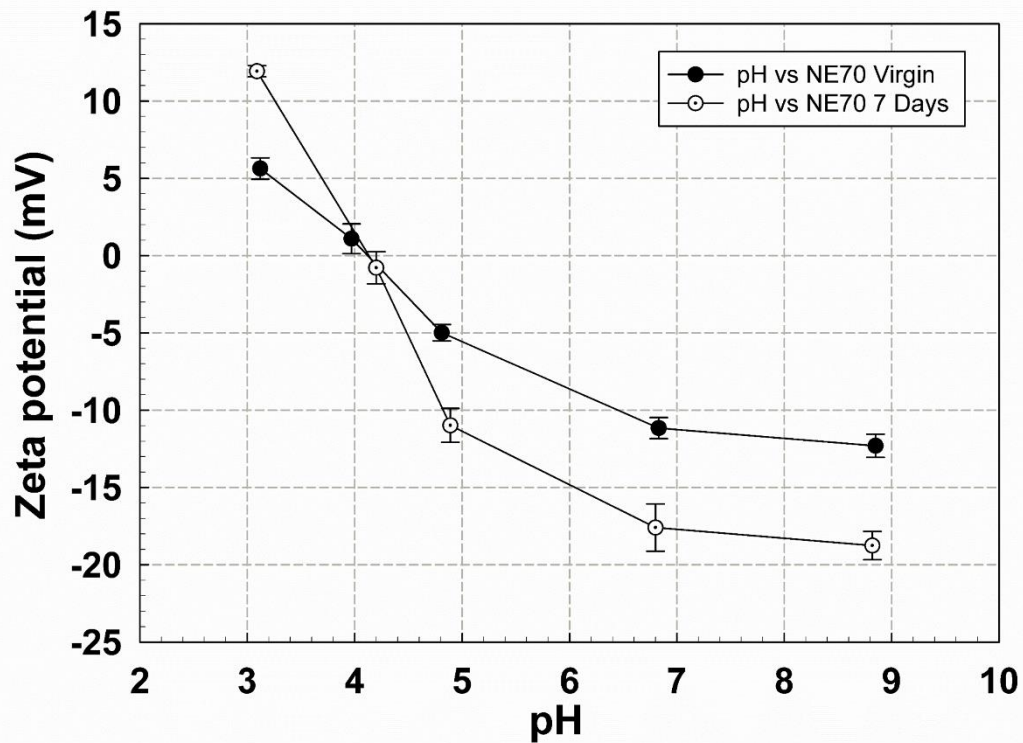


Figure 3.5 Comparison of measured surface contact angles of NF membranes along with increasing acid-soaking time.

(a) NE70 virgin vs 7 Days



(b) NE90 virgin vs 63 Days

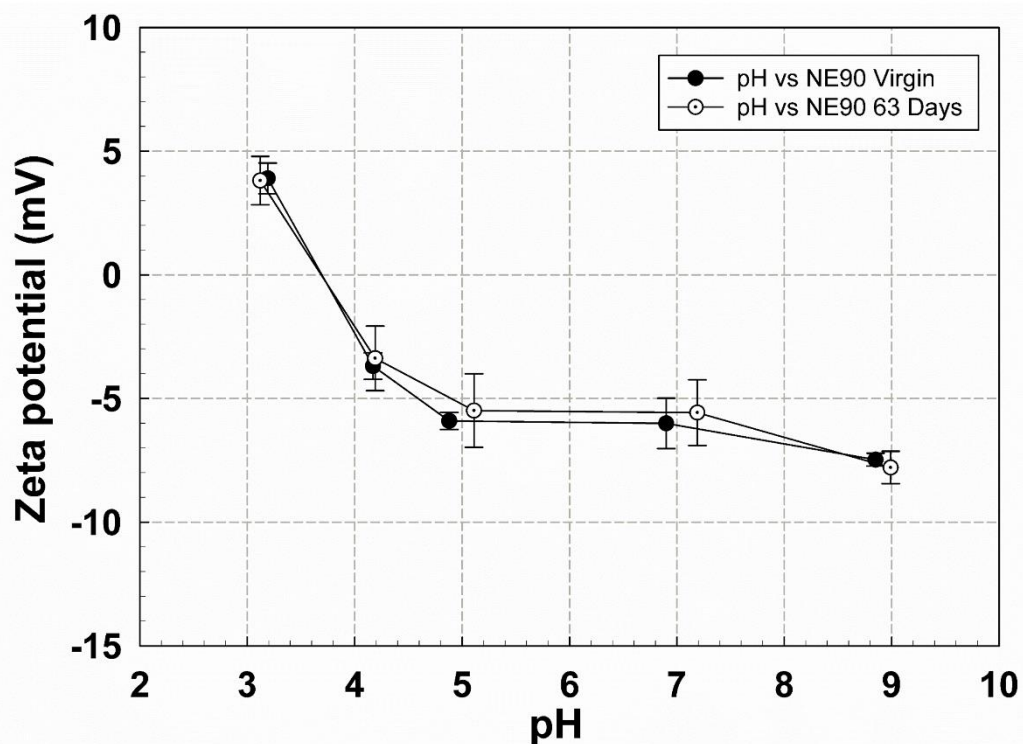
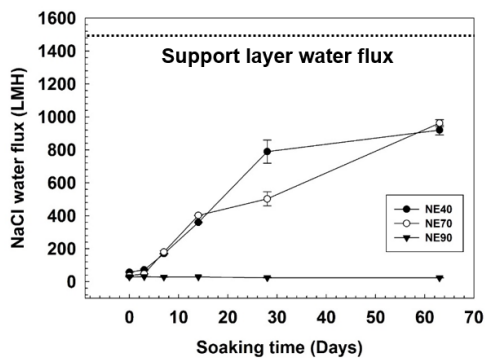


Figure 3.6 Zeta potential of the (a) NE70 virgin and NE70 7 Days, and (b) NE90 virgin and NE90 63 Days.

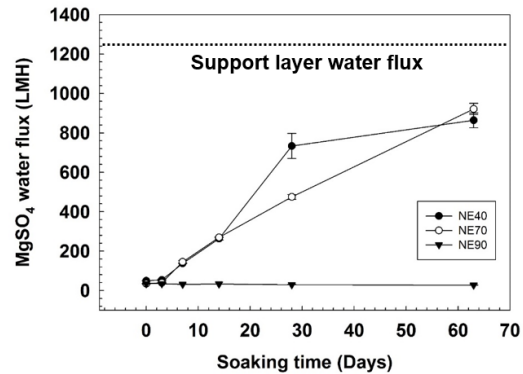
3.3.2 Permeation of the virgin and hydrolyzed membranes

The performance of TFC virgin NF membranes (NE40, 70, and 90) and acid-soaked membranes (3, 7, 14, 28, and 63 Days) were investigated in order to study the effect of acidic soaking on the membrane performance. Permeation properties (water flux and rejection) of NF membranes at various exposure times to acid are shown in Fig. 3.7. Water flux of piperazine-based NE40 and NE70 membranes dramatically increased with increasing exposure to acid in the case of both NaCl and MgSO₄ feed solutions (Fig. 3.7 (a) and (b)). The rejection of NaCl and MgSO₄ became close to 0% after only exposed to 7 Days in acid (Fig. 3.7 (c) and (d)). On the other hand, MPD-based NE90 membrane maintained both water flux and salt rejection (Fig. 3.7 (a) ~ (d)). The permeation properties of the PSf support layer are hardly affected by acid due to its high chemical stability [42], as shown in Table 3.3. In other words, hydrolyzed NE40/70 membrane's water flux was close to the support layer's water flux with increasing exposure time in acid (Fig. 3.7). The permeation properties in Fig. 3.7 proved MPD-based NE90 membrane has higher chemical stability than piperazine-based NE40 or NE70. Different chemical stability between piperazine-based and MPD-based NF membranes was investigated in section 3.3.3 using computational analysis in terms of both reaction energy and twist angle.

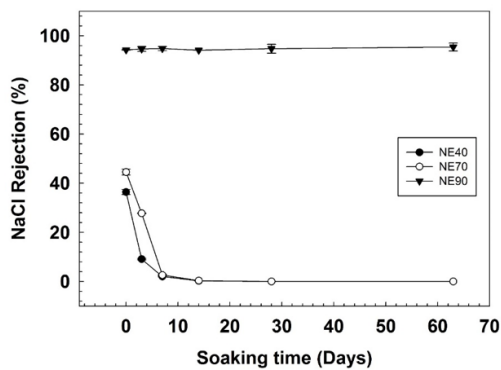
(a) NaCl water flux



(b) MgSO₄ water flux



(c) NaCl Rejection



(d) MgSO₄ Rejection

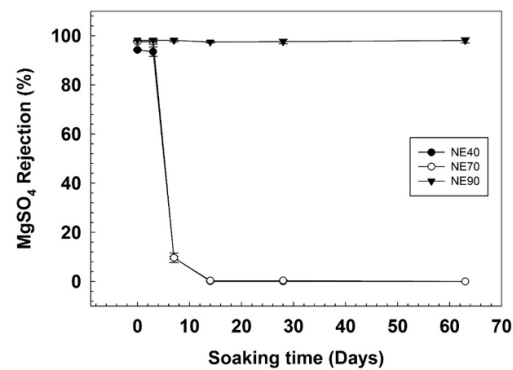


Figure 3.7 Permeation properties (water flux and rejection) of NF membranes with increasing acid-soaking time (tested at 75 psi, using 2,000 ppm NaCl or MgSO₄ single solution).

**Table 3.3 Permeation properties (water flux and rejection)
of polysulfone support layer UF membranes with increasing acid-soaking time
(tested at 75 psi, using 2,000 ppm NaCl or MgSO₄ single solution).**

Support layer soaked time in acid	0 Day (Virgin)	27 Days	63 Days
NaCl, flux (LMH)	1504 ± 57	1546 ± 25	1477 ± 69
MgSO ₄ , flux (LMH)	1228 ± 33	1199 ± 59	1193 ± 40
NaCl, rejection (%)	~0	~0	~0
MgSO ₄ , rejection (%)	~0	~0	~0

3.3.3 Computational analysis to interpret degradation of NE70 and NE90

In an acidic condition, the amide bond spontaneously protonates [81]. Our calculation results also showed the spontaneous protonations of oxygen and nitrogen in NE70 and NE90 (Step 1 to Step 2 in Fig. 3.8 (a) and (b)). As seen from other molecules containing a planar amide bond [37, 38], the protonation of oxygen was more energetically favorable, since the protonation of N induced a large deformation of the resonance structure, whereas the protonation of oxygen had little impact on the resonance structure as indicated by the small change in τ_D (Fig. 3.11 (a) and (b)). Interestingly, the most optimal protonation was found to be the protonation of oxygen in NE70, followed by that of nitrogen in NE70. Also, we found that the energy difference was correlated with τ_D at the initial state (Step 1 in Fig. 3.8), which indicates the stability of resonance structure in amide bond. For the nitrogen case, τ_D was already larger in NE70 at the initial state than NE90, so NE70 was more easily protonated due to the unstable resonance in the amide bond.

The second reaction was the dissociative adsorption of the H₂O molecule at the amide bond, which was turned out to be the rate determining step (RDS) of the degradation mechanism (Step 2 to Step 3 in Fig. 3.8 (a) and (b)). At this reaction, the highest energy barrier was found in the case of NE70(O) (*i.e.*, 42.62 kcal/mol) while the energy barrier was similar in NE90(O) (*i.e.*, 39.61 kcal/mol) and NE90(N) (*i.e.*, 39.06 kcal/mol). The lowest energy barrier was calculated in the NE70(N) (*i.e.*, 34.17 kcal/mol) with the lowest endothermic heat of reaction, so that the degradation of NE70(N) was expected to be the highest. We notify that the lowering degree of the energy barrier of NE70(N) well offsets the higher value of NE70(O). As C3 is the adsorption site for OH⁻ dissociated from H₂O, the deformation of the resonance structure mostly occurs at this carbon (Fig. 3.10). Therefore, τ_D at the protonated state (*i.e.*, Step 2) could be still used as a descriptor to indicate the stability for this reaction, which was readily seen by the linear correlation of the activation energy with τ_D (Fig. 3.11 (c)).

Lastly, the deformation of the C-N bond was an exothermic reaction (Step 3 to Step 4 in Fig. 3.8 (a) and (b)). The energy barrier for this reaction was calculated to be 13.54 kcal/mol and 5.68 kcal/mol for the cases of NE70 and NE90, respectively, since the length of the C-N bond was shorter for the case of NE70 (*i.e.*, 1.582 Å) than NE90 (*i.e.*, 1.655 Å) at Step 3. However, we presume that the difference of the energy barriers at Step 3 to Step 4 does not change the overall degradation tendency, since the RDS occurs at that reaction environment. Also, we note that in addition to investigating the monomers, the dimers and trimers of NE70 and NE90 (Fig. 3.9 and 3.11) were also tested to observe the trend of structural changes in the longer chain. With the initial values of τ_D 's, their varying trends by protonations were maintained. Thus, we conjecture that the predicted degradation reaction is highly plausible to show the degradation of the polymer. In conclusion, the degradation of NE70 proceeds relatively fast compared to NE90 for its easier protonation and the lowest energy barrier (*i.e.*,

thermodynamic dominance of nitrogen protonated) in RDS.

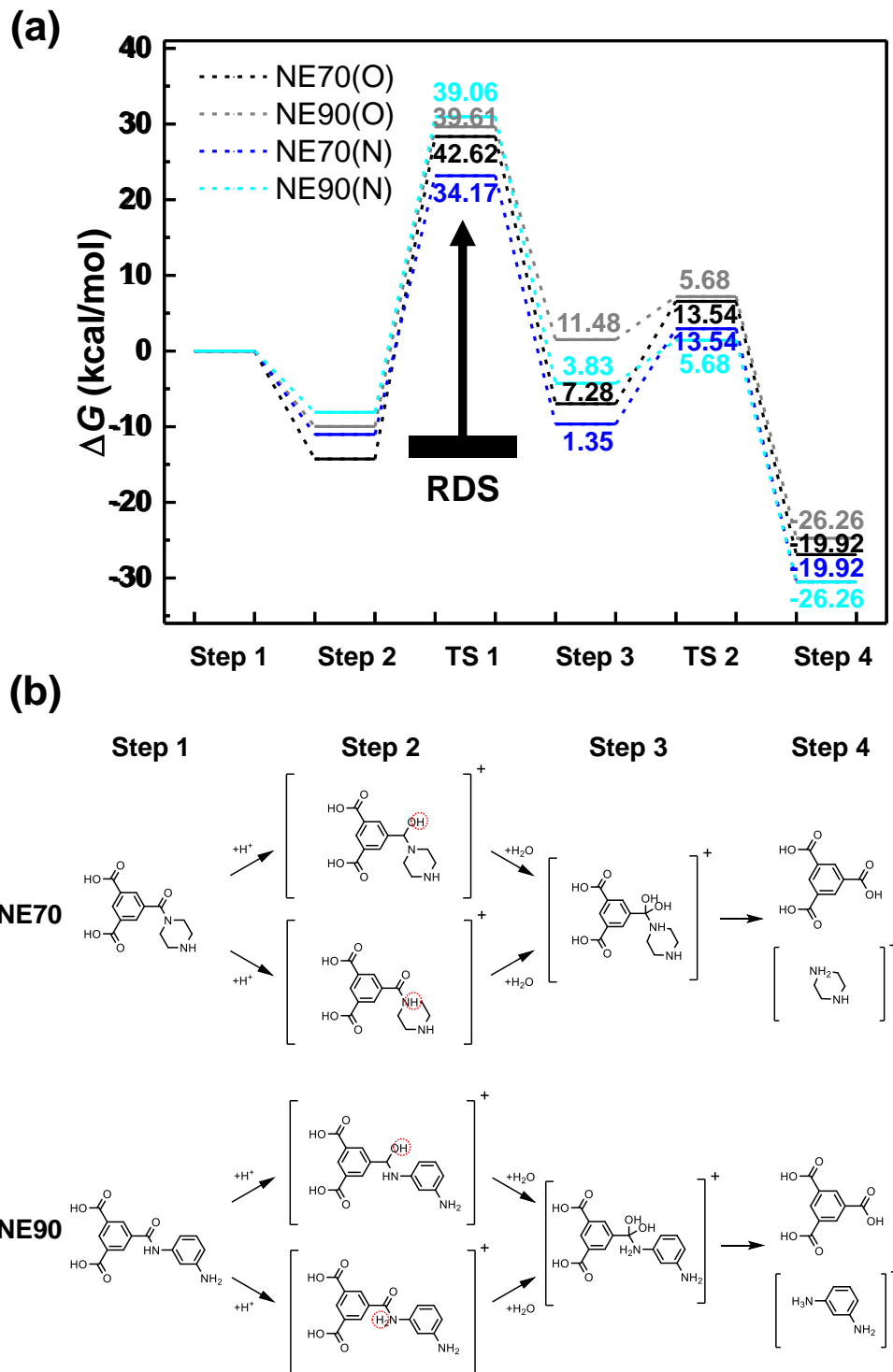


Figure 3.8 (a) Change of Gibbs free energy (ΔG at $T = 25^\circ\text{C}$) diagram of the degradation reactions of NE70 and NE90. The colored values at transition states (TS 1 and TS 2) in the graph indicate the energy barrier for the reaction, and the colored values at Step 3 and Step 4 indicate the relative Gibbs free energy of the product to the reactant. O and N in parentheses indicate the protonated sites. (b) Schematic reaction mechanism. Red-dotted circles indicate the protonated sites.

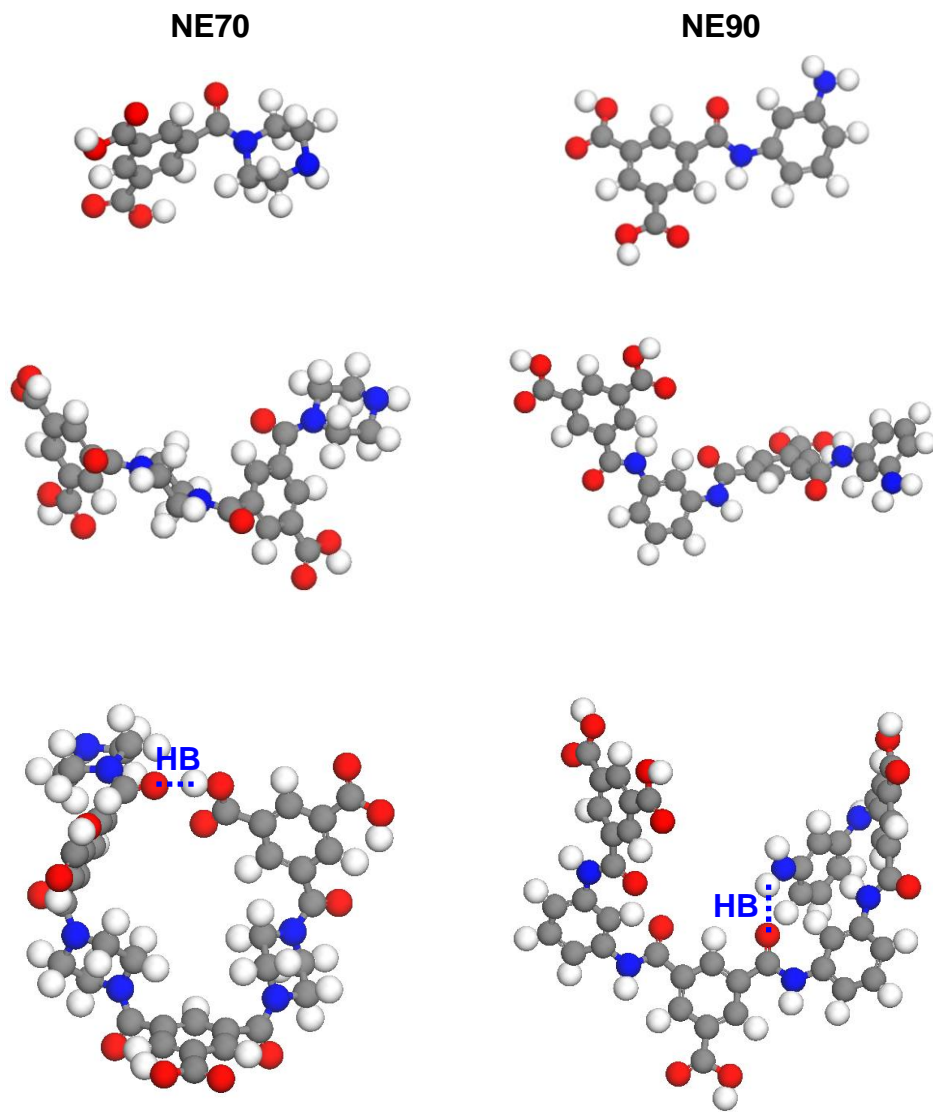


Figure 3.9 From top to bottom, monomer, dimer and trimer of NE70 and NE90 are presented, respectively. Blue dashed line indicates intermolecular hydrogen bonding (HB). Carbon, hydrogen, oxygen and nitrogen atoms are colored gray, white, red, and blue, respectively.

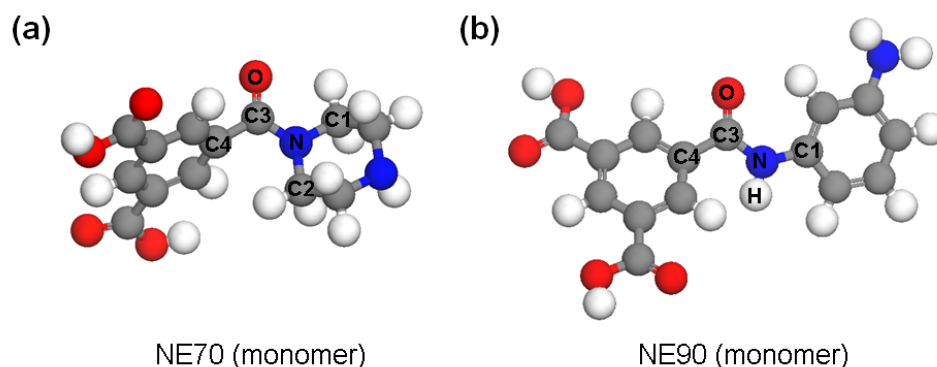


Figure 3.10 The monomer structures of NE70 (a) and NE90 (b). Out-of-plane deformations (τ_D) values are calculated from the sets of atoms as follows; For NE70, τ_D : C1-N-C3-O, C2-N-C3-C4 and for NE90, τ_D : C1-N-C3-O, H-N-C3-C4.

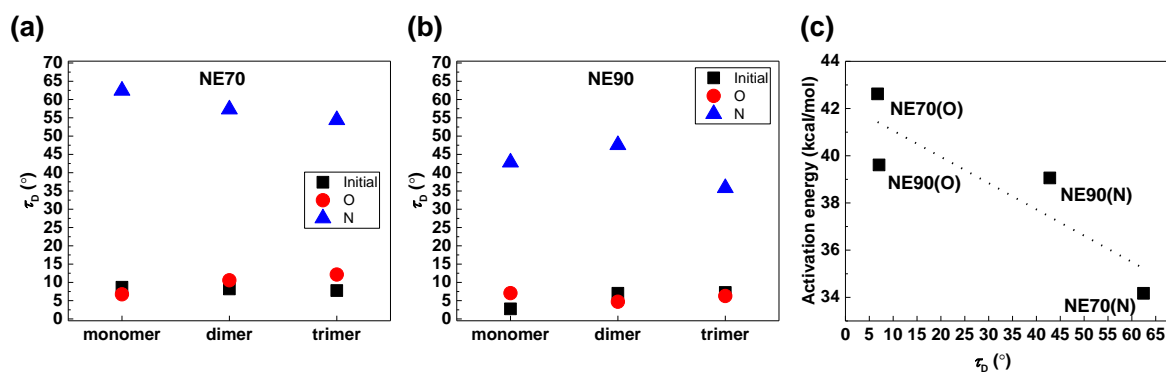


Figure 3.11 Out-of-plane deformations (τ_D) profiles of NE70 (a) and those of NE90 (b). O and N indicate the N protonated and O protonated structures of NE70 and NE90, respectively. Note that τ_D 's of dimer and trimer were calculated by averaging the values of each protonated site. (c) The correlation between activation energy at the rate determining step (*i.e.*, Step 2 to Step 3 in Fig. 3.8 (a)) and τ_D at Step 2 (Fig. 3.8 (a)). The dotted line indicates a linear trend line. O and N in parenthesis indicate the protonated sites.

3.4 Conclusions

In this work, commercially available NF polyamide TFC membranes fabricated by amine monomer (piperazine or MPD) with acyl chloride (TMC) was systemically investigated in view of the effect of acidic aqueous solution (15wt% sulfuric acid) on the membrane's physical and chemical properties. Surface morphology (SEM images), ATR-FTIR, XPS, and permeation experimental results supported that piperazine-based NE40/70 membrane has relatively lower chemical stability than MPD-based NE90 membrane. Additionally, a ToF-SIMS experiment showed the conversion of an amide group to carboxyl and amine groups by acid-catalyzed hydrolysis. These converted carboxyl and amine groups decreased the contact angle and increased the absolute value of the zeta potential on the surface of NE40 and NE70 membranes. Piperazine-based NE40 and NE70 membranes had relatively lower chemical stability than MPD-based NE90 membrane, since piperazine-based amide's monomer having N-protonation state (NE70 (N)) had the lowest energy barrier in the RDS step. These results are well correlated with surface characterization results. These energy barrier results in RDS had a close relationship with protonated amides' twist angle (τ_D), and the tendency of the twist angle was also maintained in longer molecules (dimer and trimer). The results of our study showed that the semi-aromatic membrane (NE40/70) is less chemically stable than the aromatic membrane (NE90) in terms of various surface characterization and DFT calculation results.

***Degradation of full aromatic polyamide NF
membrane by sulfuric acid and hydrogen halides:
Change of the surface/permeability properties***

This chapter has been submitted:

Byung-Moon Jun, Hyung Kae Lee, Young-Nam Kwon*,

'Degradation of full aromatic polyamide NF membrane by sulfuric acid
and hydrogen halides:Change of the surface/permeability properties',

Journal of Membrane Science (MEMSCI_2017_3148)

Abstract

We systematically investigated the effects of both sulfuric acid (pH 0 to 2) and hydrogen halides (pH 0) on the physical, chemical, and performance properties of full aromatic nanofiltration (NF) polyamide (PA) NE90 membrane. Surface characterizations of the degraded membranes were conducted by Scanning Electron Microscopy (SEM), Attenuated Total Reflectance-Fourier Transform Infrared spectroscopy (ATR-FTIR), X-ray photoelectron spectroscopy (XPS), goniometer, and zeta potential analyzer. No noticeable changes were observed in the surface properties of the membrane exposed to sulfuric acid; however, the permeable characteristics were changed due to the distortion of hydrogen bonding from additionally generated proton bridge for O-protonation and the formation of tetrahedral structure for N-protonation. On the other hand, the membrane's physico-chemical properties were much affected by hydrogen halides compared with sulfuric acid. Amide peaks N-H bending at 1541 cm^{-1} and C=O stretching at 1663 cm^{-1} in ATR-FTIR were reduced because of the halogenation reacted with halogens produced by oxidation of hydrogen halides. The increment in halogenation on PA was in the order HCl, HBr, and HI, and it was the same as the order of temporary dipole moment from the effect of molecular size. Water flux after exposure to hydrogen halides was severely decreased due to broken hydrogen bonding by halogenation. Investigation of sulfuric acid and hydrogen halides on the change of the physico-chemical characteristics in the NE90 can be utilized when full aromatic NF membrane is applied to treat/recycle several industrial processes, which include sulfuric acid or hydrogen halides.

4.1 Introduction

Water is essential for humans, and at many locations on the Earth, fresh water shortages need to be solved. In consequence, membrane technology to supply alternative fresh water has been widely researched because of its lower operation and maintenance cost, as well as lesser land space requirement [4]. Nanofiltration (NF) membrane, which has ~ 0.5 to ~ 2.0 nm of pore diameter, has been rapidly attracted during the last decades due to its low operating pressure and high rejection for divalent salts or organic molecules with low molecular weight in the range from 200 to 1000 g mol^{-1} [5]. The high rejection of NF can be explained by the combination of two different separation mechanisms which are the solution diffusion mechanism and steric/electrostatic sieving mechanism [6]. Current commercial NF thin-film composite (TFC) polyamide (PA) membranes have generally been fabricated by interfacial polymerization (IP) technique using both *m*-phenylenediamine (MPD, aromatic amine monomer) and trimesoyl chloride (TMC, acyl chloride monomer) for the active layer [7, 8]. This IP technique is a good way to fabricate TFC NF membranes, because the thin and dense full aromatic PA active layer results in high membrane performance despite low operating pressure, and the membrane performance can be controlled by various fabrication factors such as the concentration of monomers/additives, reaction/curing time, and temperature for post-treatment [9].

The NF technique has been widely applied to the reutilization/removal of target compounds under acidic conditions: 1) purification of nitric acids in picture tube production [13], 2) treatment of acidic effluents in the pulp and paper industry [15], 3) regeneration of acidic streams in dairy cleaning-in-place processes (CIP) [14], 4) removal of heavy metals [18] and sulfate ions [19] in the mining and metal industry, 5) recovery of phosphorus in sewage sludge [16, 17], and 6) separation or recycling of abundant acids such as HBF_4 , HCl , HNO_3 , H_2SO_4 , and H_3BO_3 in effluents from rinsing, fermentation, and extraction processes [11]. Furthermore, NF technique can be applied to wastewater containing HCl , HBr and HI from etching process for semiconductors [20-22]. Acid-resistant NF membranes are needed to use the above processes which operate at low pH condition. However, high-performance commercial NF full aromatic PA membranes, which are fabricated by MPD with TMC, are limited in the range of pH 2 to 11 [24]. Therefore, additional research on the degradation of full aromatic PA membrane by acid is needed to apply the above processes which have less than pH 2 acidic condition. Liu et al. [25] studied the effect of 0.5 mol/l HCl on full aromatic reverse osmosis PA membrane, and PA was hydrolyzed after 30 Days filtration, following more permeations of water and salt. However, to the best of our knowledge, the effects of degradation by acid on full aromatic membrane using different pH

range of acid and various kinds of acid containing sulfuric acid and hydrogen halides have not previously been researched. Therefore, the degradation of full aromatic membrane in various acidic conditions, with $\text{pH} < 2$ condition of sulfuric acid and hydrogen halides, requires systematic investigation.

Plentiful research has been conducted on the hydrolysis of amide by the biological importance of proteolytic reactions [32]. An amide bond's stability originates from the delocalization of electrons between lone pairs of the nitrogen atom in amide and the carbonyl π_{CO} bond [34, 37, 39]. Acid-catalyzed hydrolysis reactions firstly undergo protonation on oxygen (O) or nitrogen (N) in amide group. The O/N-protonation twists the amide's C-N bond to lose the resonance between carbonyl π_{CO} bonds and nitrogen lone-pair electrons, and accordingly accelerates the amide's hydrolysis [38, 39, 81]. Ma et al. [81] explains the O- or N-protonation pathways, which compete with each other (e.g., undistorted amides are normally protonated at the oxygen [38]). When acid-catalyzed hydrolysis occurs on the PA membranes, permeations of water and salt increased as shown in previous researches [6, 25]. However, the occurrence of mainly O/N-protonation without hydrolysis would also affect membrane performance because of the change of hydrogen bonding and deformation of polymer structure. Firstly, when the O-protonation occurs in amide group, it changes hydrogen bonding between a hydrogen-accepting carbonyl group and a hydrogen-donating H atom (e.g., connecting N atom in amide), due to the protonated carbonyl group generated by proton bridge [112, 113]. Witt et al. [113] studied several diamides which generate a rigid and strong proton bridge between the amide groups after the O-protonation, because it can be further stabilized by changing conformations including those with axial substituents. Furthermore, Addario et al. [112] reported N-acetylated amino acids made proton bridges after the O-protonation for not only the stabilizing effect between two atoms by proton bridge, but also better stabilization for amide resonance of the N-acetyl group itself. Likewise, spatial rearrangement of protonated amide can occur by proton bridge, because of the more stabilized state. In terms of the N-protonation, on the other hand, rotation of N-C(O) bond occurs, due to the formation of a tetrahedral structure at the nitrogen in amide. That is, when a progressive pyramidalization of the N from sp^2 (planar) to sp^3 (tetrahedral) geometry occurs, a rotation about the N-C(O) bond of 30° takes place [34]. Because the spectral interpretation of polymeric materials is quite difficult, benzanilide can be used for the model compound of full aromatic PA membrane [114]. If the benzanilide is assumed for the model compound of full aromatic PA membrane, the amount of N-protonation in $\text{pH} 0$ and 1 is 76% and 24% , respectively, because the pK_a value for N-protonation of benzanilide is 0.5 [115]. These spatially distorted structures caused by O/N-protonation in acidic condition can possibly affect the performance of the full aromatic PA membrane, because the application of high pressure could collapse or locally compact or mainly

distort the polymer chain [116]. Hydroiodic acid (HI) is known as an unstable chemical, so it oxidizes to molecular iodine (I_2) in air [117, 118]. Table 4.1, which shows the chemical reaction for generating halogen gases by oxidation of hydrogen halides, shows that these phenomena can be explained by spontaneous reaction. Subsequently, molecular chlorine (Cl_2) and molecular bromine (Br_2) can be generated from hydrochloric acid (HCl) and hydrobromic acid (HBr) in the same manner. Henry's constants (H^{CP}) of these halogens (Cl_2 , Br_2 , and I_2) in water are 9.2×10^{-4} , 7.2×10^{-3} , and 2.8×10^{-2} , respectively (Fig. 4.1) [119]. These generated halogens are another possible source to affect the surface characterization/performance of the full aromatic polyamide membrane, given that research has been widely conducted on the effect and mechanism of halogenation on the polyamide membrane [8, 120]. For example, chlorination mechanisms on polyamide membrane are mainly divided into two kinds of mechanisms: polymer depolymerization and polymer deformation (*e.g.*, N-chlorination) [8]. Firstly, mechanisms of polymer depolymerization due to chlorination were suggested by Koo et al. [121] and Avlonitis et al. [122]. They suggested polyamide's oxidative chain cleavage and Hoffmann degradation in alkaline chlorine solutions, respectively. Secondly, in the case of polymer deformation, nitrogen atom in a polyamide can react with chlorine to generate N-chloroamide, because the nitrogen is electron-donating group by lone pair electrons which can share with the electron-withdrawal chlorine ($Cl^{\delta+}$) created by a temporary dipole moment [123, 124]. Figure 4.1 shows a schematic description of the possible pathway of halogenated polyamide due to halogenation, which in this work explains the formation of N-halogenation. Membrane degradation due to chlorination affects membrane flux and rejection of inorganic salts as well as pharmaceutically active compounds [125]; however, systematic studies of membrane halogenation in the presence of HCl, HBr, and HI have not yet been reported.

In this work, systematic physico-chemical characterization was conducted to explain the effect of degradation by sulfuric acid in the range of pH 0 to 2 as well as hydrogen halides at pH 0 on the full aromatic membrane. Degraded membrane samples were characterized by various analytical tools such as (1) scanning electron microscopy (SEM) for observation of surface morphology, (2) attenuated total reflectance Fourier transform infrared spectroscopy (ATR-FTIR) for measurement of chemical bonds on surface, (3) X-ray photoelectron spectroscopy (XPS) for confirmation of the surface's atomic percentages, (4) goniometer for contact angle of membrane surface, (5) zeta potential analyzer by electrophoresis for surface charge of the membrane surface. Finally, filtration experiments were investigated to explain the effects of degradation by acid on membrane performance. As far as we know, this is the first study to systematically investigate the degradation of commercial NF full aromatic membrane by sulfuric acid as well as by hydrogen halides.

Table 4.1 Chemical reaction for generating halogen gases by oxidation of hydrogen halides and gibbs energy in standard state (for one mole at 298K and 1 bar).

Chemical reaction formula for generating halogen gases from oxidation of hydrogen halides	Gibbs energy for reaction (kJ·mol⁻¹)
$4 \text{HCl (g)} + \text{O}_2 \text{(g)} \rightarrow 2\text{Cl}_2 \text{(g)} + 2\text{H}_2\text{O (g)}$	-76.0
$4 \text{HBr (g)} + \text{O}_2 \text{(g)} \rightarrow 2\text{Br}_2 \text{(g)} + 2\text{H}_2\text{O (g)}$	-236.9
$4 \text{HI (g)} + \text{O}_2 \text{(g)} \rightarrow 2\text{I}_2 \text{(g)} + 2\text{H}_2\text{O (g)}$	-423.6

Compound	Gibbs energy (kJ·mol⁻¹)
HCl (g)	-95.3
HBr (g)	-53.5
HI (g)	1.3
O ₂ (g)	0
Cl ₂ (g)	0
Br ₂ (g)	3.13
I ₂ (g)	19.38
H ₂ O (g)	-228.6

Mechanism of **halogenation** on PA membrane

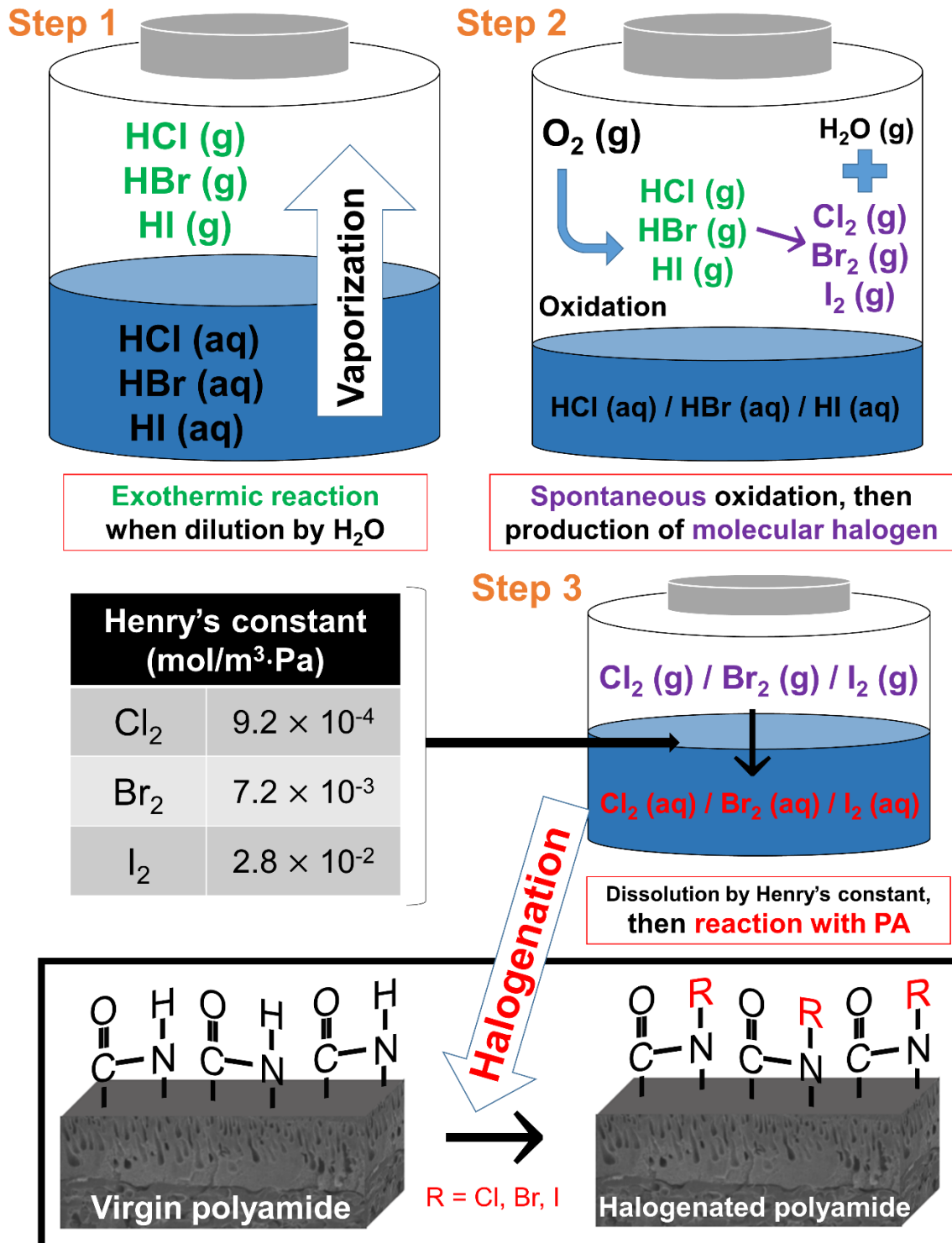


Figure 4.1 Schematic description of possible pathway of halogenated polyamide due to halogenation generated by hydrogen halides and oxygen.

4.2 Materials and methods

4.2.1 Chemicals and materials

Commercial TFC PA NE90 membrane was obtained from Toray Chemical Korea Inc (Korea), and used as a representative membrane to investigate the effect of degradation by acid on full aromatic PA, because the NE90 was already known as an MPD-based PA membrane without hydrophilic coating layer [92].

The following chemicals were used without further purification: Sulfuric (95% assay) and hydrochloric acid (35-37% assay) were purchased from DaeJung Chemicals Co., Ltd. (Busan, Korea), and hydrobromic (47-49% assay) and hydroiodic acid (57% assay) were purchased from Yakuri Pure Chemicals Co., Ltd. (Kyoto, Japan) to analyze the effect of degradation by acid on full aromatic PA membrane. To perform filtration test of the virgin NE90 and degraded membranes, sodium chloride (NaCl, 99% assay) for monovalent ion and magnesium sulfate heptahydrate ($\text{MgSO}_4 \cdot 7\text{H}_2\text{O}$, 98% assay) for divalent ion were chosen and obtained from Samchun Pure Chemicals Co., Ltd (Seoul, Korea) and Sigma-Aldrich Co., Ltd. (MO, USA), respectively. Pure water produced by Milli-Q equipment (18 M Ω resistivity, Millipore®, Merck Millipore, Germany) was used for the preparation of acidic solutions by the dilution of concentrated sulfuric and hydrogen halides as well as for the soaking and rinsing of the membrane samples.

4.2.2 Membrane degradation protocol

In this work, full aromatic NE90 membrane was investigated to study the effect of degradation by acid under (1) sulfuric acid in the range of pH 0 to 2, and (2) hydrogen halides at pH 0 during 7, 14, 28, 42, 63 Days of exposure time. Solution pH was checked by Orion ROSS Sure-Flow pH electrode purchased from Thermo Fisher Scientific Inc. (New York, U.S.A.), which, according to the supplier, guarantees pH range from (0 to 14). Degradation experiments were conducted in 1 L bottle consisting of amber color of the material with PP (polypropylene) cover for immersion of the NE90 membranes' coupons (10 × 15 cm²) at room temperature (25°C). The membrane samples were rinsed thoroughly with Milli-Q water after exposure to each acidic condition, followed by storage in Milli-Q water until usage for characterization and filtration tests.

4.2.3 Characterization of membranes

4.2.3.1 Scanning electron microscopy (SEM)

To investigate the effect of degradation by acid on surface morphology, surface images of the NE90 virgin and degraded membranes were measured by a Field Emission-Scanning Electron Microscopy (FE-SEM) (Cold FE-SEM SU8000, Hitachi, USA). We referred to the experimental procedure in our previous work to measure the surface morphology of the membranes [6]. In brief, the vacuum-dried membrane samples were fixed by a conductive carbon tape for platinum (Pt) coating. Then, Turbo Pumped High-Resolution Chromium Sputter Coater (K575X, EMITECH, Lohmar, Germany) was used for Pt coating during 1 min at 20 mA in 2×10^{-3} mbar to relieve artifacts from electrostatic charge. All of the SEM images were analyzed at 10,000 resolutions.

4.2.3.2 Attenuated total reflectance-Fourier transform infrared spectroscopy (ATR-FTIR)

Attenuated total reflectance-Fourier transform infrared spectroscopy (ATR-FTIR) was used to measure the change of chemical properties between the NE90 virgin and degraded membranes using Nicolet 6700 spectrometer (Thermo Scientific, Waltham MA, USA). A flat plate germanium ATR crystal was equipped in spectrometer to measure the TFC membranes [91]. All of the membrane samples were vacuum-dried, before measurements of ATR-FTIR. Prior to measurement of membrane samples, the background spectrum of air was firstly measured with purging by nitrogen gas, then membrane samples were measured with 64 scans of average spectra from 1000 to 4000 cm^{-1} with a resolution of 4 cm^{-1} . OMNIC software (version 8.1) was used to record the FTIR spectra, correct the peaks' baseline, and normalize the baselined peaks. Peaks for full aromatic PA such as amide I band at 1663 cm^{-1} and amide II band at 1541 cm^{-1} were mainly focused on investigate the effect of acid on the chemical properties of PA. In order to compare the peak change of the virgin NE90 and degraded membranes, all of the sample peak were normalized by the 1250 cm^{-1} peak, which is strong C–O–C asymmetric stretching vibration of polysulfone support layer [126].

4.2.3.3 X-ray photoelectron Spectroscopy (XPS)

X-ray photoelectron Spectroscopy (XPS) (K Alpha, Thermo Scientific, USA) was conducted to study effect of degradation by acid on content of halogen percentages on degraded membranes' surface. Wide survey XPS spectra were scanned by sweeping in the range of electron binding energy

from 0 to 1000 eV using a 1 eV resolution. The X-ray beam can penetrate about 5 to 10 nm depth from top surface, analyzing the elemental composition of the membranes' surface. All of the membrane samples were vacuum-dried prior to XPS measurement. In this work, binding energy of Cl2p, Br3d, and I3d were detected at 200, 68, and 620 eV, respectively to obtain content of halogen percentage on the degraded membrane surface [8, 127].

4.2.3.4 Contact angle

The surface hydrophilicity of the virgin and degraded membranes was investigated by the contact angle value of the membrane surface using a goniometer (Phoenix 300Plus, Surface & Electro Optics Co. Ltd., Korea). To attain representative contact angle values of virgin and degraded membranes, 50 contact angle measurements were conducted, using coupons from two different membranes. Sessile drops method was applied to calculate the contact angles of the membrane surface. All of the membrane samples were vacuum-dried at the same time for the same condition.

4.2.3.5 Zeta potential

The surface zeta potentials of the NE90 and degraded membranes were analyzed by the electrophoresis method to investigate the effect of degradation by acid on membrane surface charge according to our previous work [6]. In contrast with the preparation for SEM, ATR-FTIR, XPS, and contact angle, membrane samples for zeta potential were kept in Milli-Q water over 1 Day until the measurement of zeta potential. The surface zeta potentials of the wet membrane samples were measured by electrophoretic light scattering spectrophotometer (ELS-8000, Photal, Otsuka Electronics, Japan). The membrane samples were fixed at a plate sample cell, followed by measurement of surface zeta potential using a 10 mM NaCl electrolyte solution containing polystyrene latex particles (diameter: 520 nm) (Otsuka Electronics, Osaka, Japan) in the range of pH 3 to 9 adjusted by 1 N HCl or NaOH.

4.2.4 Filtration tests

The NE90 virgin and degraded membranes were performed using filtration test cells to investigate the effect of degradation by acid on the permeation properties according to our previous research [4]. Filtration test were operated at 1 L min⁻¹ flow rates at room temperature with 2,000 ppm

NaCl or MgSO₄ single electrolyte solution, and three different membranes of 19.6 cm² effective area were installed in the filtration test system. The operating procedure of filtration test was firstly compaction at 150 psi for 1 hr, and subsequently, 30 min stabilization at 75 psi, before measurement of the water flux and salt rejection. The permeate water flux (J_w (L m⁻²h⁻¹ or LMH)) was calculated by mass change of permeate solution per unit time and membrane area as shown in Eq. (4.1). Calibrated conductivity meter (Ultrameter IITM, Myron L Company, USA) was then used to calculate the NaCl or MgSO₄ salt rejection by Eq. (4.2), conversion of conductivity of feed and permeate solution to each concentration.

$$J_w = \frac{\Delta \text{ weight}}{\Delta \text{ time} \times \text{effective membrane area} \times \text{water density}} \left(\frac{\text{L}}{\text{m}^2\text{h}} \text{ or LMH} \right) \quad (4.1)$$

$$R = \left(1 - \frac{[\text{NaCl or MgSO}_4]_{\text{permeate}}}{[\text{NaCl or MgSO}_4]_{\text{feed}}} \right) \times 100 (\%) \quad (4.2)$$

To investigate the effect of degradation by acid on the permeation properties, firstly, the NE90 virgin membranes were normalized by the initial permeation results to perform only the compaction effect of high-pressure (Virgin membrane's normalized flux¹ or rejection¹). Secondly, the degraded membranes were also normalized by the initial permeation results to confirm both the compaction effect of high pressure, and degradation by acid (Degraded membranes' normalized flux¹ or rejection¹). Finally, the permeation results of the virgin membrane subtracted from those of the degraded membranes could come only from degradation by acid, and these normalized results were defined as normalized flux² or rejection² as clearly explained in Table 4.2, using an example of the calculation.

Table 4.2 Example of calculation to calculate normalized flux².

Normalized condition (Days)	0	7	14	28	42	63
Normalized flux ¹ of NE90 virgin (Only compaction)	1.000	0.935	0.903	0.901	0.905	0.896
Normalized flux ¹ after soaking in acid (Compaction + damage of acid)	1.000	0.886	0.774	0.772	0.747	0.733
Normalized flux ² after soaking in acid (Only damage of acid)	1.000	0.951	0.871	0.871	0.842	0.837

4.3 Results and discussion

4.3.1 Characterizations of degraded membranes

4.3.1.1 Effect of degradation by acid on surface morphology (SEM)

The surface morphology of the full aromatic NE90 virgin and degraded membranes was characterized by SEM images. Figure 4.2 (a) shows a representative SEM image of the NE90 virgin, and its surface morphology has ridge-and-valley structure, compared to the piperazine-based semi-aromatic PA membrane, which has smooth surface morphology [105]. This full aromatic PA layer is formed by connecting the tufts from interfacial polymerization, diffusing from MPD amine solution into TMC organic solvent, until termination of the polymerization due to the high solubility and diffusivity of MPD in organic solvent [49]. That is, the tufts, which have higher molecular weight than the laterally spreading base layer, become the ridge part, resulting in high roughness characteristics of the MPD-based full aromatic PA membrane [49]. Figure 4.2 shows the SEM images for the surface morphology of (a) the NE90 virgin, and the degraded membranes soaked in pH 0 (b) H₂SO₄ (c) HCl, (d) HBr, and (e) HI until 63 Days for exposure times. However, surface morphology was not changed after degradation by acid checked from maintaining a similar ridge-and-valley structure, so the ATR-FTIR and XPS results will be discussed in the following section, to investigate the effect of degradation by acid on the surface's chemical properties.

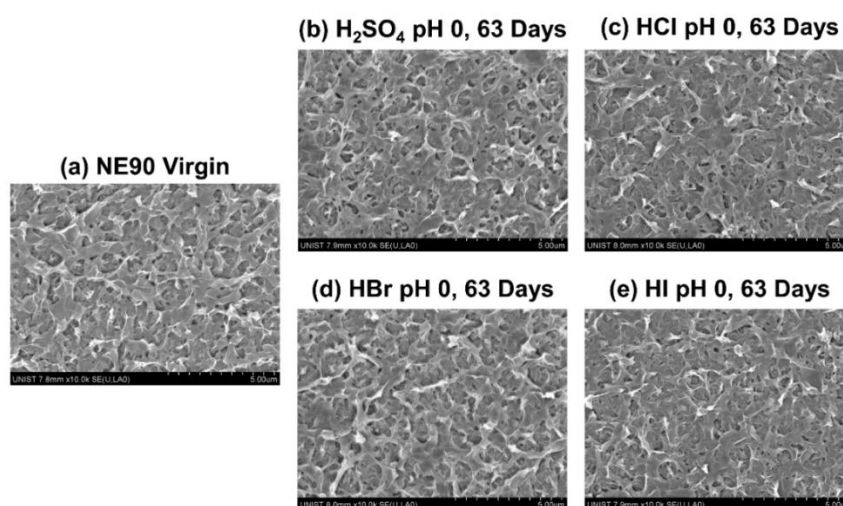


Figure 4.2 SEM images of the surface of the active layer of the NE90 virgin (a) and degraded membranes soaked in pH 0 (b) H₂SO₄ (c) HCl, (d) HBr, and (e) HI until 63 Days for exposure times.

4.3.1.2 Effect of degradation by acid on change of membrane surface's chemical bond and atomic percentages (ATR-FTIR and XPS)

ATR-FTIR spectra of the virgin NE90 and degraded membrane by acid were analyzed to study the effect of degradation on chemical bonding of the membrane surface, including both the PA layer and polysulfone support layer due to the large penetration depth of the IR [106]. Figure 4.3 shows spectra of the NE90 virgin and degraded membranes under (a) H₂SO₄ (b) HCl, (c) HBr, and (d) HI pH 0 acidic conditions in the range from 1000 cm⁻¹ to 4000 cm⁻¹ of characteristic bands. Amide I band at 1663 cm⁻¹ and amide II band at 1541 cm⁻¹ correspond to C=O stretching and N-H bending motion of amide, respectively [92], and these peaks were mainly focused on investigate the effect of acid on the chemical properties of PA. In the case of pH 0 H₂SO₄ acidic condition, neither amide I or II peak was affected, as shown in Fig. 4.3 (a). However, in the case of pH 0 hydrogen halides (Fig. 4.3 (b) to (d)), amide II peak was continuously decreased with increasing exposure time due to replacing the hydrogen in amide bond by the bounding of molecular halogens [128]. Furthermore, the disappearance of the peak in amide II by the bounding of molecular halogens increased from HCl (Fig. 4.3 (b)) to HI (Fig. 4.3 (d)) acidic condition. These phenomena occurred by electron-withdrawal halogen (e.g., Cl^{δ+}) created by a temporary dipole moment [123]. Temporary dipole moment increases with the size of molecule, because a smaller molecule is less polarizable and has smaller dispersion forces due to tightly holding electrons, on the other hand, a larger molecule is more polarizable and has larger dispersion forces because of many electrons [33]. That is, temporary dipole moment increases in the molecular size order from Cl₂ to I₂ among the halogens, and this characteristic was reflected in the disappearance of the amide II peak as shown in Fig. 4.3 (b) to (d). In particular, both amide I and II peak in the HI condition (Fig. 4.3 (d)) were shifted to higher and lower wavenumber, respectively. Kwon et al. [126] proposed that the reason for shifting of amide I and II after chlorination resulted from broken and weakened hydrogen bonds, respectively, so shifting of the amide I and II peaks in the HI condition is also thought to result from changed hydrogen bonds.

Subsequently, XPS analyses were conducted to support the ATR-FTIR results, which show bounding of molecular halogens on the membrane surface after exposure to acidic solution containing hydrogen halides. Figure 4.4 indicates the atomic percent of halogen in the degraded membranes' surface after exposure to hydrogen halides. The content of halogen on the degraded membrane surface monotonically increased with increasing acid-soaking time, and the content of halogen increased incrementally with molecular size order from Cl₂ to I₂. That is, the amount of bounding by electron-withdrawal halogens in hydrogen of amide bond increased from HCl to HI. These results support the ATR-FTIR results, which are decreasing amide II peak after exposure to hydrogen halides as well as

shifting amide I and II peaks in the case of HI due to severely decreased hydrogen bonds from the relatively higher content of halogen on the membrane surface.

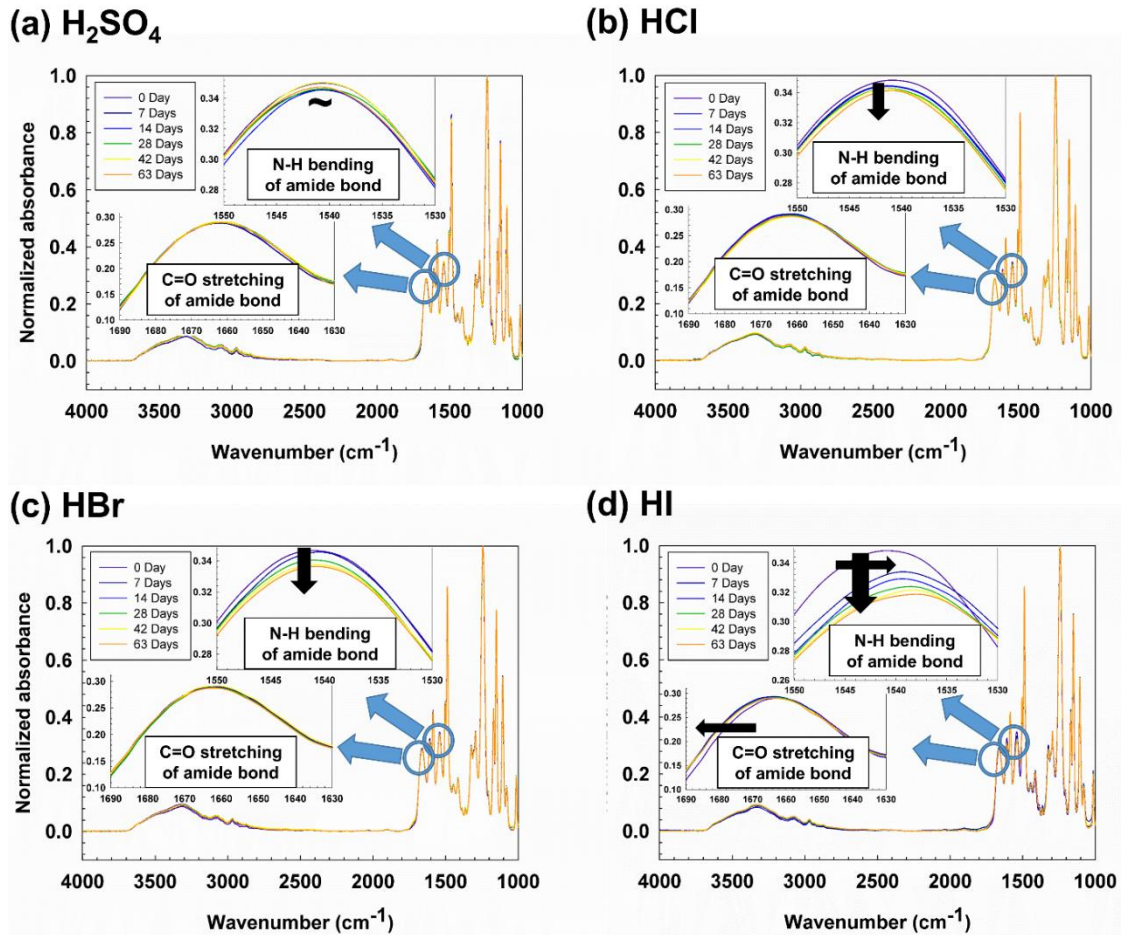


Figure 4.3 ATR-FTIR spectra of the NE90 virgin and degraded membranes soaked in pH 0 (a) H_2SO_4 (b) HCl , (c) HBr , and (d) HI until 63 Days for exposure times.

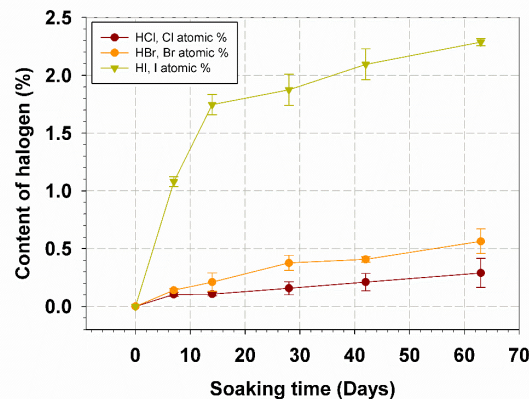


Figure 4.4 Atomic percent of halogen in the degraded membranes after exposure to pH 0 HCl , HBr , and HI until 63 Days.

4.3.1.3 Effect of degradation by acid on change of membrane surface's hydrophilicity and surface charge (contact angle and zeta potential)

The measurement of contact angle can analyze the tendency of the liquid wettability on the solid surface, by calculating the angle between the air/water interface and solid surface. From the point of view of the membrane surface, there is a higher tendency to wet the membrane surface by water when the contact angle value is lower. Table 4.3 shows the contact angle values of the NE90 virgin and degraded membranes that were measured to investigate the effect of degradation by acid on the membranes surface's hydrophilicity. After exposure to pH 0 H₂SO₄ acidic condition during 63 d, the degraded membrane surface's hydrophilicity was not changed; however, the membranes degraded by hydrogen halides changed to slightly more hydrophilic (Table 4.3). Such an increment in hydrophilicity after exposure to hydrogen halides would be related to the bounding of molecular halogens, as checked by the ATR-FTIR and XPS results (Figs. 4.3 and 4.4), because previous researches reported that after chlorination, the surface became more hydrophilic [125, 128]. Kwon *et al.* [128] studied that decreased contact angle value after exposure to sodium hypochlorite solution resulted from the greater polar membrane surface due to the introduction of unbalanced dipole moments. Furthermore, Do *et al.* [129] proposed that hydrolysis of C-N bond after chlorination can cause an increase in hydrophilicity due to carboxylic functional group. Therefore, increased hydrophilicity after degradation by hydrogen halides is also thought to result from the introduction of unbalanced dipole moments and hydrolysis phenomenon.

Measurement of the membrane surface's zeta potential was performed by the electrophoresis method to explain the effect of degradation by acid on the membrane surface charge. Figure 4.5 shows the surface zeta potential of the NE90 virgin and degraded membranes in the range pH from 3 to 9. Figure 4.5 shows that the isoelectric point (IEP) of the NE90 virgin membrane is about pH 3.5. The surface of full aromatic PA membrane generally become more negative with increasing pH (at higher than IEP value) due to the deprotonation of the carboxyl groups converted from unreacted TMC [111], and adsorption of hydroxyl ions on the membrane surface [128]. On the other hand, the membrane surface at less than IEP value has a positive charge due to the protonation of unreacted amino groups [128] or amide group [129]. After degradation by pH 0 H₂SO₄ acidic condition during 63 Days, the membrane's surface zeta potential was not affected; however, the membranes degraded by hydrogen halides resulted in a more negative charge from HCl to HI condition (Fig. 4.5). More negative charge after exposure to hydrogen halides also resulted from bounding of molecular halogens on hydrogen in amide group, because increasing negative charge is consistent with previous publications related to chlorination [128, 129]. Negative surface charge of chlorinated membrane was attributed to: (1) -NH₂⁺

groups converted from amide nitrogen to N-Cl bond formation no longer being formed [129], (2) increased carboxylic groups after cleavage of C-N bond [125], and (3) introduction of unbalanced dipole moments by substitution of chlorine in amide bond [128]. Hence, both the contact angle and zeta potential results clearly supported the bounding of molecular halogens on membrane surface after exposure to acidic solution containing hydrogen halides as discussed in the ATR-FTIR results.

Table 4.3 Contact angle of the NE90 polyamide membranes soaked in pH 0 H₂SO₄, HCl, HBr, and HI until 63 Days for exposure times.

Sample Condition	NE90 Virgin	H ₂ SO ₄ 63 Days	HCl 63 Days	HBr 63 Days	HI 63 Days
Contact angle (°)	45.2 ± 3.2	45.3 ± 3.3	44.3 ± 2.8	43.8 ± 3.4	42.9 ± 3.6

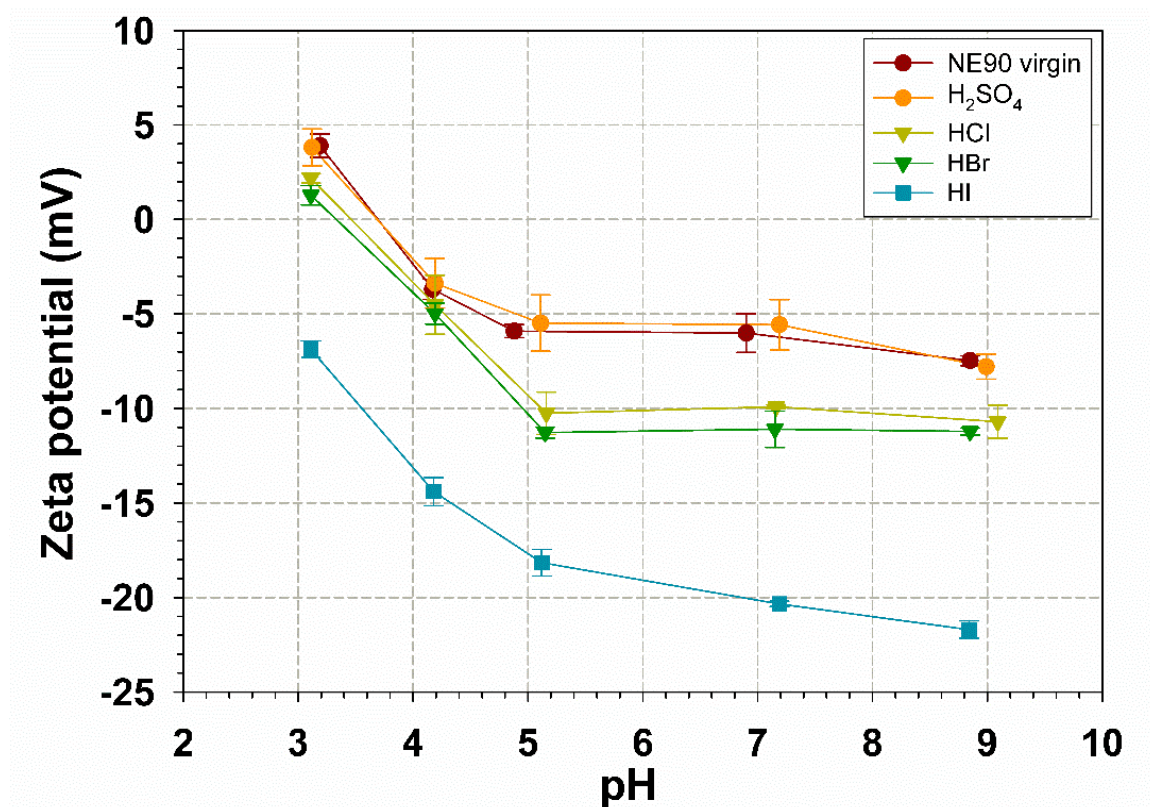


Figure 4.5 Zeta potential of the NE90 virgin and degraded membranes soaked in pH 0 H₂SO₄, HCl, HBr, and HI until 63 Days for exposure times.

4.3.2 Effect of degradation by sulfuric acid (pH 0 to 2) on permeability properties

Prior to study sole effect of degradation by acid on the permeation properties, compaction effect by high operating pressure was firstly performed through the NE90 virgin membrane samples soaked in Milli-Q water. The NE90 virgin membranes were normalized by the initial permeation results to easily understand compaction effect on the permeation properties, and it is expressed by normalized flux¹ or rejection¹ as shown in Fig. 4.6. Normalized water flux¹ decreased and salt rejection¹ increased until 14 Days, then maintained until 63 Days (Fig. 4.6), and these results are consistent with the results of RO membrane compaction in Pendergast *et al.* [130]. According to their study, changes of permeation properties by the compaction effect were explained by the decreased effective path length for water and solute diffusion. In other words, pores of the support membrane polymer become narrower due to the compaction effect, resulting in increased diffusion distance in the support layer. Thus, water and NaCl salt permeability should decrease. Even though both water and NaCl permeability decreased, salt rejection tended to increase, because the decline of NaCl permeability was much more affected than the water permeability [130].

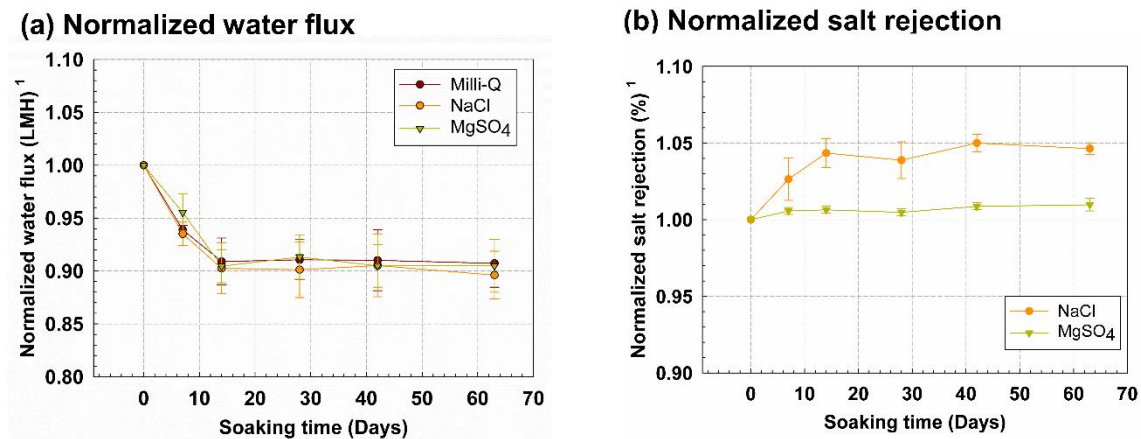


Figure 4.6 The effect of compaction on membrane flux and salt rejection of the NE90 virgin membrane kept in Milli-Q water (tested at 75 psi, using Milli-Q, 2,000 ppm NaCl and MgSO₄ single electrolyte solution).

To study the effect of degradation by H_2SO_4 acidic solution of the pH on permeation properties, degraded membranes were firstly normalized by the initial permeation results, then the compaction effect subtracted, as explained in Fig. 4.6. The calculated water flux and salt rejection are expressed by the normalized flux² and rejection², as explained in Table. 4.2, and this value indicates the sole effect of degradation by acid on the changed water flux and salt rejection. Figure 4.7 indicates the effect of sulfuric acid in the range from pH 0 to 2 and its exposure time on the permeation properties of the NE90 membrane. Water flux and salt rejection were maintained after exposure to pH 2 H_2SO_4 acidic condition, and this is in good agreement with the manufacturer's product catalog, which limits the operational pH range from 2 to 11 (Fig. 4.7).

Water flux increased and salt rejection decreased with increasing exposure time in the pH 1 H_2SO_4 acidic condition; on the other hand, water flux monotonically decreased in the pH 0 H_2SO_4 acidic condition, as shown in Fig. 4.7. The change of salt rejection by degradation of pH 0 H_2SO_4 acidic condition was not significant compared with the change of water flux. The different tendency of permeation properties between pH 0 and pH 1 H_2SO_4 acidic condition would be explained by the distorted hydrogen bonding and deformation of polymer structure, because amide II band at 1541 cm^{-1} and amide I band at 1663 cm^{-1} after degradation by H_2SO_4 were not disappeared, as shown in Fig. 4.3 (a). Namely, the O/N-protonation on amide spontaneously occurs before the occurrence of acid-catalyzed hydrolysis [81], so hydrogen bonding between amides can be distorted by proton bridge [112, 113] in the case of O-protonation and pyramidalization from planar to tetrahedral geometry in the case of N-protonation in nitrogen of amide [34], resulting in deformation of the PA structure. These phenomena are explained in Fig. 4.8 using a schematic of the NE90 PA membrane when O/N-protonation occurs. Firstly, O-protonation changes hydrogen bonding between a hydrogen-donating H atom and a hydrogen-accepting carbonyl group by proton bridge, because the changed conformation can be a more stabilized state as already discussed in previous papers using several diamides [113] and N-acetylated amino acids [112]. Secondly, protonation at N atom in amide changes from planar N-C(O) bond to about 30° distorted N-C(O) bond due to the formation of tetrahedral structure. If benzanilide is a model compound of the NE90 virgin membrane, the total amount of N-protonation in pH 1 and 0 is 24 and 76% state, respectively, calculated from the 0.5 pK_a value of benzanilide [115]. Thus, in pH 0 condition, decreased water and salt flux would result from mainly collapsed or compacted polymer structure by the 10 times higher number of hydrogen ion than that in pH 1 condition. However, in the pH 1 condition, water and salt flux would be easily permeated through the partially twisted polymer structure, because pH 1 condition has a relatively lower number of distorted hydrogen bonding. Furthermore, increased water flux and decreased salt rejection in pH 1 condition is a similar

phenomenon to the membrane swelling effect at low or high pH [4, 131, 132]. However, the effect of collapsed or compacted polymer structure is overwhelming compared to membrane swelling in pH 0 condition, resulting in decreased water and salt flux.

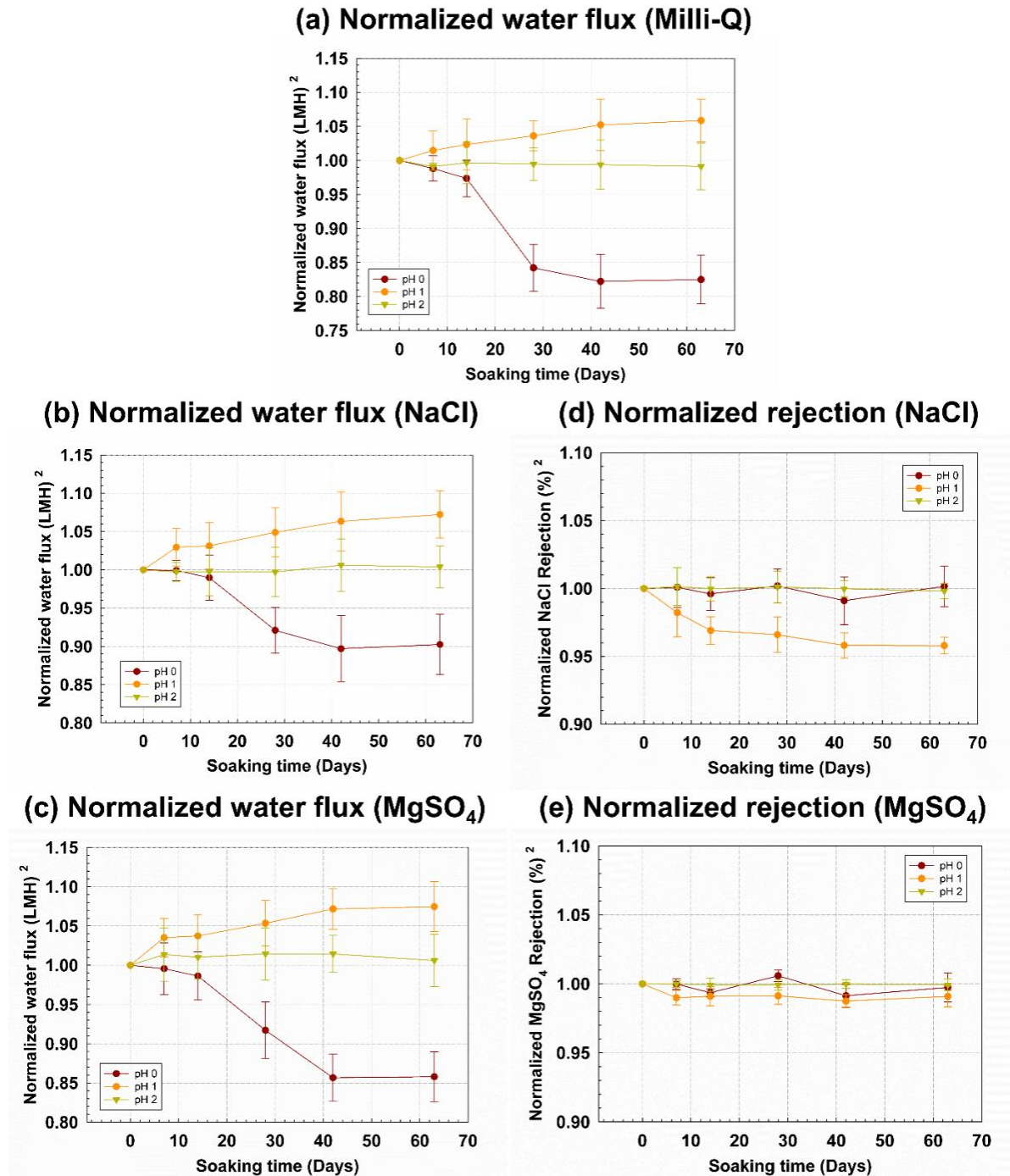


Figure 4.7 The effect of sulfuric acid's pH (pH 0-2) and exposure time on membrane flux and salt rejection of the NE90 membrane (tested at 75 psi, using Milli-Q, 2,000 ppm NaCl and MgSO₄ single electrolyte solution).

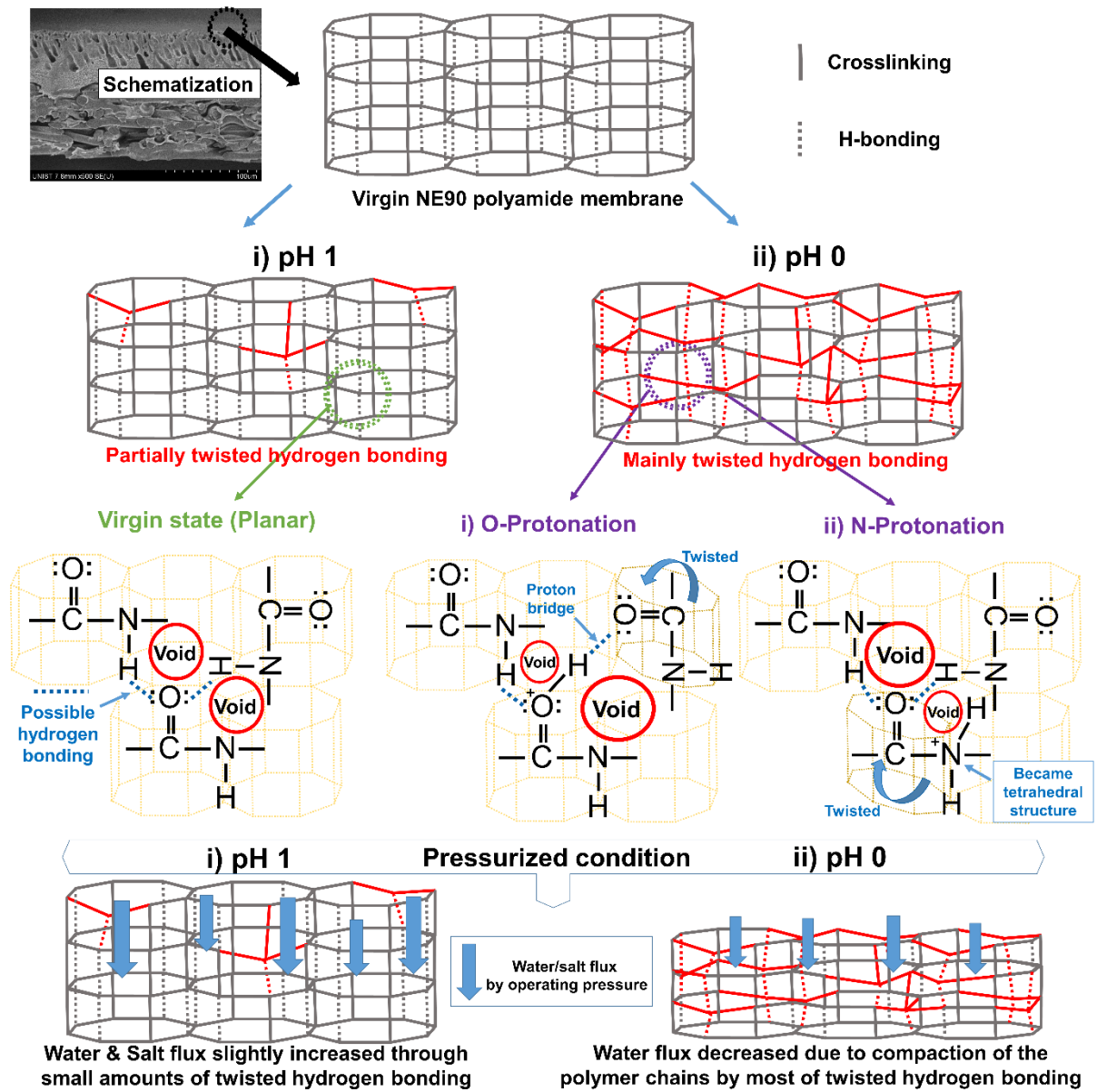


Figure 4.8 Schematic diagram of possible mechanisms to change membrane performance due to different pH condition of sulfuric acid.

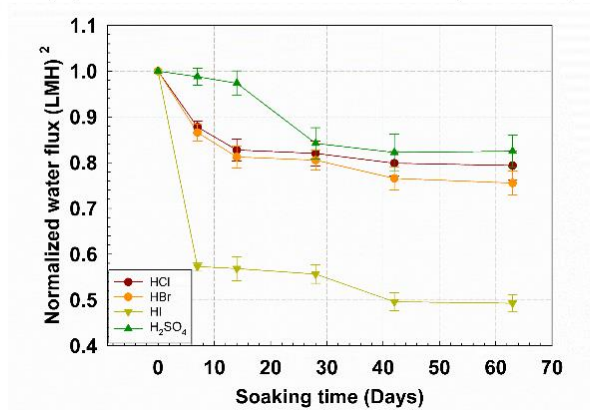
4.3.3 Effect of degradation by hydrogen halides (pH 0) on permeability properties

Normalized flux² or rejection² as explained in Table. 4.2 were also used to study the sole effect of degradation by pH 0 H₂SO₄ and hydrogen halides acidic solution on the permeation properties. Figure 4.9 shows the effect of sulfuric acid and hydrogen halides at pH 0 condition on the permeation properties of the NE90 membrane. Water flux after exposure to both pH 0 H₂SO₄ and hydrogen halides tended to decrease, and salt rejection after exposure to hydrogen halides also tended to decrease with increasing exposure time (Fig. 4.9). Such decrements of water flux and salt rejection were in the order H₂SO₄, HCl, HBr, and HI.

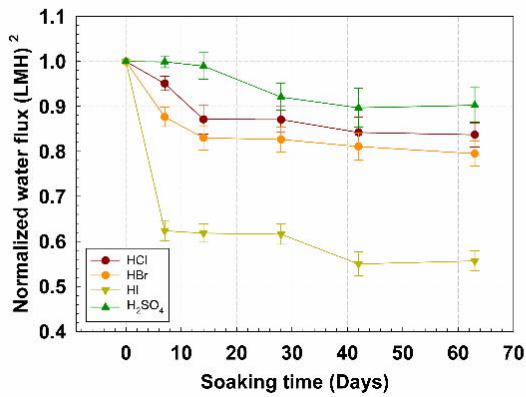
Decrement in the order of water flux between sulfuric acid and hydrogen halides at pH 0 condition resulted from reduced hydrogen bonding due to halogenation, because amide II band at 1541 cm⁻¹ and amide I band at 1663 cm⁻¹ after degradation by hydrogen halides were decreased, compared with that by sulfuric acid as shown in Fig. 4.3 (a) to (d). In other words, broken hydrogen bonding causes increased the flexibility of the PA structure, rather than twisted hydrogen bonding from O/N-protonation, and this increased the rotational freedom results in deformation/compaction of the PA structure, when applied to high pressure [126]. In other words, broken hydrogen bonding causes increased the flexibility of the PA structure, rather than twisted hydrogen bonding from O/N-protonation, and this increased the rotational freedom results in deformation/compaction of the Therefore, the decrease in water flux in the case of degradation by hydrogen halides was much higher than that by the degradation by sulfuric acid. Figure 4.10 describes these phenomena using schematics of the NE90 PA membrane when halogenation occurs. In addition, the order of decreasing water flux in hydrogen halides was equal to the molecular size order from Cl₂ to I₂, and this is highly related to the content of halogens on the membrane surface, as already discussed in the ATR-FTIR and XPS results PA structure, when applied to high pressure (Fig. 4.3 and 4.4).

When the membrane surface has a high absolute value of zeta potential, salt rejection generally increases, due to the increased Donnan exclusion effect [6]. Even though the membrane after exposure to hydrogen halides had a more negative surface charge (Fig. 4.5), the decrease of salt rejection seemed to be due to hydrolysis of the C–N bond, and this result shows a similar tendency to previous studies related to chlorination [8, 125]. Therefore, when the full aromatic NF membrane is applied to the reutilization/removal of target compounds in various acidic conditions, the changes of surface characteristics and permeable properties should be considered.

(a) Normalized water flux (Milli-Q)



(b) Normalized water flux (NaCl)



(d) Normalized rejection (NaCl)

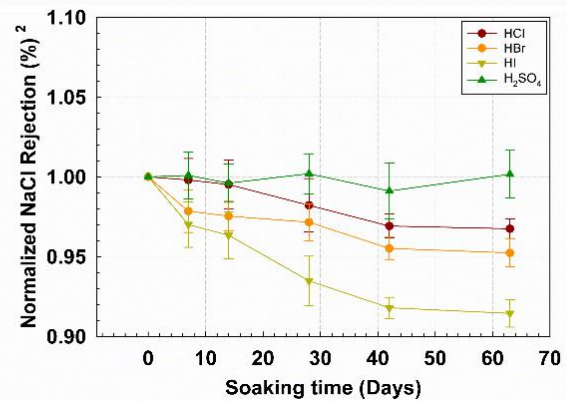
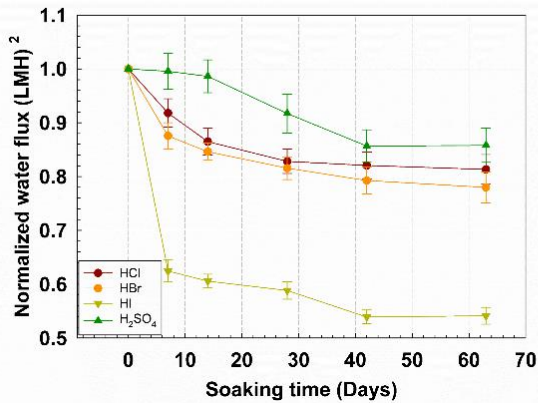
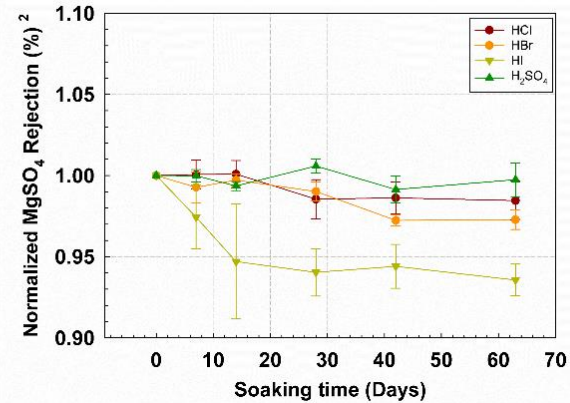
(c) Normalized water flux (MgSO₄)(e) Normalized rejection (MgSO₄)

Figure 4.9 The effect of halogen halide (pH 0) and exposure time on membrane flux and salt rejection of the NE90 membrane (tested at 75 psi, using Milli-Q, 2,000 ppm NaCl and MgSO₄ single electrolyte solution).

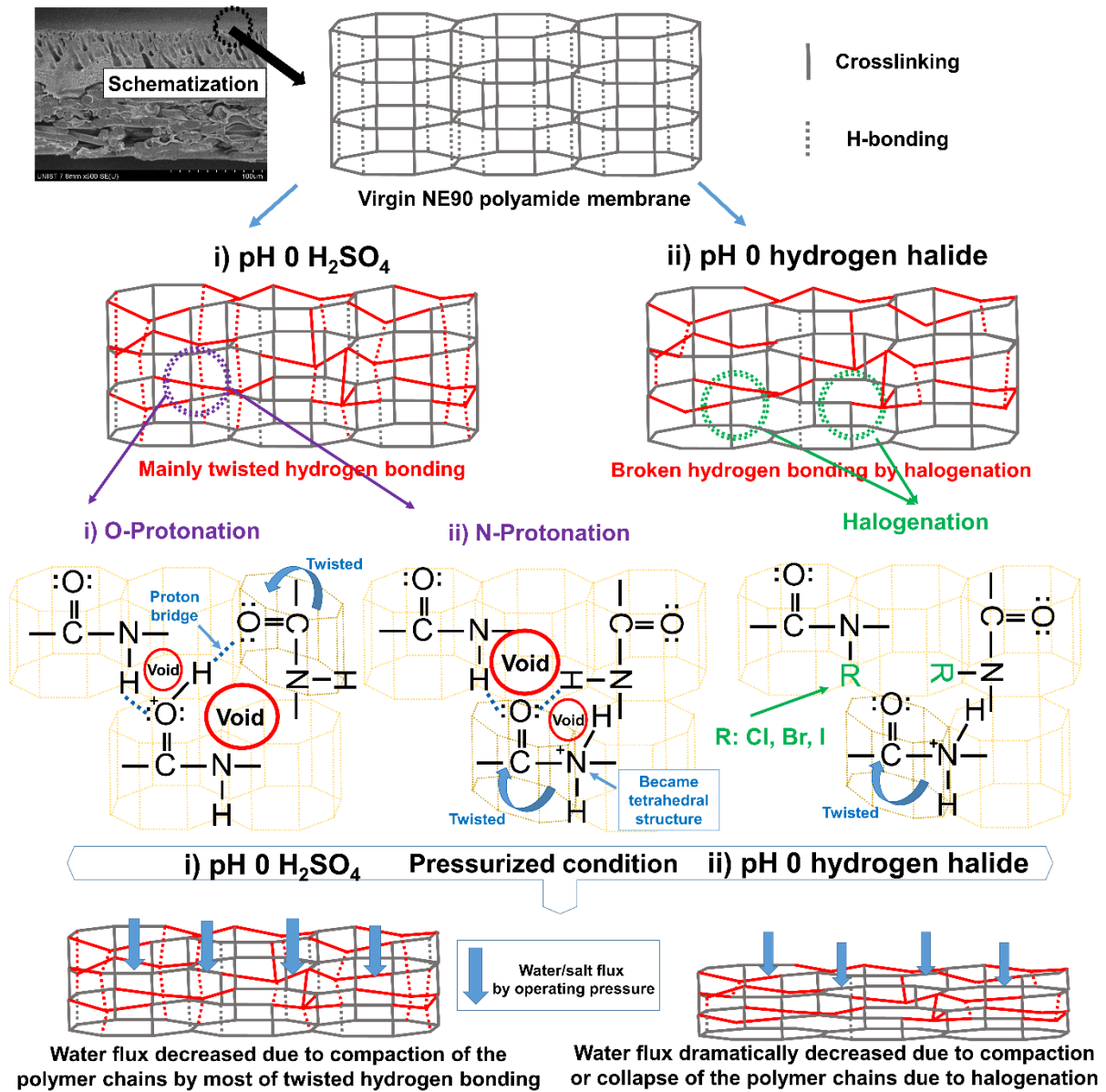


Figure 4.10 Schematic diagram of possible mechanisms to change membrane performance due to different acidic condition.

4.4 Conclusions

In this work, full aromatic NF PA membrane fabricated by MPD as an amine monomer and TMC as an acyl chloride was systemically studied for investigation of various acidic conditions (pH 0 to 2 sulfuric acid and pH 0 hydrogen halides) on the membrane's physico-chemical properties. In the case of membrane degraded by sulfuric acid, no distinct change was observed by SEM, ATR-FTIR, contact angle, and zeta potential. However, when the membrane was exposed to pH 1 condition, water flux increased and salt rejection decreased; on the other hand, when membrane was degraded by pH 0 condition, water flux decreased and salt rejection maintained. These phenomena are explained by the distorted hydrogen bonding between amides through proton bridge for O-protonation, and the formation of tetrahedral structure for N-protonation. Meanwhile at pH 0 condition, the membrane's physico-chemical properties were much more influenced by hydrogen halides than by sulfuric acid. In ATR-FTIR results, after degradation by hydrogen halides, amide II band (N-H) at 1541 cm^{-1} and amide I band (C=O) at 1663 cm^{-1} were decreased due to halogenation reacted with halogens generated by oxidation of hydrogen halides. To support ATR-FTIR results, XPS, contact angle, and zeta potential were also conducted. These amounts of halogenation increased in the order HCl, HBr, and HI, and the order was equal to the order of temporary dipole moment caused by the size of molecule. Water flux after exposure to hydrogen halides tended to severely decrease with increasing exposure time, resulting from broken hydrogen bonding due to halogenation. This work suggests that when full aromatic NF membrane is applied to treat/recycle several industrial processes that include sulfuric acid and hydrogen halides, changes of the surface characteristics and permeability should be contemplated.

*Acid-catalyzed hydrolysis of
semi-aromatic polyamide NF membrane
and its application to water softening
and antibiotics enrichment*

This chapter has been published:

Byung-Moon Jun, Hyung Kae Lee, Young-Nam Kwon*,

‘Acid-catalyzed hydrolysis of semi-aromatic polyamide NF membrane
and its application to water softening and antibiotics enrichment’,

Chemical Engineering Journal 332 (2018) 419–430

Abstract

The effect of post-treatment by acid-catalyzed hydrolysis of a commercial NE70 semi-aromatic polyamide (PA) membrane was systemically investigated to determine feasibility of use in water softening and antibiotic enrichment applications. The surface of a post-treated PA membrane was characterized using various analytical tools: SEM (Scanning Electron Microscopy) for surface morphology, ATR-FTIR (Attenuated Total Reflectance-Fourier Transform Infrared spectroscopy) for chemical bonds, contact angle for hydrophilicity of membrane surface, and electrophoretic light scattering spectrophotometer for surface charge of membrane surface. Conversion of amide groups to amine and carboxyl groups by post-treatment increased hydrophilicity and absolute value of surface charge as well as pore size and molecular weight cut off (MWCO) value. Post-treated membrane under optimal condition showed enhancement of water flux (~10%) as well as ~20% ideal selectivity ($\text{Na}^+/\text{Mg}^{2+}$) for water softening using a single electrolyte solution. In addition, mixture selectivity ($\text{Na}^+/\text{Mg}^{2+}$) using a mixture solution at pH 3 was also improved ~2.6 times. Post-treated membranes at pH 0.25 for 7 and 14 days as optimization points were also applied to enrichment of antibiotics which are erythromycin (ERY) and vancomycin (Van). Optimized post-treatment membranes showed higher water flux and lower NaCl rejection as well as competitive rejection of antibiotics when compared to virgin NE70 membrane or other commercial/fabricated membranes. The approach to post-treatment of semi-aromatic membrane by the acid-catalyzed hydrolysis method can be utilized as a multipurpose usage in the future depending on characteristics of the target compound (e.g. surface charge (positive/negative) or size diversity).

5.1 Introduction

Over the past several decades, nanofiltration (NF) technology has gradually evolved and the transportation mechanisms of NF membrane have been intensively investigated. Separation by NF membrane with nominal pore size of 1~100 nm mainly achieved via solution-diffusion mechanism or steric/electrostatic sieving mechanism [133, 134]. The NF process can be operated under the condition of low pressure and low energy consumption, however, the rejection of divalent ions and organic molecules from 200 to 1000 Da is high [135, 136]. Due to the high separation of multivalent ions and organic molecules, NF technology has been widely used in the fields of purification and concentration such as removal of dyes from wastewater, extraction or purification of woody biomass, food concentration in food industries, water softening of groundwater, and rejection of heavy metal and environmental pollutants [7, 133, 135, 136].

Commercial NF polyamide thin-film composite (TFC) membranes are generally prepared by interfacial polymerization (IP) techniques using piperazine and trimesoyl chloride (TMC) as an aliphatic amine with acyl chloride monomers for the fabrication of thin active layer [137]. The chair structure of the piperazine molecule in its lowest energy state makes the thin active layer difficult to compact, providing a large free volume inside the active layer and high permeability of water molecules through the thin layer [47]. Further enhancement of membrane performance has been achieved by addition of additives and surface modification as post-treatment. Amhed et al. investigated the effect of trimethylamine (TEA) added as an acid acceptor during IP [51], and reported that the TEA can not only prevent protonation of piperazine but also keep reactivity of piperazine, causing enhanced amount of cross-linking and a subsequent increase in salt rejection. Mansourpanah et al. studied the additive effect of cationic surfactant on membrane performance and showed that cetyltrimethyl ammonium bromide (CTAB) increases water flux without loss of salt rejection due to the enlarged free-volume in the active layer [52]. As a surface modification method, Mi et al. [138] introduced N-aminoethylpiperazine propane sulfonate (AEPPS), a zwitterionic compound, onto a TFC membrane to react with unreacted TMC monomer, thereby increasing hydrophilicity and water flux from 28 to 58 ($\text{Lm}^{-2}\text{h}^{-1}$ or LMH) without loss of Na_2SO_4 rejection. Furthermore, surface modification by grafting has been reported to enhance hydrophilicity using hydrophilic monomer such as polyethylene glycol, acrylic acid, or methacrylic acid [137]. However, to the best of our knowledge, there has been no published paper that applied acid-catalyzed hydrolysis as a post-treatment to semi-aromatic (piperazine-based) amide membrane.

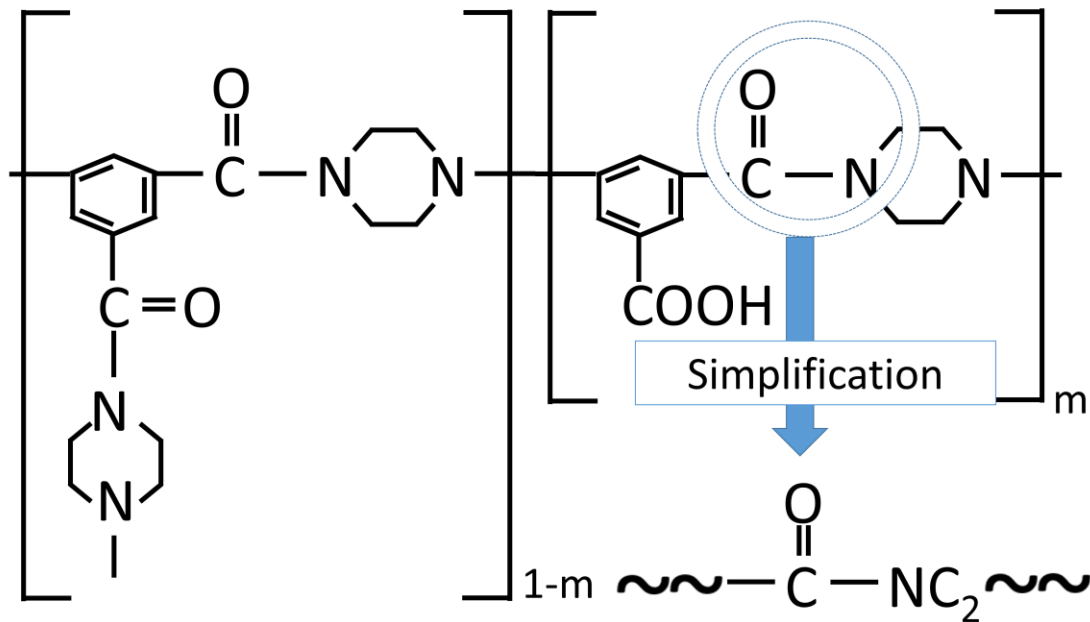
Amide hydrolysis has been already studied significantly due to the biological importance of proteolytic reactions [32]. Figure 5.1 shows schematic diagram of (a) piperazine-amide chemical structure and (b) acid-catalyzed hydrolysis reaction of the amide group. During the hydrolysis reaction of the amide group, the C-N piperazine-amide bond breaks, causing depolymerization of the amide group into carboxyl and amine groups [32, 80]. The carboxyl and amine groups converted during the depolymerization increase amount of surface charges on the membranes and the surface property change make the membranes applied to particular process requiring high electrostatic repulsion (Donnan exclusion effect [139]). For example, the removal of divalent cations (Ca^{2+} , Mg^{2+}) are important in water softening process since water with high concentration of divalent cations can cause clogging of water pipes and deterioration of industrial equipment such as boilers and cooling towers [140]. In this view, modification of polyamide membrane using the acid-catalyzed hydrolysis can be used to water softening process by utilizing enhanced electrostatic repulsion interaction between the divalent ions and membranes. In addition, modification using acid-catalyzed hydrolysis can tailor the pore size of the membrane for specific purposes, such as enrichment of antibiotics.

Antibiotics have been generally applied to treat bacterial infections in the medical field for the last 80 years, since they are highly effective for the control of microorganisms with minimal toxicity to people [141, 142]. The antibiotics' molecular masses range from about 200 to 1500 Da [143], which are similar or slightly higher than the MWCO of NF membranes, because molecular weight cut off (MWCO) of regular semi-aromatic piperazine based polyamide ranges from ~200 to 400 Da [137, 144]. Antibiotics are mostly prepared by fermentation of bacteria or fungi in the broths [142], then, ultrafiltration system is conducted to quarantine the microorganisms in a purification process [145]. Finally, purified products are extracted by solvent, followed by vacuum distillation to enrich the products [141]. Some paper [141, 142] suggested that NF techniques could be used to help both the solvent extraction and vacuum distillation processes by decreasing the volume of the feed solution, resulting in improved efficiency. In order to apply NF membrane to the recovery of the antibiotics, the membrane should have a high rejection of antibiotics but a low rejection of salt. Larger amounts of antibiotics retained in the feed side of the membrane due to high rejection minimizes the loss of product, whereas the salt enrichment on the feed side causes a build-up of concentration polarization and osmotic pressure, subsequently decreasing the permeability of the solution and overall energy efficiency [146].

In this work, physico-chemical properties of a commercial NF semi-aromatic polyamide TFC membrane was systemically investigated during the post-treatment of the membrane via acid-catalyzed hydrolysis under various acidic conditions. Characterizations were conducted using various analytical tools such as (1) SEM (scanning electron microscope) for surface morphology, (2) ATR-FTIR (attenuated total reflectance Fourier transform infrared spectroscope) for measurement of changed chemical bonds, (3) contact angle analyzer for hydrophilicity of membrane surface, (4) electrophoretic

light scattering spectrophotometer for measuring surface charge of the membrane, and (5) filtration test equipment for measuring MWCO as well as permeation properties of water flux, rejection, and selectivity. The hydrolysis condition was optimized based on the characterization study, and the membrane was modified for use in water softening and antibiotics enrichment processes.

(a) Piperazine-amide chemical structure



(b) Acid-catalyzed hydrolysis of amide group

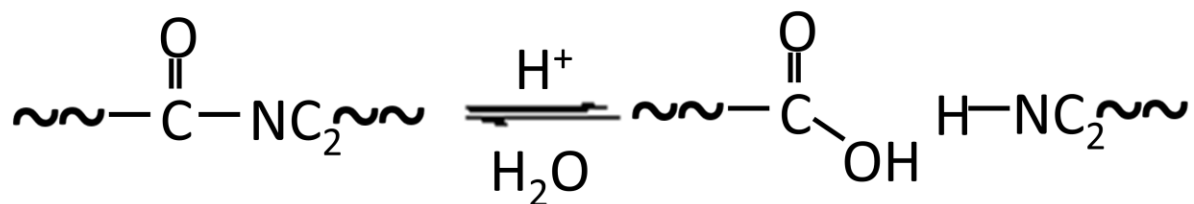


Figure 5.1 Schematic diagram of (a) piperazine-amide chemical structure and (b) acid-catalyzed hydrolysis reaction of the amide group.

5.2 Materials and methods

5.2.1 Chemicals and materials

Commercially available NE40 and NE70 thin-film composite (TFC) NF membrane, obtained from Toray Chemical Korea Inc (Korea), were used to represent a semi-aromatic polyamide (PA) membrane. Characteristics of the membranes reported by the manufacturer are given in Table 5.1 [4].

The following chemicals were used without further purification: Sulfuric acid was purchased from DaeJung Chemicals (Korea) to modify the membrane via acid-catalyzed hydrolysis. Nitric acid was used to adjust pH in the water softening experiment and obtained from Sigma-Aldrich Co., Ltd. (MO, USA). Sodium chloride (NaCl) and magnesium sulfate ($\text{MgSO}_4 \cdot 7\text{H}_2\text{O}$) were purchased from Samchun Chemicals (Seoul, Korea) and Sigma-Aldrich Co., Ltd. (MO, USA), respectively, for the filtration test. Neutral solutes of polyethylene glycol (PEG, M_w 200, 300, 400, 600, and 1000 Da), and sugars (glucose (M_w 180 Da), saccharose (M_w 342 Da), raffinose (M_w 594 Da), and α -cyclodextrin (M_w 972 Da)) were selected to evaluate MWCO of virgin and post-treated membrane, and these chemicals were purchased from Tokyo Chemical Industry (TCI) Co., Ltd. (Tokyo, Japan) and Sigma-Aldrich Co., Ltd. (MO, USA), respectively. Erythromycin ($M_w \sim 734$ Da, $850 \mu\text{g mg}^{-1}$) and vancomycin hydrochloride ($M_w \sim 1486$ Da, $900 \mu\text{g mg}^{-1}$) were purchased from Sigma-Aldrich Co., Ltd. (MO, USA) as representative antibiotics. Milli-Q water (18 $M\Omega$ resistivity, Millipore®, Merck Millipore, Germany) was utilized as the solvent for preparing aqueous solutions as well as rinsing the membrane samples.

Table 5.1 Specifications of NE 40 and 70 membranes from supplier.

Membrane	Manufacturer	Water permeation	Monovalent ion rejection	Test condition	Operating pH range
NE 40 (NE4040-40)	Toray Chemical Korea	49.8 L/m ² h	20.0-60.0%	Feed solution: 2000 mg/L NaCl Applied pressure: 75psi Effective membrane area: 7.9m ²	2-11
NE 70 (NE2540-70)	Toray Chemical Korea	28.3 L/m ² h	40.0-70.0%	Feed solution: 2000 mg/L NaCl Applied pressure: 75psi Effective membrane area: 2.5m ²	2-11

5.2.2 Characterization of membranes

In this work, the NE70 membranes (membrane area: 10cm × 15cm) were post-treated via acid-catalyzed hydrolysis under various acidic conditions of 1L volume of H₂SO₄ ranging from pH 0 to 2 during 7, 14, 28, 42, and 60 days. For the hydrolysis experiments using NE40 membrane, the membrane was exposed to 1L volume of 15 wt% sulfuric acid up to 14 days. The hydrolysis was conducted in Pyrex glass bottles with PTFE (polytetrafluoroethylene) covers. Then, the membrane samples were taken from each condition and rinsed thoroughly with de-ionized water, followed by storage in Milli-Q water at room temperature until use in filtration tests. In addition, membranes were freeze-dried for over 2 days in a vacuum freeze dryer (Biocryos, Korea) in preparation for analysis with Attenuated Total Reflectance-Fourier Transform Infrared spectroscopy (ATR-FTIR), Scanning Electron Microscopy (SEM), and contact angle.

5.2.2.1 ATR-FTIR and SEM

An attenuated Total Reflectance-Fourier Transform Infrared spectroscopy was utilized for analyzing the influence of post-treatment on the chemical properties of the membranes. The measuring method was referred to other previous papers [91, 147]. The ATR-FTIR spectrometer (Nicolet 6700, Thermo Scientific USA) was operated with a flat plate Germanium ATR crystal with an incident angle of 42°. Vacuum-dried membrane samples were continuously purged with nitrogen gas during measurement and 64 scans of spectra from 1000 to 4000 cm⁻¹ wave numbers with a resolution of 4 cm⁻¹ were averaged. The thickness of the active layers were evaluated based on peak intensities of C=O bond-stretching (1634 cm⁻¹) of semi-aromatic PA and aromatic in-plane ring bend stretching vibration (1587 cm⁻¹) of a polysulfone (PSf) support layer [92].

Surface images of the virgin and post-treated membranes were obtained using a Field Emission Scanning Electron Microscope (FE-SEM) (Cold FE-SEM SU8000, Hitachi, USA) to investigate the effect of post-treatment on membrane surface morphology. The vacuum-dried membrane was mounted on a specimen using conductive carbon tape, then all samples were coated with platinum (Pt) at 20 mA in 2 × 10⁻³ mbar for 60 sec in a Turbo Pumped High-Resolution Chromium Sputter Coater (K575X, EMITECH, Lohmar, Germany) to reduce image artifacts generated by electrostatic charge.

5.2.2.2 Contact angle and Zeta potential

Contact angle of virgin and post-treated membranes were conducted to evaluate effect of post-treatment on the membrane surface's hydrophilicity using a goniometer (Phoenix 300Plus, Surface &

Electro Optics Co. Ltd., Korea) and sessile drops method. To get representative contact angle values, measurement was conducted over 10 points using three separately prepared membranes coupons. All membrane samples were vacuum dried simultaneously to achieve the same condition.

Electrophoresis was performed to study the influence of post-treatment on membrane surface charge. The surface zeta potentials of the membranes were measured three times by an electrophoretic light scattering spectrophotometer (ELS-8000, Photal, Otsuka Electronics, Japan). Wet membrane samples soaked in Milli-Q water over 24 h were attached to a plate sample cell, then zeta potential was measured using a 10mM NaCl electrolyte solution with polystyrene latex particles (diameter: 520 nm) (Otsuka Electronics, Osaka, Japan) in the range of pH 3 to 9. The acidic and basic pH values were adjusted using 1M HCl and NaOH, respectively.

5.2.2.3 Molecular weight cut off (MWCO) and pore size of membranes

The MWCO value of the membrane was determined by the molecular weight of the neutral solute which had 90% rejection. The MWCO values of the virgin and post-treated membranes were obtained using the method which was reported in previously published papers [142, 146, 148]. Filtration tests were conducted with feed solution containing both 200 ppm single neutral solute of sugars (glucose (M_w 180 Da), saccharose (M_w 342 Da), raffinose (M_w 594 Da), and α -cyclodextrin (M_w 972 Da)) [148], and 1000 ppm polyethylene glycol (PEG, M_w 200, 300, 400, 600, and 1000 Da) [142, 146] as model solutes under 10 bar. The concentration of neutral solute in the feed and permeate solutions were measured with a Total Organic Carbon analyzer (TOC-V, Shimadzu, Japan). Pore size of NE 70 virgin and modified membranes were evaluated by the mathematical prediction using Eq. (5.1) [149, 150]. Average pore radius of membranes were calculated using rejection data of four neutral solutes (Glucose, Saccharose, Raffinose, and PEG 1000).

$$\text{Neutral solute's rejection (\%)} = 1 - \left\{ 1 - \left[\frac{r_s}{r_p} \left(\frac{r_s}{r_p} - 2 \right) \right]^2 \right\} \exp(-0.7146 \times \frac{r_s^2}{r_p^2}) \quad (5.1)$$

where r_s is the radius of solute and r_p is the radius of membrane pore.

5.2.3 Filtration tests

The virgin NF membrane (NE70) and post-treated membrane were tested in pressurized mode to investigate the effect of post-treatment on the permeation properties using a test cell [4]. Three membrane coupons with 19.6 cm² effective area were tested at flow rates of 1 L min⁻¹ at room temperature. In order to investigate single or mixture solutions of NaCl and MgSO₄ in the water softening experiment, solutions used were 2,000 ppm concentration of NaCl or MgSO₄ as single feed

solution or a combined NaCl/MgSO₄ mixture 1,000 ppm concentration of each, both with and without adjusting pH using nitric acid. The operating pressure of the filtration test was first compacted at 150 psi for 60 min, followed by a 30 min stabilization time at 75 psi before measurement of water flux and salt rejection. The permeate water flux (J_w , (Lm⁻²h⁻¹ or LMH)) and salt rejection was calculated by both Eq. (5.2) and (5.3). Concentration of ionic NaCl and MgSO₄ in feed and permeate was measured by conversion from conductivity to concentration, and conductivity of single solution was measured by a calibrated conductivity meter (Ultrameter IITM, Myron L Company, USA). In the case of NaCl/MgSO₄ mixture, the concentration of cations and anions within the feed and permeate solutions were obtained by ICP-MS (ELAN DRC-II, Perkin Elmer, Massachusetts, America) and ion chromatography (IC; Dionex ICS-3000, Thermo Fisher Scientific Inc., USA), respectively.

$$J_w = \frac{\Delta \text{ weight}}{\Delta \text{ time} \times \text{effective membrane area} \times \text{water density}} \quad (\text{Lm}^{-2}\text{h}^{-1} \text{ or LMH}) \quad (5.2)$$

$$R = \left(1 - \frac{[\text{NaCl or MgSO}_4]_{\text{permeate}}}{[\text{NaCl or MgSO}_4]_{\text{feed}}} \right) \times 100 \quad (\%) \quad (5.3)$$

5.2.4 Ideal selectivity and mixture selectivity

Membrane selectivity between A and B can be expressed in terms of α_B^A which consists of concentration ratio A to B in permeate and concentration ratio A to B in feed as shown in Eq. (5.4) where C_f and C_p are solute concentrations in the feed and permeate, respectively [140]. This selectivity value shows how much different solutes preferentially pass through the membrane.

$$\alpha_B^A = \frac{\frac{C_{A,p}}{C_{B,p}}}{\frac{C_{A,f}}{C_{B,f}}} = \frac{C_{A,p} \times C_{B,f}}{C_{B,p} \times C_{A,f}} = \frac{100 - R_A}{100 - R_B} \quad (5.4)$$

In the field of gas separation, selectivity is divided into ideal selectivity or mixture selectivity depending on whether the feed gas is a single or binary mixture, respectively [151]. Ideal selectivity is an intrinsic property of the membrane, and should be equal to mixture selectivity without consideration of the mixture species' interaction with the membrane. The interaction of mixed ion species with the membrane was investigated by comparing ideal selectivity and mixture selectivity. Ideal selectivity was measured first to select optimal conditions of pH and exposure time for the application of water softening, followed by measuring mixture selectivity using an optimized membrane in a single electrolyte condition.

5.2.5 Antibiotics separation and enrichment

The virgin NF membrane (NE70) and membrane optimized by post-treatment were used to compare permeation properties in the application of antibiotics separation and enrichment. The model antibiotics used in this study are erythromycin ($M_w \sim 734$ Da) and vancomycin ($M_w \sim 1449$ Da) [142]. Composition of antibiotics/salt mixture in feed solution (4L volume) was 100 ppm antibiotics and 10 g L^{-1} NaCl. The pH of erythromycin and vancomycin feed solution was 8.8 and 4.7 at the operating concentration, respectively, since the chemicals were used without further purification. The feed solution was concentrated under 10 bar by wasting permeate solution until 1L of feed volume remained at room temperature. 75% recovery was defined as the feed solution permeated from 4L to 1L. In order to calculate rejection, the antibiotics and NaCl concentration in the feed and permeate solutions were measured by a calibrated total organic carbon analyzer and conductivity meter, respectively. In order to compare the amount of salt enrichment between virgin and post-treated membranes, the amount of salt enrichment when unit amount of antibiotics is recovered can be expressed by $\Delta C_{antibiotic}^{salt}$, which consists of salt concentration ratio of initial (at 0% recovery of feed solution) to final (at 75% recovery of feed solution) in feed solution and antibiotics concentration ratio of initial to final in feed solution (Eq. (5.5)). A lower $\Delta C_{antibiotic}^{salt}$ value is desired in the enrichment of antibiotics, because it has lower amount of osmotic pressure generated by enrichment of salt during simultaneous enrichment of antibiotics. The flux reduction ratio of each membrane was evaluated through Eq. (5.6) using permeated initial (at 0% recovery of feed solution) and final water flux (at 75% recovery of feed solution) according to the modification of method developed by other researcher [152].

$$\Delta C_{antibiotic}^{salt} = \frac{\frac{C_{salt, at 75\% recovery of feed solution}}{C_{salt, at 0\% recovery of feed solution}}}{\frac{C_{antibiotic, at 75\% recovery of feed solution}}{C_{antibiotic, at 0\% recovery of feed solution}}} \quad (5.5)$$

$$Flux\ reduction\ ratio\ (\%) = \left(1 - \frac{J_{w, at 75\% recovery of feed solution}}{J_{w, at 0\% recovery of feed solution}}\right) \times 100\ (\%) \quad (5.6)$$

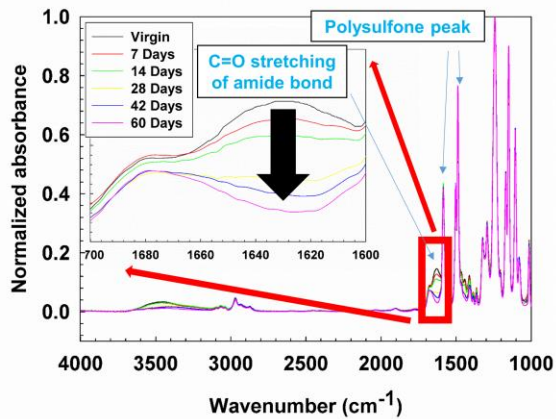
5.3 Results and discussion

5.3.1 Characterization of virgin and post-treated membrane

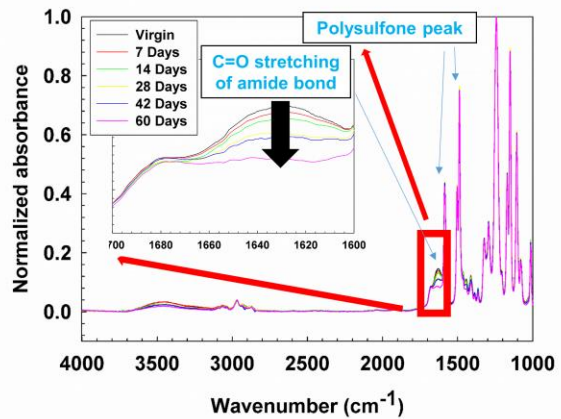
5.3.1.1. Effect of post-treatment on chemical structure of membrane and surface morphology

The ATR-FTIR spectra of virgin NE70 and post-treated membranes were measured to investigate effect of post-treatment on the chemical structure of the membrane. Since most semi-aromatic NF PA membranes are restricted to pH 2-11 [24], post-treatment of the membrane using acid-catalyzed hydrolysis was conducted with sulfuric acid at less than pH 2. Figure 5.2 shows the spectra of virgin and post-treated semi-aromatic PA membranes which were exposed to (a) pH 0, (b) pH 0.25, (c) pH 0.5, (d) pH 0.75, (e) pH 1, and (f) pH 2 for various exposure times. The spectra ranging from 1000 cm^{-1} to 4000 cm^{-1} reveals characteristic bond motions of PA in the active layer as well as PSf in the support layer due to the penetration depth of FTIR beam being deeper than thickness the of active layer. In order to evaluate the change of peak due to the post-treatment, the FTIR peaks were normalized around the 1250 cm^{-1} peak which is attributed to strong C–O–C asymmetric stretching vibration of PSf [126]. Absorbance peaks at wavenumbers 1634 and $1587/1488\text{ cm}^{-1}$ are attributed to the amide (I) band of semi-aromatic PA and aromatic in-plane ring of PSf substrate, respectively [92]. The C=O stretching amide bond peak at 1634 cm^{-1} continuously decreased with both increasing strength of acid and exposure time due to acid-catalyzed hydrolysis. However, peaks of PSf at $1587/1488\text{ cm}^{-1}$ were not decreased, because the PSf support layer is widely known as a polymer with high chemical stability [42].

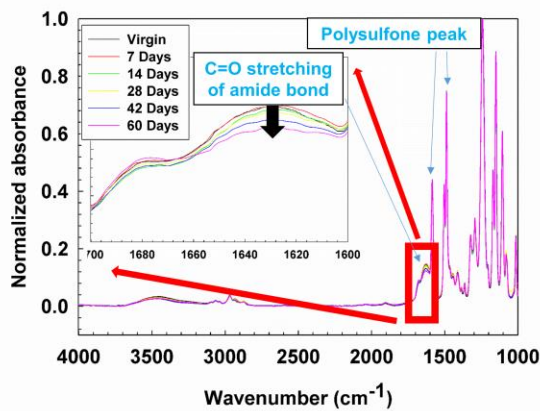
(a) pH 0



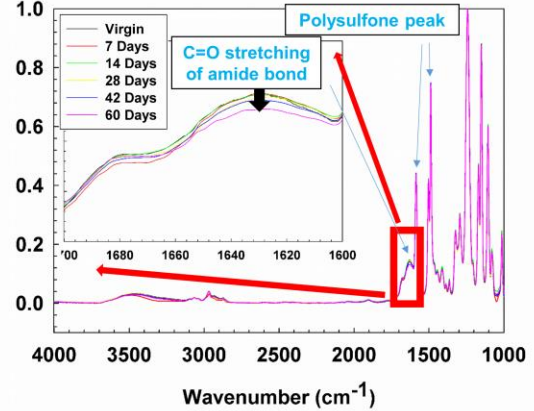
(b) pH 0.25



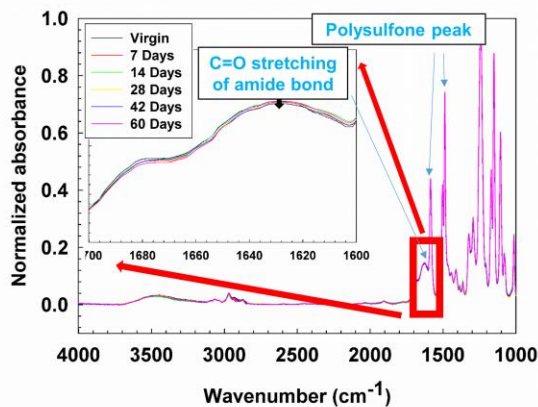
(c) pH 0.5



(d) pH 0.75



(e) pH 1



(f) pH 2

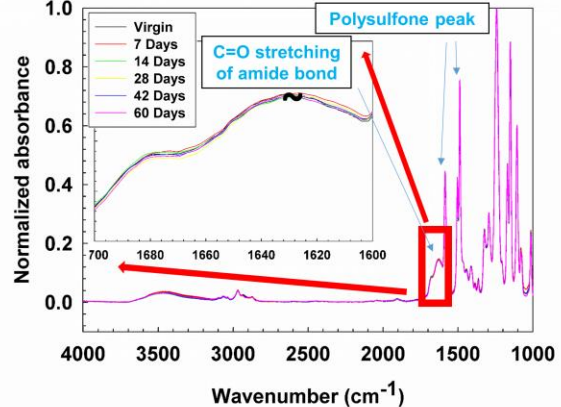


Figure 5.2 ATR-FTIR spectra of semi-aromatic NE70 virgin and post-treated polyamide membranes under (a) pH 0, (b) pH 0.25, (c) pH 0.5, (d) pH 0.75, (e) pH 1, and (f) pH 2 conditions with characteristic bands from 1000 cm^{-1} to 4000 cm^{-1} related to the membrane polyamide active layer and polysulfone support layer. Absorbance peaks at wavenumbers 1634 and 1587/1488 cm^{-1} are attributed to the amide (I) band of semi-aromatic polyamide and polysulfone layer, respectively.

The surface morphology of virgin and post-treated membranes was characterized by SEM images (Fig. 5.3). Piperazine-based semi-aromatic NF membrane is generally either grainy or smooth [137]. According to Fig. 5.3 (c) and (d), semi-aromatic PA membranes' surface were continuously peeled from the PSf support layer, revealing the PSf support layer clearly after exposure to pH 0 sulfuric acid over 14 days. These results are in good agreement with the FTIR result showing continuously decreased peak intensity of amide (I) band at wavenumber 1634 cm^{-1} . However, post-treatment at greater than pH 0.25, as shown in Fig. 5.3 (g) to (k), does not show the complete peeling of the active layer from the PSf support layer.

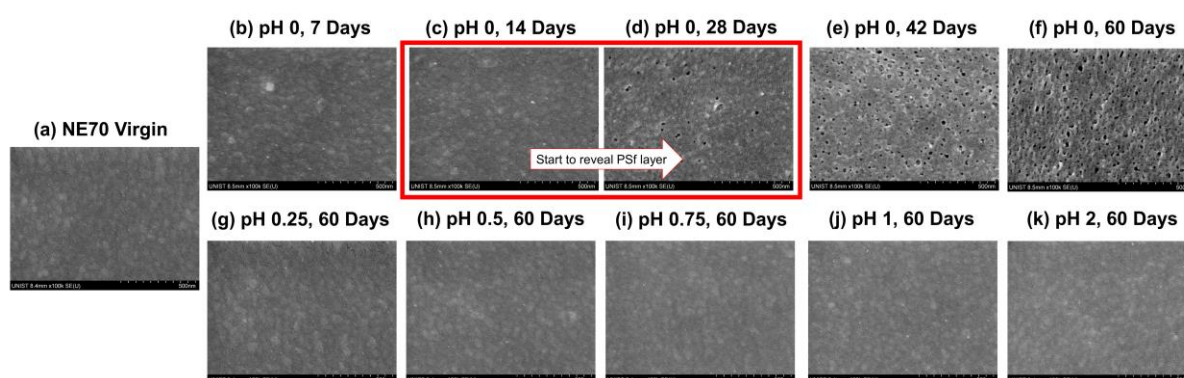


Figure 5.3 Surface morphology of virgin NE70 (a) and post-treated membranes from (b) to (k) measured by SEM in terms of strength of acid and post-treatment time.

5.3.1.2 Effect of post-treatment on permeability and salt rejection

Performance of semi-aromatic PA NE70 virgin and post-treated membranes was measured in a pressurized condition to investigate effect of post-treatment on permeability and salt rejection. Water flux and salt rejection of the membranes exposed to various strength of acid and exposure time are shown in Fig. 5.4 (a) to (f). Water flux of post-treated membrane monotonically increased and salt rejection continuously decreased with increasing strength of acid and exposure time in the case of both NaCl and MgSO_4 single feed solution (Fig. 5.4 (a) to (e)). This tendency of water flux and salt rejection is in strong agreement with the trade-off relationship between permeability and selectivity [153]. However, there seems to be no influence on the water flux and salt rejection in the case of post-treatment by pH 2 acidic condition during 60 days as shown in Fig. 5.4 (f), and manufacturer's product catalog also supported this results (operating limit of pH range is from 2 to 11).

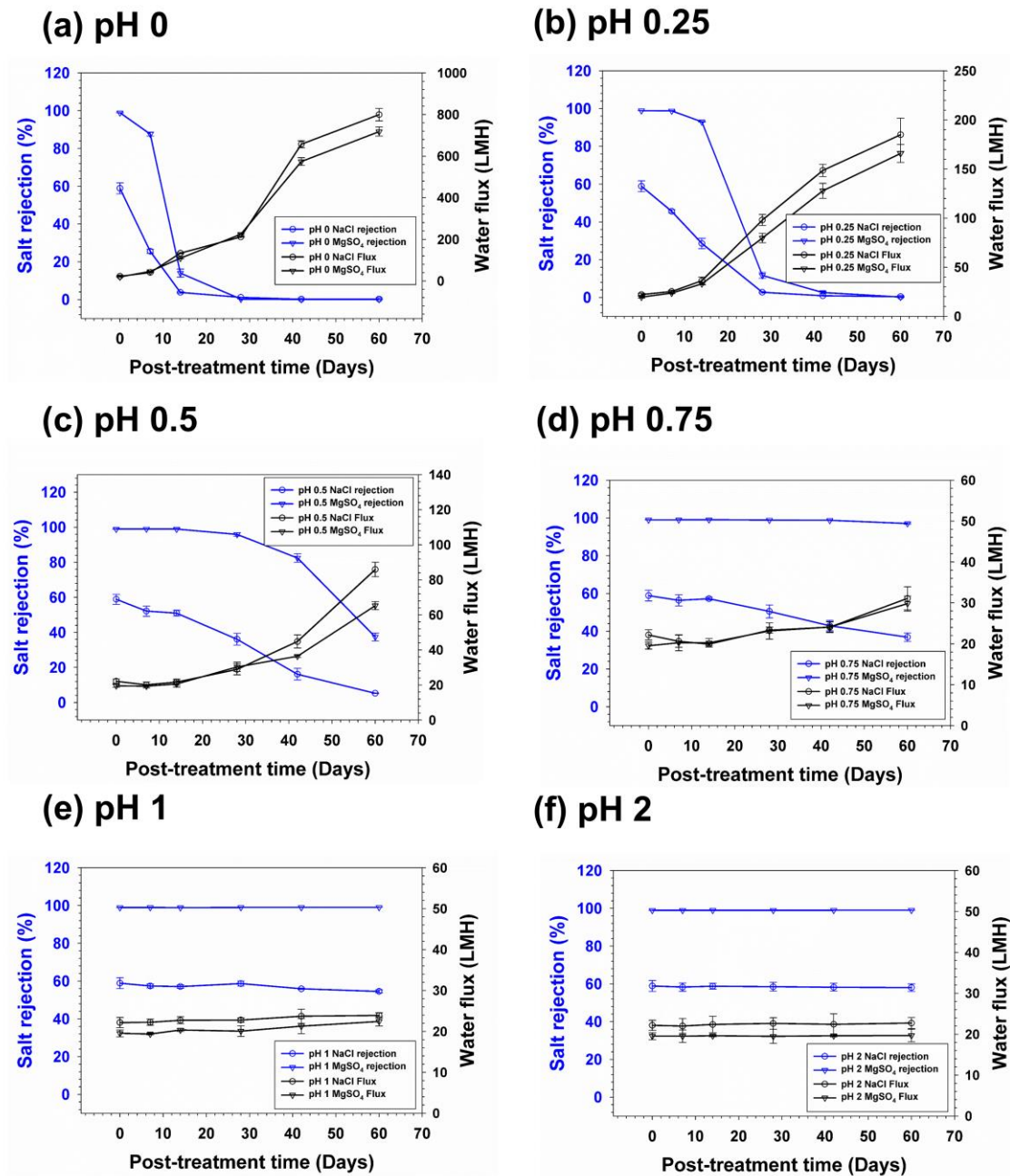


Figure 5.4 Permeation properties (water flux and rejection) of virgin and post-treated membranes with increasing strength of acid and post-treatment time (tested at 75 psi, using 2,000 ppm NaCl or MgSO₄ single solution).

5.3.1.3 Effect of post-treatment on hydrophilicity and surface charge (Contact angle and zeta potential)

Contact angle was measured to investigate effect of post-treatment on surface's hydrophilicity (Table. 5.2). The contact angle value of NE70 virgin membrane was $45.6^\circ \pm 2.4^\circ$, but the value decreased to $40.6^\circ \pm 2.3^\circ$ with increasing post-treatment time up to 28 days in pH 0.25 acidic solution. Mänttari et al. [108] studied the effect of surface charge on hydrophilicity of a membrane surface and showed that hydrophilicity increases when the surface of the membrane has positively or negatively charges. As discussed in Fig. 5.1, amide groups are converted to carboxyl and amine group by acid-catalyzed hydrolysis. The more negative charge of the carboxyl group and positive charge of the amine group at neutral pH [111] after acid-catalyzed hydrolysis could increase hydrophilicity of the membrane surface.

Table 5.2 Contact angles of NE70 virgin and post-treated membranes by pH 0.25 acidic solution for 7, 14, and 28 days using Milli-Q water.

Membrane	Virgin	Post-treated (pH 0.25 7 Days)	Post-treated (pH 0.25 14 Days)	Post-treated (pH 0.25 28 Days)
Contact angle (°)	45.6 ± 2.4	44.8 ± 2.6	43.0 ± 2.7	40.6 ± 2.3

Electrophoresis method was used to measure surface's zeta potential and to investigate the effect of post-treatment on membrane surface charge. Figure 5.5 shows zeta potential of the NE70 virgin and post-treated membranes exposed to pH 0.25 acidic solution for 7, 14, and 28 days. Isoelectric point (IEP) of NE70 virgin membrane was \sim pH 4. The surface of the semi-aromatic PA membrane becomes positively charged below IEP and negatively charged above IEP because of the protonation of the amine group of piperazine and the deprotonation of the carboxyl group, respectively [111]. Because acid-catalyzed hydrolysis of amides produces more negative charge of carboxyl groups and positive charge of amine groups on the membrane surface, absolute value of zeta potential increased with increasing post-treatment time with maintained IEP. Both contact angle and zeta potential results clearly supported that post-treatment using acid-catalyzed hydrolysis converted amide groups into amine and carboxyl groups on the membrane surface, increasing hydrophilicity and surface charges.

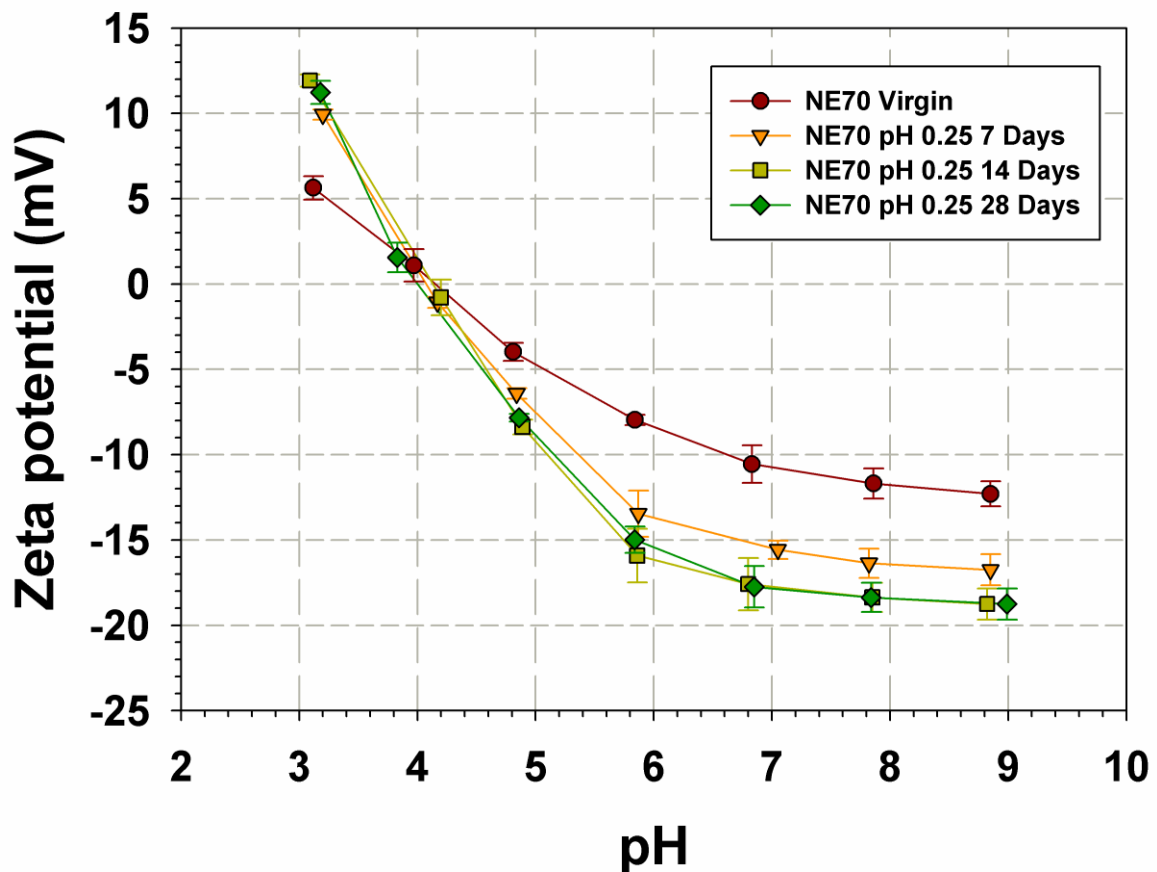


Figure 5.5 Zeta potential of the NE70 virgin and post-treated membrane by pH 0.25 acidic solution for 7, 14, and 28 days.

5.3.2 Application of post-treated membrane to water softening

Water containing high concentration of divalent cations (Ca^{2+} , Mg^{2+}) can cause serious problems in industrial equipment such as boilers, cooling towers, etc. The process to remove those divalent cations in hard water is called water softening, and NF membranes are sometimes used in this application. In this case, allowing the passage of monovalent ions through the membrane is beneficial since it can relatively reduce osmotic pressure of the feed solution, resulting in a sustained high water flux. That is, membrane for water softening requires high rejection of divalent ions (Ca^{2+} , Mg^{2+}) as well as low rejection of monovalent ions. In this work, NaCl and MgSO_4 were used to evaluate the performance of a prepared membrane in water softening as representative monovalent and divalent ions, respectively.

Selectivity has been previously used as a quantitative analytic parameter for water softening [140]. Since ideal selectivity is an intrinsic property of the membrane, it is measured firstly to select the optimization condition of pH and exposure time using a single electrolyte solution, followed by measuring mixture selectivity using NaCl/ MgSO_4 mixture solution. Figure 5.6 shows ideal selectivity of NE70 virgin and post-treated membranes exposed to acidic solution of pH 0 to 2 for various increasing post-treatment times. Ideal selectivity of post-treated membranes increased from initially 39 (NE70 virgin) up to 47 due to enhanced permeation of monovalent ion (NaCl) with sustained rejection of divalent ions when PA was partially post-treated. Afterwards ideal selectivity of post-treated membranes decreased from 47, which is a limiting ideal selectivity, to 1, a non-selective state, with decreasing pH or increasing exposure time during post-treatment because further hydrolysis permeated divalent ion (MgSO_4) along with monovalent ion. The selectivity enhancement by partial acid-catalyzed hydrolysis was also confirmed by semi-aromatic NE40 membrane which was manufactured by Toray Chemical Korea Inc (Korea). The ideal selectivity of virgin NE40 membranes was 11, but the selectivity increased up to 15 at the exposure time of 3 days, and then decreased to 1 after 14 days (Table 5.3).

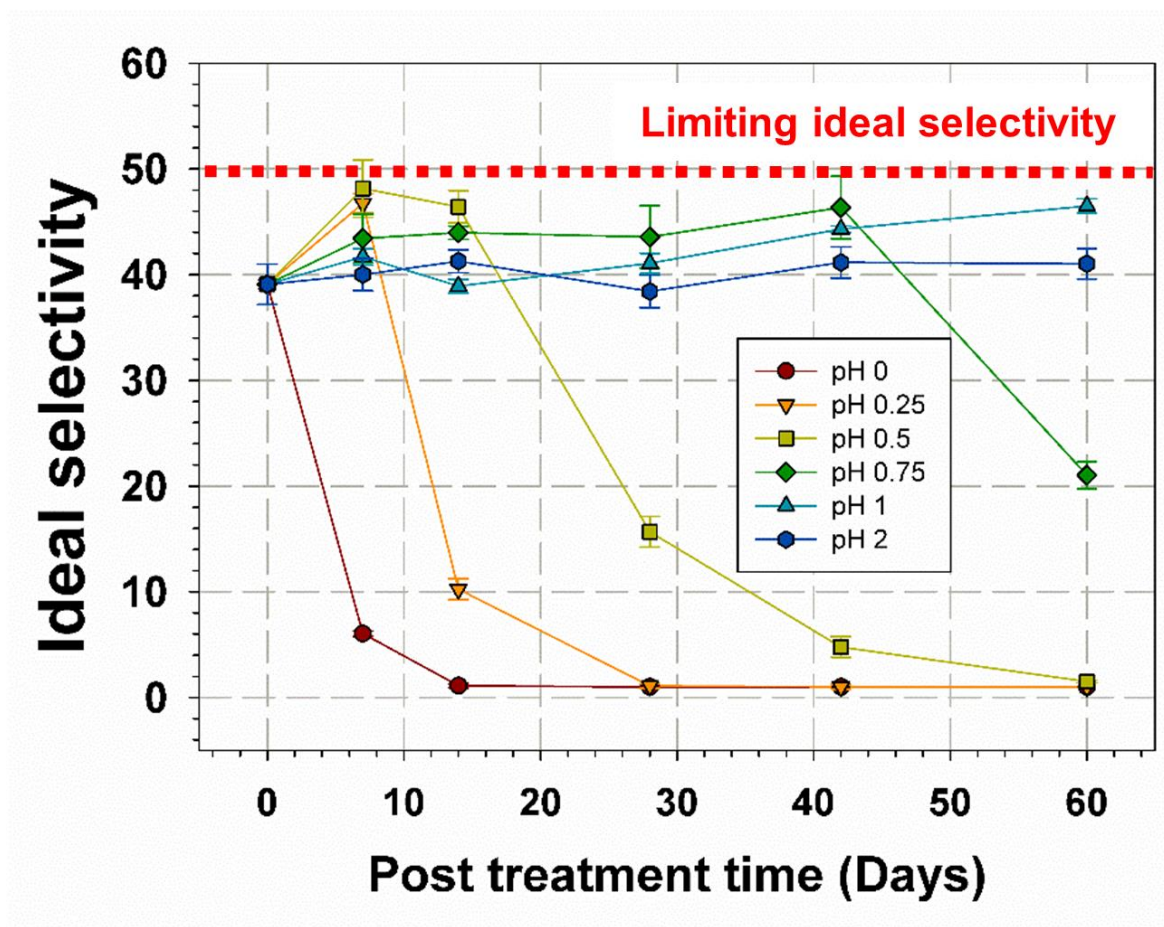


Figure 5.6 Ideal selectivity of NE70 virgin and post-treated membranes under acidic solution ranging from pH 0 to 2 with increasing post-treatment time.

Table 5.3 Permeation properties (water flux, rejection, and ideal selectivity) of NE40 virgin and post-treated membranes with increasing post-treatment time using 15 wt% sulfuric acid (tested at 75 psi, using 2,000 ppm NaCl or MgSO₄ single solution).

	NE40 virgin	NE40 3 Days	NE40 7 Days	NE40 14 Days
NaCl Flux	58.0 ± 1.6	72.1 ± 4.7	169.7 ± 1.2	359.8 ± 1.4
MgSO ₄ Flux	49.6 ± 0.1	54.0 ± 3.8	137.7 ± 0.6	263.1 ± 6.9
NaCl Rejection	36.4 ± 1.0	9.1 ± 0.3	2.1 ± 0.2	0.3 ± 0.0
MgSO ₄ Rejection	94.2 ± 0.2	94.0 ± 0.3	9.7 ± 0.6	0.1 ± 0.0
Ideal selectivity	11.0 ± 0.3	15.1 ± 0.5	1.1 ± 0.1	1.0 ± 0.0

In order to clearly summarize effects of acid concentration or exposure time during post-treatment on improvement of ideal selectivity, total post-treated membranes' ideal selectivity used in Fig. 5.6 were plotted against ATR-FTIR's peak intensity ratio of representative PSf support layer (1587 cm^{-1}) to polyamide layer (1634 cm^{-1}) (Fig. 5.7). The degree of post-treatment can be indirectly calculated by FT-IR peak intensity ratio of PSf to PA, because depolymerization occurred only in PA due to the high chemical stability of PSf [42]. Depending on degree of post-treatment, ideal selectivity increased (shown in blue oval), then decreased (shown in orange box) (Fig. 5.7). That is, effective or excessive post-treatment can be determined by degree of post-treatment based on the purpose of application.

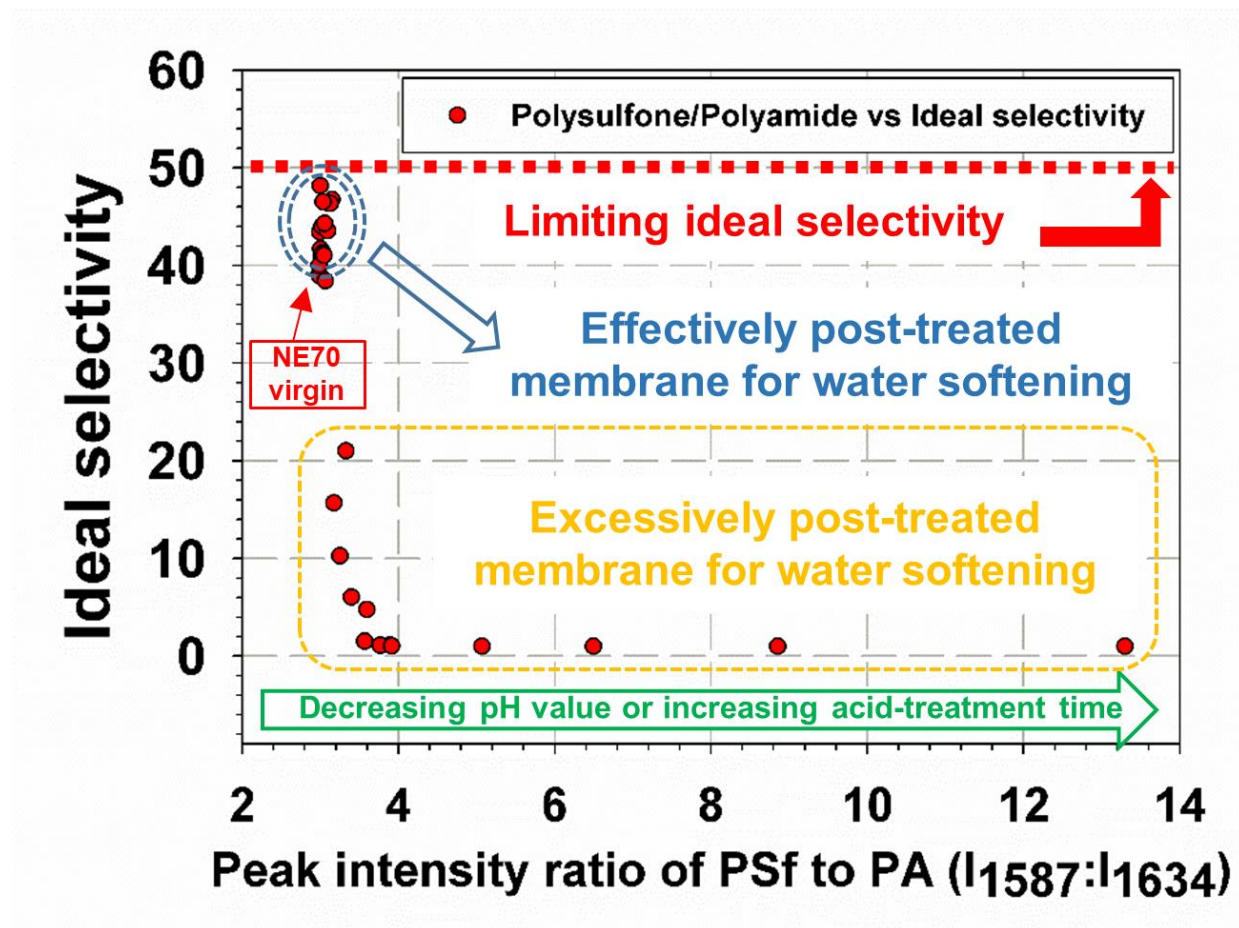


Figure 5.7 ATR-FTIR's peak intensity ratio of representative polysulfone support layer (1587 cm^{-1}) to polyamide layer (1634 cm^{-1}) for comparison of degrees of ideal selectivity with increasing acid concentration or exposure time to acidic solution.

The optimized membrane with the highest ideal selectivity was the treated under the condition of pH 0.25 for 7 days; this membrane was selected to compare with NE70 virgin membrane by measuring mixture selectivity. This optimized membrane showed an improvement of about 10% water flux and 20% ideal selectivity as shown in Table 5.4. In terms of measuring method for rejection, the conductivity meter can measure only single electrolyte solution. Thus, ICP-MS was used for measuring mixture selectivity of NE70 virgin and optimized post-treatment membrane. There was no significant difference between the two techniques for measuring salt rejection (Table 5.4).

Table 5.5 gives mixture selectivity with water flux and salt rejection of NE70 virgin and post-treated membrane. Mixture selectivity of each membrane was in contrast with ideal selectivity results. Post-treated membrane's mixture selectivity was about 3 times lower than NE70 virgin membrane. Because ideal selectivity should be equal to mixture selectivity when the interaction of mixture ion species with the membrane is not considered, the lower mixture selectivity value of the treated membrane might derive from the mixture species' interaction with membrane. Generally, rejection of organic compounds and ions by NF membranes is determined by both the relative size of the compounds compared to membrane pore size (or steric hindrance) and electrostatic repulsion [139].

Rejection of divalent cations (Mg^{2+}) in both NE70 virgin and post-treated membrane had the opposite results compared with divalent anion (SO_4^{2-}) as shown in Table 5.5. In this study, electrostatic repulsion is the dominant factor to determine salt rejection of the NF membranes. Zeta potential of post-treated membrane at pH 5.7 is much lower than NE70 virgin membrane (Fig. 5.5) due to increased carboxyl groups created by the acid-catalyzed hydrolysis of polyamide, resulting in an increased SO_4^{2-} rejection and decreased Mg^{2+} rejection by Donnan exclusion effect [139]. In this electrostatic repulsion, the co-ions (same charge with membrane) are preferentially rejected by the membrane surface, followed by rejection of same equivalent number of counter-ions (opposite charge of the membrane) to satisfy the electroneutrality condition, thus determining total salt rejection of the membrane [154]. The main difference between ideal selectivity and mixture selectivity is nonexistence or existence of monovalent ion to satisfy electroneutrality when divalent counter-ion pass through the membrane. In this view, an important factor for mixture selectivity of water softening is positive charge on the membrane surface.

According to Fig. 5.5, zeta potential of the membrane was positive in acidic conditions. When the pH of mixture electrolyte solution was adjusted with nitric acid to pH 3, mixture selectivity of the post-treated membrane was ~2.6 times higher than NE70 virgin membrane (Table. 5.5) due to high positive surface charge by increased amine group resulting from acid-catalyzed hydrolysis of polyamide. These results are in strong agreement with Ouyang et al. [140] which explains that electrostatic repulsion is major factor of Na^+/Mg^{2+} mixture selectivity. The above results suggest that the best water softening can be achieved when the optimized post-treated NF membrane is used in acidic conditions.

Table 5.4 Water flux, salt rejection, and ideal selectivity of NE70 virgin and optimized post-treatment membranes using single feed solution.

Used membranes	Feed concentration (ppm)	Rejection (%) ^a		Water flux (LMH) ^a		Ideal Selectivity (Na ⁺ /Mg ²⁺)
		NaCl	MgSO ₄	NaCl	MgSO ₄	
NE70 virgin	Single solution of	58.9 ± 2.8 ^b	98.9 ± 0.09 ^b	22.1 ± 1.2	19.5 ± 0.8	39.1 ± 1.9 ^b (47.2 ± 1.7) ^c
		(57.5 ± 2.1) ^c	(99.1 ± 0.2) ^c			
Post-treated at pH 0.25 7 Days	NaCl & MgSO ₄ 2000ppm	45.6 ± 0.9 ^b (45.5 ± 2.5) ^c	98.8 ± 0.1 ^b (99.1 ± 0.1) ^c	25.4 ± 1.2	23.6 ± 0.6	46.7 ± 0.9 ^b (60.6 ± 3.3) ^c

^a Performance test was performed at 5 bar, room temperature.

^b Concentration of feed and permeate solution was measured by conductivity meter.

^c Cation's concentration of feed and permeate solution was measured by ICP-MS.

Table 5.5 Water flux, salt rejection, and mixture selectivity of NE70 virgin and post-treated membranes using a NaCl/MgSO₄ mixture solution in neutral and acidic conditions.

Used membranes	pH condition	Feed concentration (ppm)	Rejection of each ions (%) ^a				Water flux (LMH) ^a	Mixture Selectivity (Na ⁺ /Mg ²⁺) ^b
			Na ⁺ ^b	Cl ⁻ ^c	Mg ²⁺ ^b	SO ₄ ²⁻ ^c		
NE70 virgin	Neutral (pH 5.7)	Mixture of NaCl & MgSO ₄ 1000ppm each	39.5 ± 2.7	38.1 ± 4.5	95.7 ± 1.1	98.0 ± 0.05	21.6 ± 1.3	14.0 ± 1.0
Post-treated at pH 0.25, 7 Days			30.8 ± 1.9	18.5 ± 4.4	84.3 ± 1.9	99.5 ± 0.03	27.4 ± 0.5	4.39 ± 0.3
NE70 virgin	Acidic (pH 3.0)	Mixture of NaCl & MgSO ₄ 1000ppm each	67.6 ± 0.5	64.9 ± 0.2	98.7 ± 0.1	98.5 ± 0.1	22.7 ± 1.0	25.1 ± 0.2
Post-treated at pH 0.25, 7 Days			54.0 ± 0.2	55.6 ± 1.3	99.3 ± 0.1	95.7 ± 0.1	26.8 ± 0.3	64.3 ± 0.3

^a Performance test was performed at 5 bar, room temperature.

^b Cation's concentration of feed and permeate solution was measured by ICP-MS.

^c Anion's concentration of feed and permeate solution was measured by ion chromatography.

5.3.3 Application of post-treated membrane in enrichment of antibiotics

NF membrane performance have close relevance to MWCO value which describes pore size of membrane quantitatively [139, 155], therefore, the MWCO of the membranes before and after post-treatments was investigated. Figure 5.8 shows MWCO values measured by (a) PEGs and (b) Sugars rejection curves of NE70 virgin and post-treated membrane treated with a pH 0.25 acidic solution for 0, 7, 14, and 28 days. MWCO values continuously increased with increasing post-treatment time (Fig. 5.8), showing the increase of membrane pore size by the acid-catalyzed hydrolysis [139, 155]. The pore size of the membranes before and after acid-catalyzed hydrolysis was evaluated with the mathematical prediction methods using 4 kinds of rejection data of neutral solutes (Glucose, Saccharose, Raffinose, and PEG 1000) [149, 150]. Average pore radius of the membranes exposed to a pH 0.25 acidic solution for 0 (virgin), 7, 14, and 28 days were 0.62, 0.64, 0.69, and 1.05 nm, respectively (Table 5.6) [149, 150].

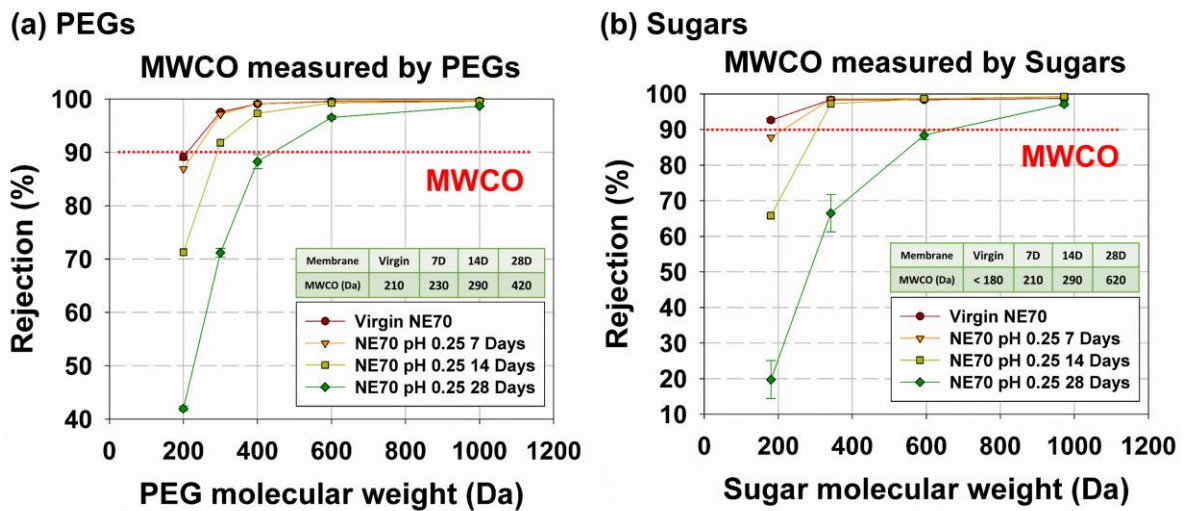


Figure 5.8 (a) PEGs and (b) Sugars rejection curves of NE70 virgin and post-treated membranes in pH 0.25 acidic solution for 7, 14, and 28 days for MWCO measurement (tested with 1000 ppm PEG aqueous solution and 200 ppm sugars aqueous solution under 10 bar).

Table 5.6 Pore radius of NE70 virgin and post-treated membranes by pH 0.25 acidic solution for 7, 14, and 28 days estimated from neutral organic compound's rejection.

Organic compound	Solute radius, r_s (nm)	r_s / r_p	Pore radius, r_p (nm)
NE70 virgin membrane			
Glucose	0.37	0.76	0.48
Saccharose	0.47	0.89	0.53
Raffinose	0.58	0.90	0.65
PEG1000	0.78	0.96	0.82
Average			0.62
NE70 7 Days			
Glucose	0.37	0.70	0.52
Saccharose	0.47	0.88	0.54
Raffinose	0.58	0.89	0.65
PEG1000	0.78	0.95	0.83
Average			0.64
NE70 14 Days			
Glucose	0.37	0.52	0.71
Saccharose	0.47	0.84	0.56
Raffinose	0.58	0.89	0.66
PEG1000	0.78	0.93	0.84
Average			0.69
NE70 28 Days			
Glucose	0.37	0.23	1.59
Saccharose	0.47	0.52	0.91
Raffinose	0.58	0.71	0.83
PEG1000	0.78	0.89	0.88
Average			1.05

MWCO values measured by different neutral solutes (PEG and sugar) revealed different tendencies. Virgin NE70 membrane's MWCO was 210 and less than 180 Da as measured by PEGs and sugars, respectively. This MWCO value of NE70 virgin membrane measured by PEGs are similar to another published paper [144]. MWCO of the membrane exposed to pH 0.25 for 28 days was 420 or 620 Da when measured by PEGs and sugars, respectively. The MWCO of the virgin NF membrane had lower MWCO at PEG, however, the MWCO of the hydrolyzed membrane showed higher MWCO with sugars. It is likely that the discrepancy of MWCO using different model compounds occurred due to the contribution of molecular shape of neutral solutes to rejection [150]. Wang et al. [150] characterized NF membrane using Cephalexin ($M_w \sim 347$ Da) and saccharose ($M_w \sim 342$ Da), which had similar molecular weight. Rejection of Cephalexin was higher than saccharose, because the Cephalexin molecule is a more rod-like than a saccharose molecule, resulting in increased steric hindrance [150]. Likewise, sugar molecules used in this study are more spherical than PEG molecules, resulting in larger steric hindrance at smaller pore-sized membrane, but lower steric hindrance at larger pore-sized membrane as schematically explained in Fig. 5.9 (a).

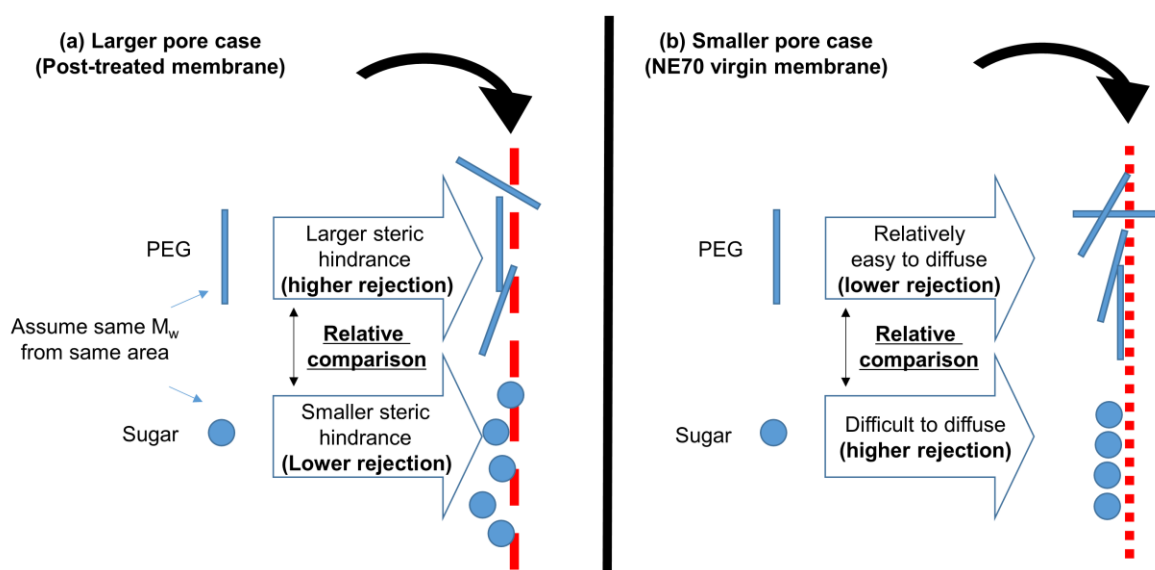


Figure 5.9 Schematic illustration of PEG and sugar's rejection in (a) larger and (b) smaller pore case.

Erythromycin (ERY, $M_w \sim 734$ Da) and vancomycin (Van, $M_w \sim 1449$ Da) were selected as representative antibiotics. On the basis of NE70 virgin and post-treated membranes' MWCO value as shown in Fig. 5.8, NE70 virgin and post-treated membranes (pH 0.25 for 7 and 14 days) were chosen for the enrichment of antibiotics for minimization of loss. $\Delta C_{antibiotic}^{salt}$ value was used to compare the amount of salt enrichment between virgin and post-treated membranes (Table. 5.7). Post-treated

membranes in terms of concentration polarization and osmotic pressure from salt enrichment were much better than virgin NE70 membrane, because lower $\Delta C_{antibiotic}^{salt}$ values represent low amounts of NaCl enrichment during simultaneous antibiotics enrichment, resulting in better water flux and energy efficiency.

Table 5.7 Relative enrichment ratio of salt to antibiotic ($\Delta C_{antibiotic}^{salt}$) and flux reduction ratio using NE70 virgin and post-treated membranes.

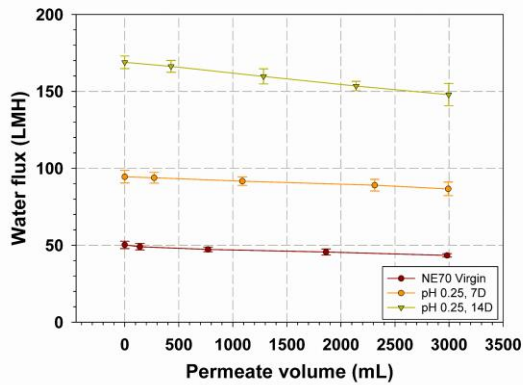
Used membranes	Target antibiotics	$\Delta C_{antibiotic}^{salt}$	Flux reduction ratio (%)
NE70		0.43	13.6
Post-treated at pH 0.25, 7 Days	Erythromycin (ERY)	0.36	8.3
Post-treated at pH 0.25, 14 Days		0.33	12.4
NE70		0.43	18.3
Post-treated at pH 0.25, 7 Days	Vancomycin (Van)	0.34	13.2
Post-treated at pH 0.25, 14 Days		0.27	11.7

The flux reduction ratio of each membrane was also evaluated (Table. 5.7). Flux reduction ratio of post-treated membranes were lower than virgin NE70 membrane in both ERY and Van concentration. The flux decline may result from both concentration polarization on the membrane surface due to salt enrichment (Fig. 5.10 (c) and Fig. 5.11(c)) [146] and membrane fouling [156]. Tang et al. [156] explained the relationship between flux reduction and initial water flux. Membrane fouling was severe at high initial water flux due to increased hydrodynamic permeate drag [156]. Although post-treated membranes had lower NaCl enrichment than virgin NE70 membranes in feed solution (Fig. 5.10 (c) and Fig. 5.11(c)), high hydrodynamic permeate drag from high initial water flux seems to play an important role on the reduction of water flux by about 10%. In addition, the gradual fouling phenomenon in the PA layer continuously increased rejection of antibiotics (Fig. 5.10 (b) and Fig. 5.11(b)), because entrapment of antibiotics in the PA layer hinders the further passage of both water and

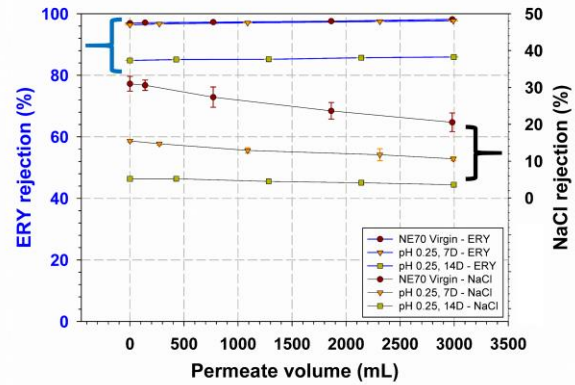
antibiotics [156]. Thus, the hindrance effect of additional fouled layers on the passage of antibiotic molecules is much higher than water molecule because of the much larger molecular size of antibiotics, which results in a higher rejection with increasing permeate volume (Fig. 5.10 (b) and Fig. 5.11(b)) [156].

Rejection of NaCl in an ERY/NaCl mixture solution gradually decreased with increasing permeate volume as shown in Fig. 5.10 (b). Continuous decrease of NaCl rejection is mainly associated with reduction of the Donnan exclusion effect, resulting from augmentation of the Na⁺ ion's shielding effect in accordance with increasing NaCl enrichment as shown in Fig. 5.10 (c) [146]. On the other hand, rejection of NaCl in Van/NaCl mixture solution (Fig. 5.11 (c)) maintains due to nearly neutral surface charge of virgin NE70 and post-treated membranes at pH 4.7 as provided in Fig. 5.5. Figure 5.10 (d) and Fig. 5.11 (d) show the concentration of antibiotics in feed. Operating times of post-treated membranes for 75% recovery of total volume were about 2 to 3 times faster than virgin NE70 membranes (pH 0.25 for 7 and 14 days, respectively), resulting from both higher MWCO values (Fig. 8) and lower amount of salt concentration (Fig. 5.10 (c) and Fig. 5.11(c)). Small amount of salt enrichment on the feed side due to the relatively low salt rejection during filtration causes less concentration polarization and less osmotic pressure build-up, increasing water flux and decreasing operation time. Consequently, post-treated membranes with higher water flux and lower NaCl rejection as well as almost maintained antibiotics rejection (except pH 0.25 14 days condition for ERY) are appropriate to produce antibiotics from concentrating the antibiotics/salt mixtures (Fig. 5.10 and 5.11).

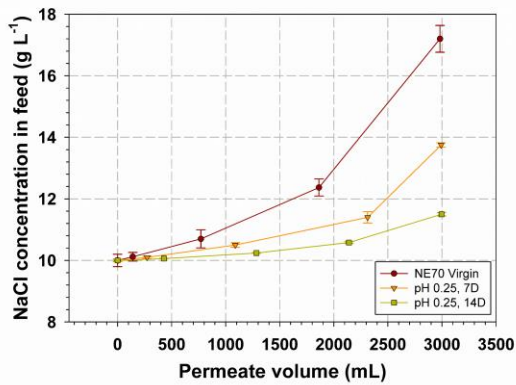
(a) Water flux



(b) ERY/NaCl rejection



(c) NaCl concentration



(d) ERY concentration

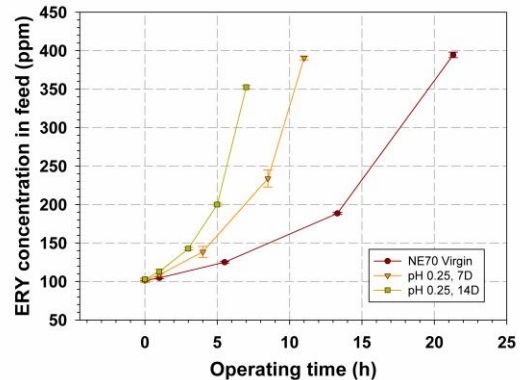
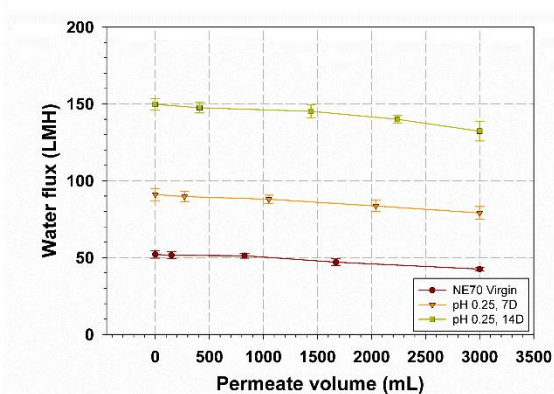
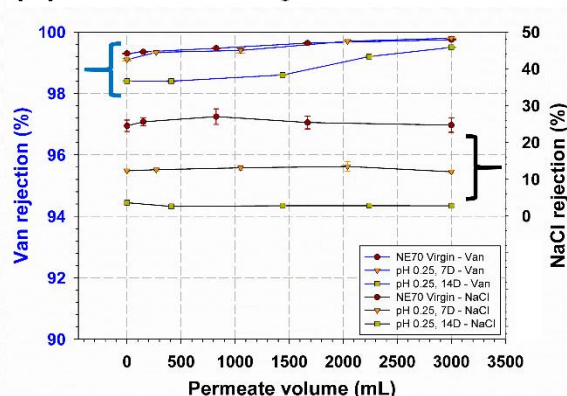


Figure 5.10 Comparison of NE70 virgin and post-treated membranes in pH 0.25 acidic solution for 7 and 14 days in terms of erythromycin (ERY) enrichment during the feed solution permeated from 4L to 1L (a) water flux, (b) ERY/NaCl rejection, (c) concentration of NaCl in feed, and (d) concentration of ERY in feed (tested at 150 psi, using mixture of 100 ppm ERY/10 g L⁻¹ NaCl at pH 8.8 because chemicals were used without further purification).

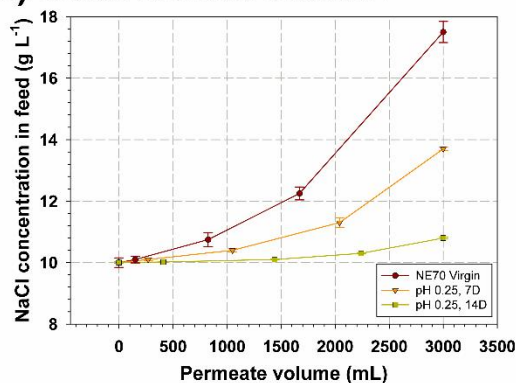
(a) Water flux



(b) Van/NaCl rejection



(c) NaCl concentration



(d) Van concentration

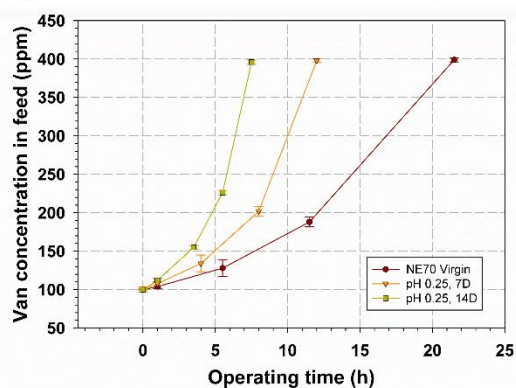


Figure 5.11: Comparison of NE70 virgin and post-treated membrane by pH 0.25 acidic solution for 7 and 14 days in terms of vancomycin (Van) enrichment during the feed solution permeated from 4L to 1L (a) water flux, (b) Van/NaCl rejection, (c) concentration of NaCl in feed, and (d) concentration of Van in feed. (tested at 150 psi, using mixture of 100 ppm Van/10 g L⁻¹ NaCl at pH 4.7 because chemicals were used without further purification).

Overall, Table. 5.8 compares post-treated membrane in this work with other commercial or fabricated membranes for separation of antibiotics, and here we demonstrate that post-treated membranes exhibited higher water flux, lower NaCl rejection as well as competitive antibiotics rejection [142, 150, 157, 158].

Table 5.8 Comparison of the performance of NE70 control and optimized membranes in the separation of antibiotics with other published papers.

Used membranes	Target antibiotics	Molecular weight of antibiotics (Da)	Rejection of antibiotics (%)	Rejection of salt (NaCl, %)	Water permeability (L m ⁻² h ⁻¹ bar ⁻¹)	Reference
NE70	Erythromycin (ERY)	734	96.9 ^b	31.0 ^b	4.9 ^b	This work
Post-treated at pH 0.25, 7 Days	Erythromycin (ERY)	734	96.4^b	15.5^b	9.5^b	This work
Post-treated at pH 0.25, 14 Days	Erythromycin (ERY)	734	84.8^b	5.2^b	16.9^b	This work
NE70	Vancomycin (Van)	1449	99.3 ^b	24.5 ^b	5.2 ^b	This work
Post-treated at pH 0.25, 7 Days	Vancomycin (Van)	1449	99.1 ^b	12.3 ^b	9.1 ^b	This work
Post-treated at pH 0.25, 14 Days	Vancomycin (Van)	1449	98.4^b	3.6^b	15.0^b	This work
ZTFCM (M0)	Erythromycin (ERY)	734	93.8 ^b	31.1 ^b	4.3 ^b	[142]
ZTFCM (M3)	Erythromycin (ERY)	734	96.5 ^b	14.4 ^b	8.4 ^b	[142]
ZTFCM (M5)	Erythromycin (ERY)	734	88.9 ^b	18.0 ^b	13.2 ^b	[142]
SR2	Tetracycline	444	75-95 ^b	24 ^a	7.5 ^a	[158]
NF90	Oxytetracycline	460	99.0 ^b	85.5 ^b	7.2 ^b	[157]
N30F	Cephalexin	347	98.0 ^a	25-35 ^a	1.0-1.8 ^a	[142, 155]
NFPES10	Cephalexin	347	88.0 ^a	10-20 ^a	5-10 ^a	[142, 155]

^a Performance test was conducted by single solution. ^b Performance test was conducted by mixture (antibiotic/salt) solution.

5.4 Conclusion

In this work, post-treatment using acid-catalyzed hydrolysis of semi-aromatic polyamide membrane was systemically investigated. Post-treatment converted polyamide group into amine and carboxyl group, resulting in increased hydrophilicity and absolute value of surface charge as well as MWCO value. In accordance with change of surface characteristics, the post-treated membrane at optimal condition (pH 0.25 for 7 days) showed about 10% enhanced water flux as well as 20% improvement of ideal selectivity of a NaCl or MgSO₄ single electrolyte solution. In the case of water softening, mixture selectivity (Na⁺/Mg²⁺) was improved about 2.6 times in acidic conditions. Optimized post-treatment membranes (at pH 0.25 for 7 and 14 days) were also applied to the enrichment of antibiotics, resulting in higher water flux, lower NaCl rejection as well as competitive antibiotics rejection compared to other commercial or fabricated membranes. Operation time of membrane modified by acid-catalyzed hydrolysis to achieve 75% recovery of antibiotics was 2 to 3 times shorter than virgin NE70 membrane. This work suggests that the post-treatment of semi-aromatic membranes by acid-catalyzed hydrolysis could be utilized as a versatile usage by different purposes.

Summary and conclusions

The NF process has been rapidly attracted during last decades due to pressure-driven separation process in acidic wastewater recovery/treatment. This work contributed to the systematical investigation of the effect of the acidic conditions on semi/full-aromatic PA membranes in terms of changes of physico-chemical properties, and suggested to mechanism for explanations of changed the properties using various analytical tools and computational calculation methods. Summary and conclusions of this work is as follows:

6.1 Comparison between semi and full-aromatic membrane

Commercially available Toray Chemical Korea © NF polyamide TFC membranes fabricated by amine monomer (piperazine or MPD) with acyl chloride (TMC) were used as representative semi and full-aromatic membrane in terms of the effect of acidic aqueous solution (15wt% sulfuric acid) on the membrane's physico-chemical properties. Characteristic results such as SEM, ATR-FTIR, XPS, and permeation experimental supported that piperazine-based NE40/70 membrane has relatively lower acid-stability than MPD-based NE90 membrane. In addition, a ToF-SIMS experiment showed the conversion of an amide group to carboxyl and amine groups by acid-catalyzed hydrolysis. These converted carboxyl and amine groups increased both the hydrophilicity and the absolute value of the zeta potential on the surface of NE40 and NE70 membranes. Because piperazine-based amide's monomer having N-protonation state (NE70 (N)) had the lowest energy barrier in the RDS step, piperazine-based NE40 and NE70 membranes had relatively lower acid-stability than MPD-based NE90 membrane. These computational calculation results are well correlated with surface characterization results. These activation energy results in RDS had a close relationship with protonated amides' twist angle (τ_D), and the tendency of the twist angle was also maintained in longer molecules (dimer and trimer). The results of our study showed that the semi-aromatic membrane has less acid-stability than the aromatic membrane in the view of various surface characterization and computational calculation results.

6.2 Effect of sulfuric acid and hydrogen halides on full-aromatic membrane

Full-aromatic NE 90 membrane was systemically investigated in various acidic conditions (pH 0 to 2 sulfuric acid and pH 0 hydrogen halides) to in-depth study of the membrane's physico-chemical properties, because full-aromatic membrane had high acid-stability than semi-aromatic membrane as

explained in section 6.1. In the case of membrane degraded by sulfuric acid, any surface characterization didn't change by observing SEM, ATR-FTIR, contact angle, and zeta potential. However, water and salt permeability increased when membrane was exposed to H₂SO₄ pH 1 condition, on the other hand, water flux decreased and salt rejection maintained when membrane was degraded by H₂SO₄ pH 0 condition. These results were explained by distorted hydrogen bonding between amides produced from proton bridge in the case of O-protonation and formation of tetrahedral structure in the case of N-protonation. Meanwhile, membrane's physical and chemical properties were much affected by pH 0 hydrogen halides condition than sulfuric acid condition. ATR-FTIR results show decreased amide II band (N-H) in 1541 cm⁻¹ and amide I band (C=O) in 1663 cm⁻¹ after exposure to hydrogen halides due to halogenation reacted with halogens generated by oxidation of hydrogen halides. XPS, contact angle, and zeta potential results also supported ATR-FTIR results. These amount of halogenation were increased in HCl, HBr, and HI order, and it was same as temporary dipole moment order produced by size of molecule. Water flux after exposure to hydrogen halides was severely decreased, and this results was caused by broken hydrogen bonding due to halogenation. This work suggests that change physico-chemical properties should be considered when full-aromatic NF membrane is utilized to treat/recycle for several industrial effluents which contain sulfuric acid and hydrogen halides at extreme low pH.

6.3 Practical application of acidic hydrolysis on semi-aromatic membrane

In the view of practical application, acid-catalyzed hydrolysis of semi-aromatic PA membrane was utilized as post-treatment using sulfuric acid in the range of pH 0 to 2, because of relatively lower acid-stability of semi-aromatic PA membrane. Post-treatment converted polyamide group into amine and carboxyl group, resulting to increase hydrophilicity and absolute value of surface charge as well as membrane pore size. Consistent with change of surface characteristics, the post-treated membrane at optimal condition (sulfuric acid pH 0.25 for 7 days) showed about 10% improved water flux as well as 20% enhanced ideal selectivity between Na⁺ and Mg²⁺ using a NaCl or MgSO₄ as a single electrolyte solution. In the case of mixture selectivity (Na⁺/Mg²⁺), it was improved about 2.6 times in acidic conditions. Additionally, optimized post-treatment membranes (at sulfuric acid pH 0.25 for 7 and 14 days) showed the possibility for application of the antibiotics enrichment due to higher water flux, lower NaCl rejection, and high antibiotics rejection compared to other commercial or fabricated membranes. Therefore, operation time of optimized membrane resulted 2 to 3 times shorter than virgin NE70 membrane. This study suggests that the post-treatment of semi-aromatic membranes by acid-catalyzed hydrolysis can be applied to a multipurpose usage depended on different applications.

REFERENCES

- [1] M. Bai, Z. Zhang, N. Zhang, Y. Tian, C. Chen, and X. Meng, "Treatment of 250 t/h ballast water in oceanic ships using $\cdot\text{OH}$ radicals based on strong electric-field discharge," *Plasma Chemistry and Plasma Processing*, vol. 32, pp. 693-702, 2012.
- [2] C. Job, "Water treatment practices at groundwater-supplied community water systems in the United States," *Ground Water Monitoring and Remediation*, vol. 32, pp. 35-36, 2012.
- [3] M. Kurihara, Y. Fusaoka, T. Sasaki, R. Bairinji, and T. Uemura, "Development of crosslinked fully aromatic polyamide ultra-thin composite membranes for seawater desalination," *Desalination*, vol. 96, pp. 133-143, 1994.
- [4] B.-M. Jun, T. P. N. Nguyen, S.-H. Ahn, I.-C. Kim, and Y.-N. Kwon, "The application of polyethyleneimine draw solution in a combined forward osmosis/nanofiltration system," *Journal of Applied Polymer Science*, vol. 132, pp. 42198-42206, 2015.
- [5] X. Q. Cheng, L. Shao, and C. H. Lau, "High flux polyethylene glycol based nanofiltration membranes for water environmental remediation," *Journal of Membrane Science*, vol. 476, pp. 95-104, 2015.
- [6] B.-M. Jun, H. K. Lee, and Y.-N. Kwon, "Acid-catalyzed hydrolysis of semi-aromatic polyamide NF membrane and its application to water softening and antibiotics enrichment," *Chemical Engineering Journal*, vol. 332, pp. 419-430, 2018.
- [7] Y.-N. Kwon, K. Shih, C. Tang, and J. O. Leckie, "Adsorption of perfluorinated compounds on thin-film composite polyamide membranes," *Journal of Applied Polymer Science*, vol. 124, pp. 1042-1049, 2012.
- [8] Y.-N. Kwon, R. Joksimovic, I.-C. Kim, and J. O. Leckie, "Effect of bromide on the chlorination of a polyamide membrane," *Desalination*, vol. 280, pp. 80-86, 2011.
- [9] A. K. Ghosh, B.-H. Jeong, X. Huang, and E. M. V. Hoek, "Impacts of reaction and curing conditions on polyamide composite reverse osmosis membrane properties," *Journal of Membrane Science*, vol. 311, pp. 34-45, 2008.
- [10] N. A. o. Engineering, *Frontiers of engineering: reports on leading-edge engineering from the 2016 symposium*. Washington, DC: The National Academies Press, 2017.
- [11] M. Liu, G. Yao, Q. Cheng, M. Ma, S. Yu, and C. Gao, "Acid stable thin-film composite membrane for nanofiltration prepared from naphthalene-1,3,6-trisulfonylchloride (NTSC) and piperazine (PIP)," *Journal of Membrane Science*, vol. 415-416, pp. 122-131, 2012.
- [12] M. P. González, R. Navarro, I. Saucedo, M. Avila, J. Revilla, and C. Bouchard, "Purification of phosphoric acid solutions by reverse osmosis and nanofiltration," *Desalination*, vol. 147, pp. 315-320, 2002.
- [13] D. Jakobs and G. Baumgarten, "Nanofiltration of nitric acidic solutions from picture tube

- production," *Desalination*, vol. 145, pp. 65-68, 2002.
- [14] E. Räsänen, M. Nyström, J. Sahlstein, and O. Tossavainen, "Purification and regeneration of diluted caustic and acidic washing solutions by membrane filtration," *Desalination*, vol. 149, pp. 185-190, 2002.
- [15] M. Nyström, L. Kaipia, and S. Luque, "Fouling and retention of nanofiltration membranes," *Journal of Membrane Science*, vol. 98, pp. 249-262, 1995.
- [16] C. Niewersch, C. N. Koh, T. Wintgens, T. Melin, C. Schaum, and P. Cornel, "Potentials of using nanofiltration to recover phosphorus from sewage sludge," *Water Science and Technology*, vol. 57, pp. 707-14, 2008.
- [17] C. Blöcher, C. Niewersch, and T. Melin, "Phosphorus recovery from sewage sludge with a hybrid process of low pressure wet oxidation and nanofiltration," *Water Research*, vol. 46, pp. 2009-2019, 2012.
- [18] S. Platt, M. Nyström, A. Bottino, and G. Capannelli, "Stability of NF membranes under extreme acidic conditions," *Journal of Membrane Science*, vol. 239, pp. 91-103, 2004.
- [19] T. J. K. Visser, S. J. Modise, H. M. Krieg, and K. Keizer, "The removal of acid sulphate pollution by nanofiltration," *Desalination*, vol. 140, pp. 79-86, 2001.
- [20] S. J. Pearton, C. R. Abernathy, and F. Ren, *Topics in growth and device processing of III-V semiconductors*: World scientific, 1996.
- [21] S. A. Vitale, H. Chae, and H. H. Sawin, "Silicon etching yields in F₂, Cl₂, Br₂, and HBr high density plasmas," *Journal of Vacuum Science & Technology A: Vacuum, Surfaces, and Films*, vol. 19, pp. 2197-2206, 2001.
- [22] C. E. Brion, M. Dyck, and G. Cooper, "Absolute photoabsorption cross-sections (oscillator strengths) for valence and inner shell excitations in hydrogen chloride, hydrogen bromide and hydrogen iodide," *Journal of Electron Spectroscopy and Related Phenomena*, vol. 144-147, pp. 127-130, 2005.
- [23] K. P. Lee, J. Zheng, G. Bargeman, A. J. B. Kemperman, and N. E. Benes, "pH stable thin film composite polyamine nanofiltration membranes by interfacial polymerisation," *Journal of Membrane Science*, vol. 478, pp. 75-84, 2015.
- [24] R. Schlesinger, G. Götzinger, H. Sixta, A. Friedl, and M. Harasek, "Evaluation of alkali resistant nanofiltration membranes for the separation of hemicellulose from concentrated alkaline process liquors," *Desalination*, vol. 192, pp. 303-314, 2006.
- [25] M. Liu, Z. Chen, S. Yu, D. Wu, and C. Gao, "Thin-film composite polyamide reverse osmosis membranes with improved acid stability and chlorine resistance by coating N-isopropylacrylamide-co-acrylamide copolymers," *Desalination*, vol. 270, pp. 248-257, 2011.
- [26] J. Tanninen, S. Platt, A. Weis, and M. Nyström, "Long-term acid resistance and selectivity of NF membranes in very acidic conditions," *Journal of Membrane Science*, vol. 240, pp. 11-18,

- 2004.
- [27] M. Dalwani, N. E. Benes, G. Bargeman, D. Stamatialis, and M. Wessling, "Effect of pH on the performance of polyamide/polyacrylonitrile based thin film composite membranes," *Journal of Membrane Science*, vol. 372, pp. 228-238, 2011.
- [28] C. J. M. v. Rijn, "Chapter 1 Overview membrane technology," in *Membrane Science and Technology*. vol. Volume 10, C. J. M. v. Rijn, Ed., ed: Elsevier, 2004, pp. 1-23.
- [29] M. Mulder, *Basic principles of membrane technology*. Dordrecht: Springer Netherlands, 1996.
- [30] S. A. El-Safty and N. D. Hoa, *Organic-Inorganic Mesoporous Silica Nanotube Hybrid Anodic Alumina Membranes for Ultrafine Filtration of Noble Metal Nanoparticles*: INTECH Open Access Publisher, 2012.
- [31] W. J. Lau, A. F. Ismail, N. Misdan, and M. A. Kassim, "A recent progress in thin film composite membrane: A review," *Desalination*, vol. 287, pp. 190-199, 2012.
- [32] T. Cohen and J. Lipowitz, "Acid-catalyzed amide hydrolysis assisted by a neighboring amide group," *Journal of the American Chemical Society*, vol. 86, pp. 5611-5616, 1964.
- [33] J. E. McMurry, R. C. Fay, and J. Topich, *Chemistry*: Pearson College Division, 2008.
- [34] A. J. Bennet, V. Somayaji, R. S. Brown, and B. D. Santarsiero, "The influence of altered amidic resonance on the infrared and carbon-13 and nitrogen-15 NMR spectroscopic characteristics and barriers to rotation about the N-C(O) bond in some anilides and toluamides," *Journal of the American Chemical Society*, vol. 113, pp. 7563-7571, 1991.
- [35] Q. P. Wang, A. J. Bennet, R. S. Brown, and B. D. Santarsiero, "Distorted amides as models for activated peptide N-C(O) units. 3. Synthesis, hydrolytic profile, and molecular structure of 2,3,4,5-tetrahydro-2-oxo-1,5-propanobenzazepine," *Journal of the American Chemical Society*, vol. 113, pp. 5757-5765, 1991.
- [36] A. Greenberg, C. M. Breneman, and J. F. Liebman, *The amide linkage : selected structural aspects in chemistry, biochemistry, and materials science*. New York: Wiley-Interscience, 2000.
- [37] X. Lopez, J. I. Mujika, G. M. Blackburn, and M. Karplus, "Alkaline hydrolysis of amide bonds: effect of bond twist and nitrogen pyramidalization," *The Journal of Physical Chemistry A*, vol. 107, pp. 2304-2315, 2003.
- [38] J. I. Mujika, J. M. Mercero, and X. Lopez, "Water-promoted hydrolysis of a highly twisted amide: rate acceleration caused by the twist of the amide bond," *Journal of the American Chemical Society*, vol. 127, pp. 4445-4453, 2005.
- [39] J. I. M. Gorostidi, "Twisted amides: characterization of their electronic structure and analysis of their accelerated hydrolysis," Doctoral Dissertation, Physical Chemistry at the Department of Chemistry University of the Basque Country, 2005.
- [40] M. Szostak, L. Yao, V. W. Day, D. R. Powell, and J. Aubé, "Structural characterization of N-protonated amides: regioselective N-activation of medium-bridged twisted lactams," *Journal*

- of the American Chemical Society*, vol. 132, pp. 8836-8837, 2010.
- [41] V. Somayaji and R. S. Brown, "Distorted amides as models for activated peptide N-C:O units produced during enzyme-catalyzed acyl transfer reactions. 1. The mechanism of hydrolysis of 3,4-dihydro-2-oxo-1,4-ethanoquinoline and 2,3,4,5-tetrahydro-2-oxo-1,5-ethanobenzazepine," *The Journal of Organic Chemistry*, vol. 51, pp. 2676-2686, 1986.
- [42] M. M. Farrukh, P. Bosch, M. Giagnorio, A. Tiraferri, and M. Sangermano, "Solvent-stable UV-cured acrylic polysulfone membranes," *Polymer International*, vol. 66, pp. 64-69, 2017.
- [43] W. J. Lau, A. F. Ismail, N. Misdan, and M. A. Kassim, "A recent progress in thin film composite membrane: A review," *Desalination*, vol. 287, pp. 190-199, 2012.
- [44] B. S. Lalia, V. Kochkodan, R. Hashaikeh, and N. Hilal, "A review on membrane fabrication: Structure, properties and performance relationship," *Desalination*, vol. 326, pp. 77-95, 2013.
- [45] K. P. Lee, T. C. Arnot, and D. Mattia, "A review of reverse osmosis membrane materials for desalination—Development to date and future potential," *Journal of Membrane Science*, vol. 370, pp. 1-22, 2011.
- [46] V. Freger, "Kinetics of film formation by interfacial polycondensation," *Langmuir*, vol. 21, pp. 1884-1894, 2005.
- [47] J. Jegal, S. G. Min, and K.-H. Lee, "Factors affecting the interfacial polymerization of polyamide active layers for the formation of polyamide composite membranes," *Journal of Applied Polymer Science*, vol. 86, pp. 2781-2787, 2002.
- [48] S.-Y. Kwak, S. G. Jung, Y. S. Yoon, and D. W. Ihm, "Details of surface features in aromatic polyamide reverse osmosis membranes characterized by scanning electron and atomic force microscopy," *Journal of Polymer Science Part B: Polymer Physics*, vol. 37, pp. 1429-1440, 1999.
- [49] A. K. Ghosh and E. M. V. Hoek, "Impacts of support membrane structure and chemistry on polyamide-polysulfone interfacial composite membranes," *Journal of Membrane Science*, vol. 336, pp. 140-148, 2009.
- [50] C. Y. Tang, Y.-N. Kwon, and J. O. Leckie, "Effect of membrane chemistry and coating layer on physiochemical properties of thin film composite polyamide RO and NF membranes: II. Membrane physiochemical properties and their dependence on polyamide and coating layers," *Desalination*, vol. 242, pp. 168-182, 2009.
- [51] A. L. Ahmad and B. S. Ooi, "Optimization of composite nanofiltration membrane through pH control: Application in CuSO₄ removal," *Separation and Purification Technology*, vol. 47, pp. 162-172, 2006.
- [52] Y. Mansourpanah, S. S. Madaeni, and A. Rahimpour, "Fabrication and development of interfacial polymerized thin-film composite nanofiltration membrane using different surfactants in organic phase; study of morphology and performance," *Journal of Membrane*

- Science*, vol. 343, pp. 219-228, 2009.
- [53] D. B. Purchas and K. Sutherland, *Handbook of filter media*. Oxford: New York, 2002.
- [54] K. Scott, "Section 2 - Membrane materials, preparation and characterisation," in *Handbook of Industrial Membranes (Second Edition)*, K. Scott, Ed., ed Amsterdam: Elsevier Science, 1998, pp. 187-269.
- [55] C. Causserand and P. Aimar, "1.15 - Characterization of Filtration Membranes," in *Comprehensive Membrane Science and Engineering*, E. Drioli and L. Giorno, Eds., ed Oxford: Elsevier, 2010, pp. 311-335.
- [56] D. J. Johnson, D. L. Oatley-Radcliffe, and N. Hilal, "State of the art review on membrane surface characterisation: Visualisation, verification and quantification of membrane properties," *Desalination*, 2017. (in press)
- [57] F. Galiano, A. Figoli, S. A. Deowan, D. Johnson, S. A. Altinkaya, L. Veltri, *et al.*, "A step forward to a more efficient wastewater treatment by membrane surface modification via polymerizable bicontinuous microemulsion," *Journal of Membrane Science*, vol. 482, pp. 103-114, 2015.
- [58] Z. Fu-Yun, W. Qi-Qi, Z. Xiao-Sheng, H. Wei, Z. Xin, and Z. Hai-Xia, "3D nanostructure reconstruction based on the SEM imaging principle, and applications," *Nanotechnology*, vol. 25, p. 1-10, 2014.
- [59] M. F. Atitar, H. Belhadj, R. Dillert, and D. W. Bahnemann, "The relevance of ATR-FTIR spectroscopy in semiconductor photocatalysis," in *Emerging Pollutants in the Environment - Current and Further Implications*, M. L. Larramendy and S. Soloneski, Eds., ed Rijeka: InTech, pp. 1-238, 2015.
- [60] N. J. Harrick and F. K. du Pré, "Effective thickness of bulk materials and of thin films for internal reflection spectroscopy," *Applied Optics*, vol. 5, pp. 1739-1743, 1966.
- [61] J. F. Watts and J. Wolstenholme, "Electron Spectroscopy: Some Basic Concepts," in *An Introduction to Surface Analysis by XPS and AES*, ed: John Wiley & Sons, Ltd, 2005, pp. 1-15.
- [62] B. D. Ratner and D. G. Castner, "Electron Spectroscopy for Chemical Analysis," in *Surface Analysis – The Principal Techniques*, ed: John Wiley & Sons, Ltd, 2009, pp. 47-112.
- [63] Y. Baek, J. Kang, P. Theato, and J. Yoon, "Measuring hydrophilicity of RO membranes by contact angles via sessile drop and captive bubble method: A comparative study," *Desalination*, vol. 303, pp. 23-28, 2012.
- [64] S. Romero-Vargas Castrillón, X. Lu, D. L. Shaffer, and M. Elimelech, "Amine enrichment and poly(ethylene glycol) (PEG) surface modification of thin-film composite forward osmosis membranes for organic fouling control," *Journal of Membrane Science*, vol. 450, pp. 331-339, 2014.
- [65] S. Yu, X. Liu, J. Liu, D. Wu, M. Liu, and C. Gao, "Surface modification of thin-film composite

- polyamide reverse osmosis membranes with thermo-responsive polymer (TRP) for improved fouling resistance and cleaning efficiency," *Separation and Purification Technology*, vol. 76, pp. 283-291, 2011.
- [66] Y. Kiso, T. Kon, T. Kitao, and K. Nishimura, "Rejection properties of alkyl phthalates with nanofiltration membranes," *Journal of Membrane Science*, vol. 182, pp. 205-214, 2001.
- [67] J. R. Du, S. Peldszus, P. M. Huck, and X. Feng, "Modification of poly(vinylidene fluoride) ultrafiltration membranes with poly(vinyl alcohol) for fouling control in drinking water treatment," *Water Research*, vol. 43, pp. 4559-4568, 2009.
- [68] A. Nabe, E. Staude, and G. Belfort, "Surface modification of polysulfone ultrafiltration membranes and fouling by BSA solutions," *Journal of Membrane Science*, vol. 133, pp. 57-72, 1997.
- [69] F. Liu, N. A. Hashim, Y. Liu, M. R. M. Abed, and K. Li, "Progress in the production and modification of PVDF membranes," *Journal of Membrane Science*, vol. 375, pp. 1-27, 2011.
- [70] H. Rho, K. Chon, and J. Cho, "Surface charge characterization of nanofiltration membranes by potentiometric titrations and electrophoresis: Functionality vs. zeta potential," *Desalination*, vol. 427, pp. 19-26, 2018.
- [71] C. Bellona, J. E. Drewes, P. Xu, and G. Amy, "Factors affecting the rejection of organic solutes during NF/RO treatment—a literature review," *Water Research*, vol. 38, pp. 2795-2809, 2004.
- [72] J. Y. Hu, S. L. Ong, J. H. Shan, J. B. Kang, and W. J. Ng, "Treatability of organic fractions derived from secondary effluent by reverse osmosis membrane," *Water Research*, vol. 37, pp. 4801-4809, 2003.
- [73] Y. Shim, H.-J. Lee, S. Lee, S.-H. Moon, and J. Cho, "Effects of natural organic matter and ionic species on membrane surface charge," *Environmental Science & Technology*, vol. 36, pp. 3864-3871, 2002.
- [74] A. Braghetta, DiGiano, F., and Ball, W, "Nanofiltration of Natural Organic Matter: pH and Ionic Strength Effects," *Journal of Environmental Engineering*, vol. 123, pp. 628-641, 1997.
- [75] A. Al-Amoudi and R. W. Lovitt, "Fouling strategies and the cleaning system of NF membranes and factors affecting cleaning efficiency," *Journal of Membrane Science*, vol. 303, pp. 4-28, 2007.
- [76] S. Hong and M. Elimelech, "Chemical and physical aspects of natural organic matter (NOM) fouling of nanofiltration membranes," *Journal of Membrane Science*, vol. 132, pp. 159-181, 1997.
- [77] M. Mänttari, L. Puro, J. Nuortila-Jokinen, and M. Nyström, "Fouling effects of polysaccharides and humic acid in nanofiltration," *Journal of Membrane Science*, vol. 165, pp. 1-17, 2000.
- [78] S. Fearn, "Characterisation of biological material with ToF-SIMS: a review," *Materials Science and Technology*, vol. 31, pp. 148-161, 2015.

- [79] J. P. Krug, P. L. A. Popelier, and R. F. W. Bader, "Theoretical study of neutral and of acid and base-promoted hydrolysis of formamide," *The Journal of Physical Chemistry*, vol. 96, pp. 7604-7616, 1992.
- [80] D. Zahn, "Theoretical study of the mechanisms of acid-catalyzed amide hydrolysis in aqueous solution," *The Journal of Physical Chemistry B*, vol. 107, pp. 12303-12306, 2003.
- [81] Q. Ma, P. J. Shuler, C. W. Aften, and Y. Tang, "Theoretical studies of hydrolysis and stability of polyacrylamide polymers," *Polymer Degradation and Stability*, vol. 121, pp. 69-77, 2015.
- [82] J. Cadotte, R. Forester, M. Kim, R. Petersen, and T. Stocker, "Nanofiltration membranes broaden the use of membrane separation technology," *Desalination*, vol. 70, pp. 77-88, 1988.
- [83] X. Lu, X. Bian, and L. Shi, "Preparation and characterization of NF composite membrane," *Journal of Membrane Science*, vol. 210, pp. 3-11, 2002.
- [84] R. Han, "Formation and characterization of (melamine-TMC) based thin film composite NF membranes for improved thermal and chlorine resistances," *Journal of Membrane Science*, vol. 425-426, pp. 176-181, 2013.
- [85] Y. Zhang, M. Guo, G. Pan, H. Yan, J. Xu, Y. Shi, *et al.*, "Preparation and properties of novel pH-stable TFC membrane based on organic-inorganic hybrid composite materials for nanofiltration," *Journal of Membrane Science*, vol. 476, pp. 500-507, 2015.
- [86] A. Greenberg, D. T. Moore, and T. D. DuBois, "Small and medium-sized bridgehead bicyclic lactams: a systematic ab initio molecular orbital study," *Journal of the American Chemical Society*, vol. 118, pp. 8658-8668, 1996.
- [87] R. S. Brown, A. J. Bennet, and H. Slebocka-Tilk, "Recent perspectives concerning the mechanism of H_3O^+ - and hydroxide-promoted amide hydrolysis," *Accounts of Chemical Research*, vol. 25, pp. 481-488, 1992.
- [88] B. Wang and Z. Cao, "Mechanism of acid-catalyzed hydrolysis of formamide from cluster-continuum model calculations: concerted versus stepwise pathway," *The journal of physical chemistry*, vol. 114, pp. 12918-27, 2010.
- [89] J. Tanninen, S. Platt, A. Weis, and M. Nyström, "Long-term acid resistance and selectivity of NF membranes in very acidic conditions," *Journal of Membrane Science*, vol. 240, pp. 11-18, 2004.
- [90] T. P. N. Nguyen, E.-T. Yun, I.-C. Kim, and Y.-N. Kwon, "Preparation of cellulose triacetate/cellulose acetate (CTA/CA)-based membranes for forward osmosis," *Journal of Membrane Science*, vol. 433, pp. 49-59, 2013.
- [91] B.-M. Jun, T. P. N. Nguyen, Y.-K. Kim, H. K. Lee, and Y.-N. Kwon, "Surface modification of TFC FO membrane using N-isopropylacrylamide (NIPAM) to enhance fouling resistance and cleaning efficiency," *Desalination and Water Treatment*, vol. 65, pp. 11-21, 2017.
- [92] C. Y. Tang, Y.-N. Kwon, and J. O. Leckie, "Effect of membrane chemistry and coating layer on

- physiochemical properties of thin film composite polyamide RO and NF membranes," *Desalination*, vol. 242, pp. 149-167, 2009.
- [93] S. Bell and J. S. Crighton, "Locating transition states," *The Journal of Chemical Physics*, vol. 80, pp. 2464-2475, 1984.
- [94] E. Alayemieka and S. Lee, "Modification of polyamide membrane surface with chlorine dioxide solutions of differing pH," *Desalination and Water Treatment*, vol. 45, pp. 84-90, 2012.
- [95] B. Delley, "An all-electron numerical method for solving the local density functional for polyatomic molecules," *The Journal of Chemical Physics*, vol. 92, pp. 508-517, 1990.
- [96] B. Delley, "From molecules to solids with the DMol3 approach," *The Journal of Chemical Physics*, vol. 113, pp. 7756-7764, 2000.
- [97] J. P. Perdew, K. Burke, and M. Ernzerhof, "Generalized gradient approximation made simple," *Physical Review Letters*, vol. 77, pp. 3865-3868, 1996.
- [98] B. Delley, "The conductor-like screening model for polymers and surfaces," *Molecular Simulation*, vol. 32, pp. 117-123, 2006.
- [99] J.-L. Fattebert and F. Gygi, "Density functional theory for efficient ab initio molecular dynamics simulations in solution," *Journal of Computational Chemistry*, vol. 23, pp. 662-666, 2002.
- [100] T. A. Halgren and W. N. Lipscomb, "The synchronous-transit method for determining reaction pathways and locating molecular transition states," *Chemical Physics Letters*, vol. 49, pp. 225-232, 1977.
- [101] N. Metropolis, A. W. Rosenbluth, M. N. Rosenbluth, A. H. Teller, and E. Teller, "Equation of state calculations by fast computing machines," *The Journal of Chemical Physics*, vol. 21, pp. 1087-1092, 1953.
- [102] B. Charlès, "Materials Studio," 2017R2 ed. San Diego, CA: BIOVIA Inc., 2017.
- [103] H. Sun, P. Ren, and J. R. Fried, "The COMPASS force field: parameterization and validation for phosphazenes," *Computational and Theoretical Polymer Science*, vol. 8, pp. 229-246, 1998.
- [104] H. Sun, "COMPASS: An ab initio force-field optimized for condensed-phase applications - overview with details on alkane and benzene compounds," *The Journal of Physical Chemistry B*, vol. 102, pp. 7338-7364, 1998.
- [105] R. J. Petersen, "Composite reverse osmosis and nanofiltration membranes," *Journal of Membrane Science*, vol. 83, pp. 81-150, 1993.
- [106] C. Y. Tang, Y.-N. Kwon, and J. O. Leckie, "Probing the nano- and micro-scales of reverse osmosis membranes—A comprehensive characterization of physiochemical properties of uncoated and coated membranes by XPS, TEM, ATR-FTIR, and streaming potential measurements," *Journal of Membrane Science*, vol. 287, pp. 146-156, 2007.
- [107] V. Freger, J. Gilron, and S. Belfer, "TFC polyamide membranes modified by grafting of hydrophilic polymers: an FT-IR/AFM/TEM study," *Journal of Membrane Science*, vol. 209, pp.

- 283-292, 2002.
- [108] M. Mänttari, A. Pihlajamäki, and M. Nyström, "Effect of pH on hydrophilicity and charge and their effect on the filtration efficiency of NF membranes at different pH," *Journal of Membrane Science*, vol. 280, pp. 311-320, 2006.
- [109] C. C. Wamser and M. I. Gilbert, "Detection of surface functional group asymmetry in interfacially-polymerized films by contact angle titrations," *Langmuir*, vol. 8, pp. 1608-1614, 1992.
- [110] K. S. Kim, K. H. Lee, K. Cho, and C. E. Park, "Surface modification of polysulfone ultrafiltration membrane by oxygen plasma treatment," *Journal of Membrane Science*, vol. 199, pp. 135-145, 2002.
- [111] O. Coronell, B. J. Mariñas, X. Zhang, and D. G. Cahill, "Quantification of functional groups and modeling of their ionization behavior in the active layer of FT30 reverse osmosis membrane," *Environmental Science & Technology*, vol. 42, pp. 5260-5266, 2008.
- [112] V. Addario, Y. Guo, I. K. Chu, Y. Ling, G. Ruggerio, C. F. Rodriguez, *et al.*, "Proton affinities of methyl esters of N-acetylated amino acids," *International Journal of Mass Spectrometry*, vol. 219, pp. 101-114, 2002.
- [113] M. Witt, D. Kreft, and H.-F. Grützmacher, "Effects of internal hydrogen bonds between amide groups: protonation of alicyclic diamides," *European Journal of Mass Spectrometry*, vol. 9, pp. 81-95, 2003.
- [114] J. Glater and M. R. Zachariah, "A mechanistic study of halogen interaction with polyamide reverse-osmosis membranes," *American Chemical Society*, vol. 281, pp. 345-358, 1985.
- [115] K. Sivakumar, T. Stalin, and N. Rajendiran, "Dual fluorescence of diphenyl carbazide and benzanilide: Effect of solvents and pH on electronic spectra," *Spectrochimica Acta Part A: Molecular and Biomolecular Spectroscopy*, vol. 62, pp. 991-999, 2005.
- [116] Y.-N. Kwon, C. Y. Tang, and J. O. Leckie, "Change of membrane performance due to chlorination of crosslinked polyamide membranes," *Journal of Applied Polymer Science*, vol. 102, pp. 5895-5902, 2006.
- [117] O. S. Kulakovich, D. V. Korbutyak, S. M. Kalytchuk, S. I. Budzulyak, O. A. Kapush, L. I. Trishchuk, *et al.*, "Influence of conditions for synthesis of CdTe nanocrystals on their photoluminescence properties and plasmon effect," *Journal of Applied Spectroscopy*, vol. 79, pp. 765-772, 2012.
- [118] E. Skorepova, M. Husak, L. Ridvan, M. Tkadlecova, J. Havlicek, and M. Dusek, "Iodine salts of the pharmaceutical compound agomelatine: the effect of the symmetric H-bond on amide protonation," *CrystEngComm*, vol. 18, pp. 4518-4529, 2016.
- [119] R. Sander, "Compilation of Henry's law constants (version 4.0) for water as solvent," *Atmospheric Chemistry and Physics*, vol. 15, pp. 4399-4981, 2015.

- [120] J. Glater, J. W. McCutchan, S. B. McCray, and M. R. Zachariah, "The effect of halogens on the performance and durability of reverse-osmosis membranes," *American chemical society.*, vol. 153, pp. 171-190, 1981.
- [121] J. y. Koo, "ESCA characterization of chlorine-damaged polyamide reverse osmosis membrane," *Polymer. Preprints*, vol. 27, pp. 391-392, 1986.
- [122] S. Avlonitis, W. T. Hanbury, and T. Hodgkiess, "Chlorine degradation of aromatic polyamides," *Desalination*, vol. 85, pp. 321-334, 1992.
- [123] R. Singh, "Polyamide polymer solution behaviour under chlorination conditions," *Journal of Membrane Science*, vol. 88, pp. 285-287, 1994.
- [124] J. S. Jensen, Y.-F. Lam, and G. R. Helz, "Role of amide nitrogen in water chlorination: proton NMR evidence," *Environmental Science & Technology*, vol. 33, pp. 3568-3573, 1999.
- [125] A. Simon, L. D. Nghiem, P. Le-Clech, S. J. Khan, and J. E. Drewes, "Effects of membrane degradation on the removal of pharmaceutically active compounds (PhACs) by NF/RO filtration processes," *Journal of Membrane Science*, vol. 340, pp. 16-25, 2009.
- [126] Y.-N. Kwon and J. O. Leckie, "Hypochlorite degradation of crosslinked polyamide membranes: II. Changes in hydrogen bonding behavior and performance," *Journal of Membrane Science*, vol. 282, pp. 456-464, 2006.
- [127] P. M. A. Sherwood, "X-ray photoelectron spectroscopic studies of some iodine compounds," *Journal of the Chemical Society*, vol. 72, pp. 1805-1820, 1976.
- [128] Y.-N. Kwon and J. O. Leckie, "Hypochlorite degradation of crosslinked polyamide membranes: I. Changes in chemical/morphological properties," *Journal of Membrane Science*, vol. 283, pp. 21-26, 2006.
- [129] V. T. Do, C. Y. Tang, M. Reinhard, and J. O. Leckie, "Degradation of polyamide nanofiltration and reverse osmosis membranes by hypochlorite," *Environmental Science & Technology*, vol. 46, pp. 852-859, 2012.
- [130] M. T. M. Pendergast, J. M. Nygaard, A. K. Ghosh, and E. M. V. Hoek, "Using nanocomposite materials technology to understand and control reverse osmosis membrane compaction," *Desalination*, vol. 261, pp. 255-263, 2010.
- [131] V. Freger, A. Bottino, G. Capannelli, M. Perry, V. Gitis, and S. Belfer, "Characterization of novel acid-stable NF membranes before and after exposure to acid using ATR-FTIR, TEM and AFM," *Journal of Membrane Science*, vol. 256, pp. 134-142, 2005.
- [132] J.-E. Gu, B.-M. Jun, and Y.-N. Kwon, "Effect of chlorination condition and permeability of chlorine species on the chlorination of a polyamide membrane," *Water Research*, vol. 46, pp. 5389-5400, 2012.
- [133] A. G. Boricha and Z. V. P. Murthy, "Preparation of N,O-carboxymethyl chitosan/cellulose acetate blend nanofiltration membrane and testing its performance in treating industrial

- wastewater," *Chemical Engineering Journal*, vol. 157, pp. 393-400, 2010.
- [134] C.-C. Ye, F.-Y. Zhao, J.-K. Wu, X.-D. Weng, P.-Y. Zheng, Y.-F. Mi, *et al.*, "Sulfated polyelectrolyte complex nanoparticles structured nanofiltration membrane for dye desalination," *Chemical Engineering Journal*, vol. 307, pp. 526-536, 2017.
- [135] G. Zeng, Z. Ye, Y. He, X. Yang, J. Ma, H. Shi, *et al.*, "Application of dopamine-modified halloysite nanotubes/PVDF blend membranes for direct dyes removal from wastewater," *Chemical Engineering Journal*, vol. 323, pp. 572-583, 2017.
- [136] Y. C. Xu, Z. X. Wang, X. Q. Cheng, Y. C. Xiao, and L. Shao, "Positively charged nanofiltration membranes via economically mussel-substance-simulated co-deposition for textile wastewater treatment," *Chemical Engineering Journal*, vol. 303, pp. 555-564, 2016.
- [137] J. M. Gohil and P. Ray, "A review on semi-aromatic polyamide TFC membranes prepared by interfacial polymerization: Potential for water treatment and desalination," *Separation and Purification Technology*, vol. 181, pp. 159-182, 2017.
- [138] Y.-F. Mi, Q. Zhao, Y.-L. Ji, Q.-F. An, and C.-J. Gao, "A novel route for surface zwitterionic functionalization of polyamide nanofiltration membranes with improved performance," *Journal of Membrane Science*, vol. 490, pp. 311-320, 2015.
- [139] V. Yangali-Quintanilla, A. Sadmani, M. McConville, M. Kennedy, and G. Amy, "Rejection of pharmaceutically active compounds and endocrine disrupting compounds by clean and fouled nanofiltration membranes," *Water Research*, vol. 43, pp. 2349-2362, 2009.
- [140] L. Ouyang, R. Malaisamy, and M. L. Bruening, "Multilayer polyelectrolyte films as nanofiltration membranes for separating monovalent and divalent cations," *Journal of Membrane Science*, vol. 310, pp. 76-84, 2008.
- [141] W. Zhang, G. He, P. Gao, and G. Chen, "Development and characterization of composite nanofiltration membranes and their application in concentration of antibiotics," *Separation and Purification Technology*, vol. 30, pp. 27-35, 2003.
- [142] X.-D. Weng, Y.-L. Ji, R. Ma, F.-Y. Zhao, Q.-F. An, and C.-J. Gao, "Superhydrophilic and antibacterial zwitterionic polyamide nanofiltration membranes for antibiotics separation," *Journal of Membrane Science*, vol. 510, pp. 122-130, 2016.
- [143] X.-m. Wang, B. Li, T. Zhang, and X.-y. Li, "Performance of nanofiltration membrane in rejecting trace organic compounds: Experiment and model prediction," *Desalination*, vol. 370, pp. 7-16, 2015.
- [144] J. Park, K. Chon, and J. Cho, "Science Walden: new horizons of combined ecological sanitation with separated urine/feces and treatment wetlands," *Desalination and Water Treatment*, vol. 54, pp. 1353-1360, 2015.
- [145] C. Christy and S. Vermant, "The state-of-the-art of filtration in recovery processes for biopharmaceutical production," *Desalination*, vol. 147, pp. 1-4, 2002.

- [146] X. Wei, X. Kong, J. Yang, G. Zhang, J. Chen, and J. Wang, "Structure influence of hyperbranched polyester on structure and properties of synthesized nanofiltration membranes," *Journal of Membrane Science*, vol. 440, pp. 67-76, 2013.
- [147] Y.-N. Kwon, R. Joksimovic, I.-C. Kim, and J. O. Leckie, "Effect of bromide on the chlorination of a polyamide membrane," *Desalination*, vol. 280, pp. 80-86, 2011.
- [148] Y. Pan, R. Xu, Z. Lü, S. Yu, M. Liu, and C. Gao, "Enhanced both perm-selectivity and fouling resistance of poly(piperazine-amide) nanofiltration membrane by incorporating sericin as a co-reactant of aqueous phase," *Journal of Membrane Science*, vol. 523, pp. 282-290, 2017.
- [149] L. D. Nghiem, A. I. Schäfer, and M. Elimelech, "Removal of natural hormones by nanofiltration membranes: measurement, modeling, and mechanisms," *Environmental Science & Technology*, vol. 38, pp. 1888-1896, 2004.
- [150] K. Y. Wang and T.-S. Chung, "The characterization of flat composite nanofiltration membranes and their applications in the separation of Cephalexin," *Journal of Membrane Science*, vol. 247, pp. 37-50, 2005.
- [151] C. Sitprasert, F. Y. Wang, V. Rudolph, and Z. H. Zhu, "Ideal and mixture permeation selectivity of flexible prototypical zeolitic imidazolate framework – 8 Membranes," *Chemical Engineering Science*, vol. 108, pp. 23-32, 2014.
- [152] Y. T. Chung, E. Mahmoudi, A. W. Mohammad, A. Benamor, D. Johnson, and N. Hilal, "Development of polysulfone-nano hybrid membranes using ZnO-GO composite for enhanced antifouling and antibacterial control," *Desalination*, vol. 402, pp. 123-132, 2017.
- [153] G. M. Geise, H. B. Park, A. C. Sagle, B. D. Freeman, and J. E. McGrath, "Water permeability and water/salt selectivity tradeoff in polymers for desalination," *Journal of Membrane Science*, vol. 369, pp. 130-138, 2011.
- [154] M. R. Teixeira, M. J. Rosa, and M. Nyström, "The role of membrane charge on nanofiltration performance," *Journal of Membrane Science*, vol. 265, pp. 160-166, 2005.
- [155] L. D. Nghiem and S. Hawkes, "Effects of membrane fouling on the nanofiltration of trace organic contaminants," *Desalination*, vol. 236, pp. 273-281, 2009.
- [156] C. Y. Tang, Q. S. Fu, C. S. Criddle, and J. O. Leckie, "Effect of flux (transmembrane pressure) and membrane properties on fouling and rejection of reverse osmosis and nanofiltration membranes treating perfluorooctane sulfonate containing wastewater," *Environmental Science & Technology*, vol. 41, pp. 2008-2014, 2007.
- [157] K. Košutić, D. Dolar, D. Ašperger, and B. Kunst, "Removal of antibiotics from a model wastewater by RO/NF membranes," *Separation and Purification Technology*, vol. 53, pp. 244-249, 2007.
- [158] M. A. Zazouli, H. Susanto, S. Nasser, and M. Ulbricht, "Influences of solution chemistry and polymeric natural organic matter on the removal of aquatic pharmaceutical residuals by

nanofiltration," *Water Research*, vol. 43, pp. 3270-3280, 2009.

ACKNOWLEDGEMENT

Looking back to the previous six years of SMART lab in UNIST, the experiences for the doctoral degree have been a very unforgettable and challenging events. The graduation is not the end but the new beginning of my life as an independent researcher, and I don't know how to express my thanks to all of people who supported me by various ways. I really appreciate all of the support, and it would have been very hard without their continuous encouragement.

First and foremost, I would like to express my sincere gratitude to my advisor, Professor Young-Nam Kwon, for endless patience and effort in supervising my dissertation through innumerable discussions. He carefully advised me how to start research and cooperate with brilliant colleagues. The experience and accomplishments under the guidance of my advisor was a best of luck in my life. I would also like to thank Professor Jaeweon Cho, Changha Lee, Sang Kyu Kwak, and Dr. In-Chul Kim for serving their noble comments on my research as committee members. Furthermore, fusion research by collaboration with Professor Sang Kyu Kwak and his student Su Hwan Kim will never be forgotten.

I am particularly grateful to all of the SMART lab members, Jung-Eun Gu, Thi Phuong Nga Nguyen, Hyung Gyu Park, Eun-Ho Kim, Eun-Tae Yun, Sang-Woo Han, Yu-Kyung Kim, Hyung Kae Lee, Woojeong Kim, Jong Hyeok Kim, Ji Hun Park, Shashi Prabha Dubey, and Jayalakshmi Ayyavoo.

Besides, I would like to thank other lab members in the same department, Jongkwan Park, Hojung Rho, Taewoo Nam, and Huijin Heo in Professor Jaeweon Cho's (OWIE) lab as well as Hongshin Lee, Hyung-Eun Kim, Hye-Jin Lee, Min Sik Kim, Jiwon Seo, Hak-Hyeon Kim, Minjung Shin, Junyoung Jeong, Ki-Myeong Lee, and Taewan Kim in Professor Changha Lee's (ART) lab.

Last but not least, I would like to thank my parents and older brother for their continuous encouragement and support. I would not have come without their unconditional love, and I am so proud of myself who lives with beloved family. This dissertation consists of not my own efforts but love and support of all people.

This research was financially supported by both the Global Ph.D Fellowship (GPF) from the Korean Ministry of Education & the National Research Foundation, and the industrial fundamental technology development program (10050503) from the Ministry of Trade, Industry & Energy. I would like to acknowledge the Toray Chemical Korea© for kindly providing the membrane samples.